PNNL-27276

Prepared for U.S. Army Corps of Engineers & U.S. EPA through
agreement with Washington State Department of Ecology

Pacific Northwest
NATIONAL LABORATORY

Proudly Operated by **Battelle** *Since 1965*

Simulation of Salish Sea Response to Climate Change and Sea Level Rise Scenarios

Tarang Khangaonkar
Wenwei Xu
Adi Nugraha
Karthik Balaguru

February 2018

U.S. DEPARTMENT OF
ENERGY

Prepared for the U.S. Department of Energy
under Contract **DE-AC05-76RL01830**

DISCLAIMER

PACIFIC NORTHWEST NATIONAL LABORATORY
operated by
BATTELLE
for the
UNITED STATES DEPARTMENT OF ENERGY
under Contract DE-AC05-76RL01830

PNNL-26748

Simulation of Salish Sea Response to Climate Change and Sea Level Rise Scenarios

Tarang Khangaonkar
Wewei Xu
Adi Nugraha
Karthik Balaguru

February 2018

Prepared for U. S. Army Corps of Engineers & U.S. EPA through
agreement with Washington State Department of Ecology
CWFO Agreement No C0900121
under U.S. Department of Energy Contract DE-AC05-76RL01830

Pacific Northwest National Laboratory
Seattle, Washington 98109

Executive Summary

Researchers from various state and federal agencies engaged in efforts related to ecosystem management and restoration of the Salish Sea are assessing issues such as nutrient pollution and shoreline development pressures that require hydrodynamic and water quality information. To address these needs, Pacific Northwest National Laboratory, in collaboration with Washington State Department of Ecology, developed the Salish Sea Model (SSM). It is a predictive ocean-modeling tool for coastal estuarine research, restoration planning, water-quality management, and climate change effect assessment. This was accomplished through the U.S. Environmental Protection Agency's National Estuary Program project titled *Puget Sound Dissolved Oxygen Modeling Study*.

Salish Sea researchers are concerned that climate change will affect surface temperatures, freshwater runoff, sea level rise, and coastal upwelling, and these changes may result in entry of low-dissolved oxygen, high-pH, nutrient-rich water to the Salish Sea ecosystem. The U.S. Army Corps of Engineers and Environmental Protection Agency, seeking to better understand and manage the nexus of mitigation and adaptation initiatives within their overall climate change programs, collaborated on developing the scope for this project. The premise for this effort is that estimates of future meteorological and oceanic climate derived from the applications of large-scale general circulation models (GCMs) can be used to drive finer scale ecosystem models. The GCMs provide simulations of the Earth's past, present, and future climate states on a global scale. The resulting data products are typically on a grid (e.g., 30 km x 30 km) that cannot adequately resolve coastal nearshore estuarine systems. On the other hand, numerous site-specific models, such as the SSM, exist around the U.S. coastlines that operate on a much finer scale (250 m to 800 m typical range) with the ability to refine to ≈25 m in the nearshore intertidal regions. These models have demonstrated the ability to simulate estuarine processes in the nearshore environment; however, they have not been tested using downscaled data from global scale models, especially in the nearshore fjord-like estuarine environment of the Salish Sea.

This project is a proof-of-concept level effort where the objective was to evaluate if it is feasible to simulate nearshore estuarine response using off-the-shelf products available from the climate change research community to provide inputs and boundary conditions. This study also evaluated whether the SSM used by water quality management agencies in the State of Washington had sufficient resolution and sophisticated kinetics suitable for propagating the climate change effects into the nearshore coastal environment. The major objectives of this effort were to:

- Functionally link *downscaled* climate change models (e.g., meteorology, ocean chemistry, and hydrology) for Salish Sea to a marine circulation and water quality model that has been developed for the Puget Sound, Georgia Basin, and Strait of Juan de Fuca, namely the SSM
- Profile the projected interaction of riverine and marine systems at the estuarine/nearshore interface for selected locations, scenarios, and variables.

The SSM, with its recent improved kinetics for sediment diagenesis and carbonate chemistry and expanded domain encompassing Vancouver Island and covering the continental shelf (Khangaonkar et al. 2018), was applied for this effort. The model ocean boundary was adjusted to align better with the shelf break. To evaluate climate change effects in the intertidal environment, the model grid was refined in the Snohomish sub-basin that was selected as a test site based on availability of data. An improvement to heat

flux routines was implemented that allowed the model to function stably in regions with shallow/dry or standing water.

The inputs and boundary conditions for the simulations were obtained from the latest future climate predictions from the Coupled Model Intercomparison Project. This project produced a set of coordinated model experiments of future emissions scenarios that were simulated by numerous modeling groups around the world and were used in the development of Intergovernmental Panel on Climate Change's 5th assessment report. The Community Earth System Model (CESM), a global circulation model from the National Center for Climate Research, was selected for this study.

Projections of future climate vary across different GCMs due to several reasons, such as: (1) uncertainty in forcing applied, (2) differences in parametrizations, and (3) internal variability associated with each model. The common approach is to address uncertainty through the use of an 'ensemble', where the mean across several models is used to indicate the general direction of change. CESM ranks among the top CMIP5 models with regards to its skill in simulating the Pacific Northwest climate, and the multi-model mean for both temperature and precipitation. The availability of associated future ocean biogeochemistry directly from CESM and derived downscaled meteorological and hydrological predictions for the Pacific Northwest were also key factors that led to this selection.

Results were extracted from CESM model experiments corresponding to historical emissions and a future high-emission scenario titled RCP8.5. Future climate change effects on the Salish Sea circulation and biogeochemistry were evaluated relative to historical conditions defined by conditions averaged over 10 years of simulations from 1995 to 2004 representing the year (Y) 2000 scenario. This historical scenario established the "present conditions" baseline. The future scenario was defined by conditions averaged over 10 years of simulation from 2091 to 2100 (Y2095 RCP8.5 scenario). The historical Y2000 meteorological, hydrological, and oceanic conditions from downscaled CESM products were bias-corrected to observed data and this bias correction was applied to inputs for future simulations with SSM.

The model results show that under the RCP8.5 emissions scenario, numerous water quality variable responses are driven by predicted global changes. These responses include overall warming, depletion of dissolved oxygen (DO) levels, shift of algal species towards those with preference for higher temperatures, and continued ocean acidification. Effects of global ocean acidification and DO depletion propagate into the Salish Sea. A Salish Sea-wide average increase in temperature of 1.8˚C, decrease in DO of 0.7 mg/L, and reduction in pH of 0.12 units is predicted in future Y2095 relative to historical Y2000 conditions. The algal biomass in the Salish Sea is predicted to increase by 23% and the region of annually recurring hypoxia that occupies <1% of the Salish Sea in the present or Y2000 conditions is predicted to cover nearly 16% in the future.

The results also provide a new finding that the Salish Sea response in the future is less severe in magnitude when compared to the global change as reflected in the outer ocean near the edge of the continental shelf, where an average increase in temperature of 2.4˚C, decrease in DO of 1.7 mg/L, and reduction in pH of 0.23 units is predicted in future Y2095 relative to historical Y2000 conditions based on downscaled CESM products. The apparent resilience of the Salish Sea is attributed to benefits from the existence of strong estuarine circulation and healthy primary production.

At the intertidal scale, the combined effects of warming of freshwater streamflow and seawater intrusion will likely reduce the available fish habitat in estuaries such as the Snohomish River estuary based on simulated future scenarios.

This study accomplished the primary objective when it demonstrated the feasibility of using a leading coastal estuarine hydrodynamic and biogeochemical model to propagate climate change effects from a global scale to the nearshore estuarine scale. Downscaled products from global climate change experiments of future emissions scenarios are available in major coastal estuaries around the United States and may be used for testing the response in the nearshore environment using a suitable coastal ocean model that has been tested and reached an acceptable level of robustness and maturity. The SSM developed by Pacific Northwest National Laboratory, in collaboration with Ecology, through funding from the Environmental Protection Agency, demonstrated readiness level for this assessment and successfully simulated Salish Sea response to future climate conditions.

Acronyms

CAM	Community Atmosphere Model
ICM	integrated compartment model
CCSM4	Community Climate System Model version 4.0
CESM	Community Earth System Model
CESM-LE	Community Earth System Model – large ensemble
CICE	Community Ice Code
CLM	Community Land Model
CMIP5	Coupled Model Intercomparison Project, fifth phase
DFO	Canadian Department of Fisheries and Oceans
DIC	dissolved inorganic carbon
DIN	dissolved inorganic nitrogen
DO	dissolved oxygen
DOC	dissolved organic carbon
DON	dissolved organic nitrogen
EPA	Environment Protection Agency
FVCOM	Finite Volume Coastal Ocean Model
GCM	general circulation model
ICM	integrated compartment model
IPCC	Intergovernmental Panel on Climate Change
NOAA	National Oceanic and Atmospheric Administration
OBC	Open Boundary Conditions
PNNL	Pacific Northwest National Laboratory
psu	practical salinity unit
POP	Parallel Ocean Program
RCP	representative concentration pathways
RMSE	root mean square error
SOD	sediment oxygen demand
SSM	Salish Sea Model
TA	total alkalinity
USACE	U.S. Army Corps of Engineers
WRF	Weather Research and Forecasting
WSS	Willmott Skill Score
WWTP	wastewater treatment plant
Y	year

Contents

Figures

Tables

1.0 Introduction

There is a growing concern about the resilience of coastal waters and estuaries to stressors associated with climate change and sea level rise. Coastal ecosystems in the Pacific Northwest encompass numerous tide flats, marshes, and eelgrass beds that support thousands of species of fish and wildlife, which in turn are vital to the regional economy, culture, and quality of life. These habitats are present in the large and complex estuarine reaches within the Salish Sea, which includes the Puget Sound, Strait of Juan de Fuca, and Georgia Strait sub-basins in U.S. and Canadian waters. Potential changes to coastal physical and biogeochemical processes from climate change and sea level rise are of utmost importance here; therefore, adaptive management actions must be considered to ensure long-term coastal protection and sustainable use of nearshore resources (National Wildlife Federation 2007).

Over the global scale, effects of climate change—such as increases in air and sea surface temperatures, sea level rise, and changes in precipitation, cloud cover, and ocean chemistry with lower pH and higher nutrient concentrations—are expected to result in numerous ecosystem impacts (Doney et al. 2011, National Research Council 2011). On smaller riverine or estuarine scales, however, responses such as changes to stratification, circulation, and water quality may vary based on site-specific conditions. In the absence of information on local hydrodynamic and environmental characteristics, community-wide uncertainty about the magnitude of potential future impacts often hinders efforts to plan and implement adaptive management measures. Availability of suitable modeling tools that can simulate potential impacts from future climate conditions and the application and testing of numerous potential scenarios is essential for making informed planning and management decisions.

1.1 Project Background

This project supports a joint effort between the U.S. Army Corps of Engineers (USACE) and Environmental Protection Agency (EPA) that applies a coastal estuarine hydrodynamic and biogeochemical model to assess projected future climate impacts in the estuarine environment of the Puget Sound sub-basin within the Salish Sea. This effort seeks to better understand the nexus of mitigation and adaptation initiatives within their overall climate change programs. Many agencies, including the USACE and EPA, are increasingly expected to undertake and report on the results of mitigation efforts and incorporate adaptation features in their core programs. Yet, mitigation and adaptation efforts are often organizationally and functionally separate from one another. Until recently, this separation may have seemed reasonable, but current and projected fiscal and policy developments are creating new incentives and pressures for agencies to craft more integrated climate change programs that promote strategic investments, efficiencies, synergies, and sustainable solutions wherever possible.

Researchers from various state and federal agencies, who are responsible for management of nearshore coastal ecosystems, natural resources, and water quality, regularly encounter planning challenges that require hydrodynamic and water quality information describing the present environment and anticipated future conditions. Capital improvement projects must address questions related to conditions that will be encountered in the future given 50- to 100-year performance designs. The information or estimates of future meteorological and oceanic climate are typically based on research and publications derived from the applications of general circulation models (GCMs) that represent physical processes in the atmosphere, ocean, cryosphere and land surface. GCMs are the most advanced tools currently available for simulating response of the global climate system to increasing greenhouse gas

concentrations and provide simulations of the Earth's past, present, and future climate states on a global scale. These data products are typically on a grid (e.g., 30 km x 30 km) that cannot adequately resolve coastal nearshore estuarine systems. Site-specific models such as the Salish Sea Model (SSM) in the pacific northwest (Khangaonkar et al. 2011, 2012, and 2017) or the Chesapeake Bay Model on the east coast of United States (Cerco et al. 2010, Irby et al. 2016, Jiang and Xia 2016, and Ye et al. 2017) are typical examples of coastal estuarine models that have the required nearshore resolution. They are normally operated in the "hind-cast" mode using observed river flow, ocean boundary, and meteorological data. Use of these high-resolution models with GCM predictions as inputs to propagate the predicted future conditions into nearshore environments is relatively new.

This project is a proof-of-concept application of the SSM with its higher nearshore resolution (250 m to 800 m typical range with ≈25 m in the nearshore intertidal regions) to simulate future hydrodynamic and biogeochemical response, using data products from GCM for forcing the simulations. This effort is a first step towards assisting agencies that are engaged in developing climate change program policies, strategies, priorities, decision support, and performance management systems that consider mitigation and adaptation program functions in a more integrated context.

1.2 Introduction to Salish Sea Model

With the goal of resolving the interbasin exchange and biogeochemical response to nutrient pollution from over 100 wastewater outfalls, nineteen major rivers, and runoff from watersheds in the inner waters of the Salish Sea, Pacific Northwest National Laboratory (PNNL), in collaboration with the Washington State Department of Ecology, developed an externally coupled hydrodynamic and biogeochemical model of the Salish Sea. The combined model was constructed using the unstructured grid finite-volume coastal ocean model (FVCOM) framework (Chen eta al. 2003) and the CE-QUAL integrated compartment model (ICM) biogeochemical water quality kinetics (Cerco et al. 1994). This early version of the model was limited in that the ocean boundaries were set near the entrances to the Strait of Juan de Fuca and north boundary of the Georgia Strait. As a result, accurate simulation of estuarine exchange with the Pacific Ocean through the Strait of Juan de Fuca and Johnstone Strait required extensive boundary adjustment as part of model calibration. Another limitation was that sediment water interaction was prescribed as uniform fluxes of nutrients and dissolved oxygen. The model worked reasonably well in most sub-basins, but could not achieve domain-wide calibration for near bed dissolved oxygen (DO) levels. With prescribed uniform sediment fluxes, hypoxia in regions such as Lynch Cove in Hood Canal could not be reproduced.

Several updates to the model code and grid were made as part of this effort to overcome the prior limitations. This report presents an assessment with the improved version of the unstructured grid FVCOM based on the SSM. To facilitate better exchange with the Pacific Ocean, the SSM grid was expanded to include coastal waters around Vancouver Island and the continental shelf from Queen Charlotte Strait to the north in Canada to Waldport, south of Yaquina Bay, Oregon. The discharges of the Willapa, Chehalis, and Columbia Rivers to the shelf were also included in the domain. Johnstone Strait at the north end of Georgia Strait offers a second pathway for exchange with the Pacific Ocean along the east shores of Vancouver Island. Khangaonkar et al. (2017) showed that this pathway could be significant and is now explicitly included.

A new sediment diagenesis module was added that allows directly coupled interaction between water column and sediments through the processes of organic sediment settling and burial and remineralization (Pelletier et al. 2017a; Bianucci et al. 2017 in press). The sediment module generates nutrient fluxes including sediment oxygen demand (SOD). The model was also updated to include carbonate chemistry with dissolved inorganic carbon (DIC), total alkalinity (TA), pCO_2, and pH (Pelletier et al. 2017b; Bianucci et al. 2017 in press). With the aid of improvements described above, and a recalibration effort using data from 2014, observed biogeochemical monitoring data (salinity, temperature, DO, nitrate, algal biomass, and pH) in the Salish Sea, including near bed hypoxia in locations such as the Lynch Cove region of Hood Canal, have been reproduced (Khangaonkar et al. 2017 under review).

1.3 Study Objectives and Approach

The high-level objective of this project is to provide USACE, EPA, and their partners with new and valuable insights on how mitigation and adaptation initiatives in the nearshore estuarine environments may be impacted by climate change. At a basic level, these insights would help to more comprehensively inform decision-making on prioritization and coordination of future resource investments in mitigation and adaptation work. This project serves as a proof-of-concept effort to develop procedures and methods to downscale global-scale GCM data products to drive nearshore estuarine simulations.

The specific objectives of this effort are to:

1. Functionally link downscaled climate change models (i.e., meteorology, open-ocean chemistry, and hydrology) for the Pacific Northwest to the marine circulation and water-quality model that has been developed for the Salish Sea.
   - Improve the SSM to facilitate its use with climate change data products from GCMs. These improvements include site-specific grid and model code refinements for application in the intertidal zone as well as expansion of model domain around Vancouver Island, Canada, and to the continental shelf Pacific Ocean boundary.
   - Evaluate model performance and conduct skill assessment for the ability to accurately simulate water surface elevation, salinity, temperature, nutrients, DO, and pH.
2. Identify, evaluate, and import climate change, hydrological, and meteorological model simulations downscaled for the Pacific Northwest as inputs to the SSM.
   - Select climate models and scenarios of interest for use as inputs to the SSM based on screening criteria for identified projections, accounting for differences in spatial and temporal scope and resolution.
   - Design and apply a methodology to reconcile climate model estimates of current conditions and the observational records currently underpinning the SSM. Import the climate projections into SSM inputs.
3. Profile the projected interaction of riverine and marine systems at the estuarine-nearshore interface for selected locations, scenarios, and variables. Run climate-change scenarios and post-process SSM output.
4. Document and disseminate project results in a study report.

2.0 Acquisition and Review of Simulated Future Climate Data

This section provides a review of available global climate models, configurations, future climate scenarios, and the data products acquired for this study. Procedures used in extraction and processing of the climate data are described. This section also provides a detailed description of the meteorological, hydrological, and ocean boundary conditions that were developed from the available GCM data products to force the SSM under climate change scenarios.

2.1 Climate Models and Climate Change Scenarios

The Intergovernmental Panel on Climate Change (IPCC) published its fifth assessment report (IPCC 2014) just prior to the start of this project. The project team decided to use the latest future climate predictions from the set of coordinated climate model experiments that were used in the development of this report. These experiments comprise the fifth phase of the Coupled Model Intercomparison Project (CMIP5) and were developed with inputs from numerous climate modeling groups from around the world. To select a suitable global climate model and its predictions for this project, the global climate models that participated in CMIP5 were reviewed and evaluated for their suitability for one-way external coupling with the nearshore environment of the Salish Sea. In this case, external coupling would be accomplished by processing GCM outputs through spatial and temporal interpolation to develop inputs and boundary conditions corresponding to future climate conditions based on CMIP5 (Taylor et al. 2012), which includes predictions from more than 60 global climate models (submitted by more than 20 institutes). Among the models, spatial resolution and level of complexity vary, but at the most basic level all models include a coupled atmospheric component and ocean component.

One of the objectives of the project was to assess the feasibility of simulating nearshore response to climate change using available off-the-shelf products. This objective recognized the fact that incorporating GCM climate projections to a resolution and scale that is suitable for nearshore estuarine model would require a statistical or dynamic downscaling effort. Preparing each of the ocean, atmospheric, and hydrological boundary conditions would be a challenging task by itself and hence the focus on the use of previously prepared products. From the perspective of GCMs, the SSM represents the high-resolution nearshore model. Its inputs include freshwater runoff from watershed and rivers, nutrient loads, meteorological forcing on a regional scale, and ocean boundary chemistry. During the data acquisition phase of the project, the availability of meteorological and hydrological future predictions for the Salish Sea region was researched. Downscaled meteorological products from CMIP5 scenarios for the Pacific Northwest were directly available from PNNL. These were previously generated through dynamical downscaling with the Weather Research and Forecasting (WRF) model and a regional hydrology model using inputs from a GCM called Community Earth System Model or CESM (Hurrell et al. 2013). Rupp et al. (2013) and Gao et al. (2014) showed that CESM ranks among the top CMIP5 models with regards to the simulation of the Pacific Northwest climate and reproduces the multi-model mean for both temperature and precipitation very well. Of particular importance was access to compatible global ocean predictions from the same CMIP5 scenarios. The availability of associated future ocean biogeochemistry directly from CESM and derived downscaled meteorological and hydrological predictions resulted in selection of CESM and associated data products for this study.

CESM was funded by the National Science Foundation and U.S. Department of Energy and is administrated at the National Center for Atmosphere Research. As a fully coupled global climate model, CESM comprises four component models:

- Atmosphere: Community Atmosphere Model (CAM)
- Ocean: Parallel Ocean Program (POP)
- Land surface: Community Land Model (CLM)
- Sea ice: Community Ice Code (CICE).

CESM is one of the leading CMIP5 models in its ability to simulate global patterns of observed temperature and precipitation (Knutti et al. 2013) and has supported many research projects around the world. CESM has some new capabilities that can be coupled in different configurations, such as with the latest version of the CAM (CESM1-CAM5), or with active biogeochemistry and a prognostic carbon cycle with nitrogen limitation. In this research, we leveraged two configurations in preparing for SSM's boundary conditions (see Table 2.1). One of the configurations is the Community Climate System Model version 4.0 or CCSM4 (Gent et al. 2011), which is the earlier version that precedes CESM1 but is still supported as a configuration in CESM1. The other configuration is the Community Earth System Model – large ensemble (CESM-LE) project (Kay et al. 2015), which is based on the CESM1-CAM5. CESM-LE simulations not only calculate land carbon cycle as in CESM1-CAM5, but also include diagnostic biogeochemistry calculations for the ocean ecosystem and atmospheric carbon dioxide cycle, which are required for preparing SSM ocean water quality boundary conditions. Both CCSM4 and CESM-LE use 1.25˚ (longitude) by 0.9˚ (latitude) horizontal resolution for all model components, including atmosphere, land, sea ice, and ocean.

Table 2.1. Selected CESM Model Configurations

Selected Model Configuration	Atmosphere Component	Land Component	Sea Ice Component	Ocean Component	Ocean Biogeochemistry
CCSM4	CAM4	CLM4	CICE4	POP2	No
CESM-LE	CAM5	CLM4	CICE4	POP2	Yes

As mentioned previously, the metrological inputs to SSM were derived from dynamical downscaling products of CCSM4 meteorological datasets to 0.125˚ spatial resolution using the WRF model version 3.2 coupling with the CLM (Gao et al. 2014). Another product is Hejazi et al. (2015) hydrological projections (stream flow and temperature) over the continental United States based on Gao et al. (2014) downscaled meteorology. These hydrological predictions corresponding to future climate scenarios were used to develop hydrological loading for SSM. For the ocean boundary conditions, since CCSM4 does not resolve ocean water quality, we used CESM-LE to generate ocean temperature, salinity, and water quality boundary conditions to force SSM. Since CCSM4 and CESM-LE are two configurations from CESM, from this point on in we will use CESM as a broad reference for both CCES4 and CESM-LE.

The standard design of CMIP5 model simulation periods includes historical runs (1850-2005) and future runs (2006-2100). To assess climate change impacts at the Salish Sea, we designed our historical

scenario to reflect the current condition and future scenario to reflect long-term changes in the future. The historical scenario was designated as a 10-year period centered on year (Y) 2000 (1995-2005). The future scenario was designated as a 10-year period centering on Y2095 (2091-2100). For each of the scenarios, we developed a single-year time series to serve as the boundary condition for SSM using the average of 10-years of CESM output.

CMIP5 adopted a new set of scenarios called representative concentration pathways (RCPs) as described in Moss et al. (2010) to project different future greenhouse gas concentration (not emissions) scenarios. The four RCPs (RCP2.6, RCP4.5, RCP6, and RCP8.5) represent a possible range of radiative forcing values in Y2100 relative to pre-industrial values (+2.6, +4.5, +6.0, and +8.5 Watt per square mile, respectively). Moss et al. (2010) stated that these RCPs are neither forecasts nor policy recommendations but provide a broad range of climate outcomes for climate change research purposes. Given limited resources and broad interest in potential changes (i.e., upper bound) in the Salish Sea due to climate change, we decided to use RCP8.5, the reasonable highest emissions scenario available, as our future scenario.

2.2 Future Ocean Boundary Conditions for the SSM

The existing configuration of SSM has 87 open boundary condition (OBC) nodes, which require inputs of temperature, salinity, and water quality forcing in the form of time series profiles. To generate the historical and future OBC forcing under climate change scenarios, we used CESM-LE (Kay et al. 2015), which fully resolves the biogeochemical dynamics in the ocean that meet the SSM water quality OBC requirements. CESM-LE includes 30 ensemble members of fully coupled CESM simulations for the period 1920-2100. Each member is subject to the same radiative forcing scenario (historical and future RCP8.5) but begins from a slightly different initial atmospheric state. By using multiple ensemble members from CESM, we can reduce the model uncertainty introduced from model initialization. Here, 3 evenly spaced arbitrary ensembles out of the 30 members (Ensemble #2, Ensemble #15, and Ensemble #28), were selected and averaged to generate OBC forcing information.

Figure 2.1 shows the CESM ocean biogeochemistry simulation grid nodes and the SSM OBC nodes, with the location of a representative SSM OBC node #45 indicated. For each SSM OBC node, we selected CESM nodes that were within 1-degree radius and averaged the available water column profile data from CESM nodes to generate an OBC profile corresponding to the selected SSM node. The same process was used for temperature, salinity, and water quality variables. During the data quality assurance and control process, the CESM node at latitude 51.18 and longitude 231.91 was found to be biased and was removed from consideration.

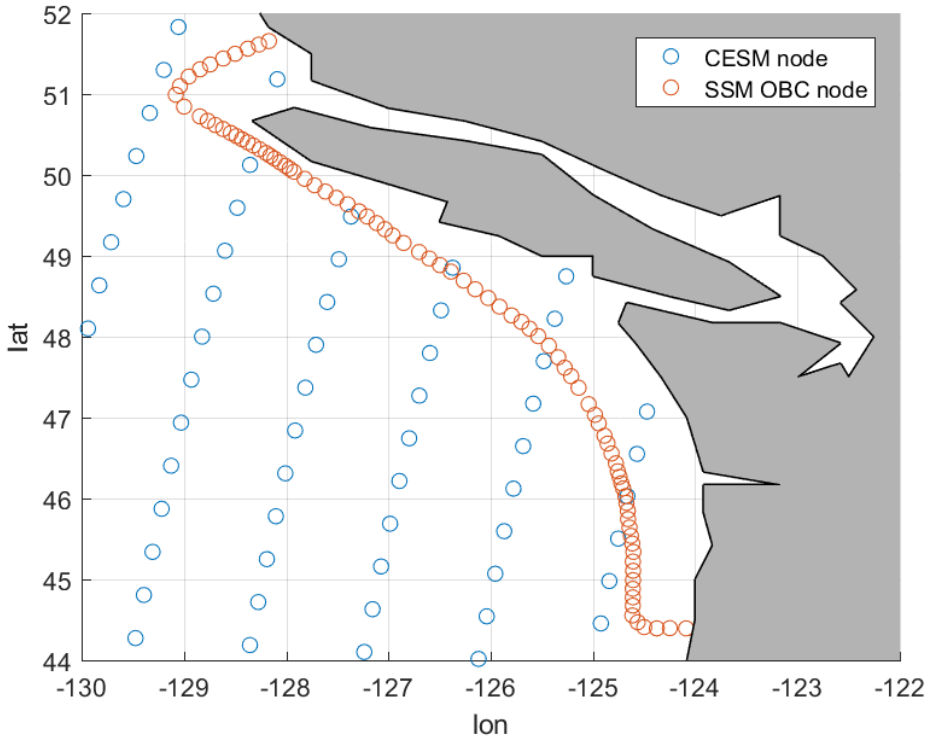

Figure 2.1. Overview of CESM Model Grid and SSM Boundary Nodes

2.2.1 Temperature and Salinity

The historical predictions from the CESM model for Y2000, for temperature and salinity at the SSM boundary nodes, were compared with measured data collected by the Canadian Department of Fisheries and Oceans (DFO). This comparison serves as a validation step to assess the accuracy of the CESM in predicting temperature and salinity over the Pacific Northwest continental shelf adjacent to the Salish Sea. The comparisons were conducted qualitatively (profile shape and stratification) and quantitatively by computing bias or mean error and root mean square error (RMSE) error between DFO measured data and CESM predictions (see Appendix A1). The historical scenario predictions corresponding to Y2000 at the SSM boundary locations from CESM were found to be comparable with DFO temperature and salinity data. As presented in Appendix A1, a mean error of 0.34˚C and RMSE of 1.02˚C for temperature and a mean error of -0.54 and RMSE of 0.6 for salinity were considered within acceptable limits and similar to typical model validation skill assessments. As a result, no bias correction was applied to temperature and salinity variables obtained from the CESM results for use as boundary conditions for SSM.

Figure 2.2 and Figure 2.3 provide comparison between historical and future scenarios for the temperature and salinity profiles at a representative SSM OBC node (#45 directly across from the entrance to the Strait of Juan De Fuca) as an example in both plots. Across all the OBC nodes, future temperature is on an average 2.44˚C higher than the historical scenario. Salinity profiles in the future are not predicted to change significantly relative to the historical scenario; however, the increased presence of freshwater in the surface layers in the winter and spring is noticeable (≈1 practical salinity unit [psu]).

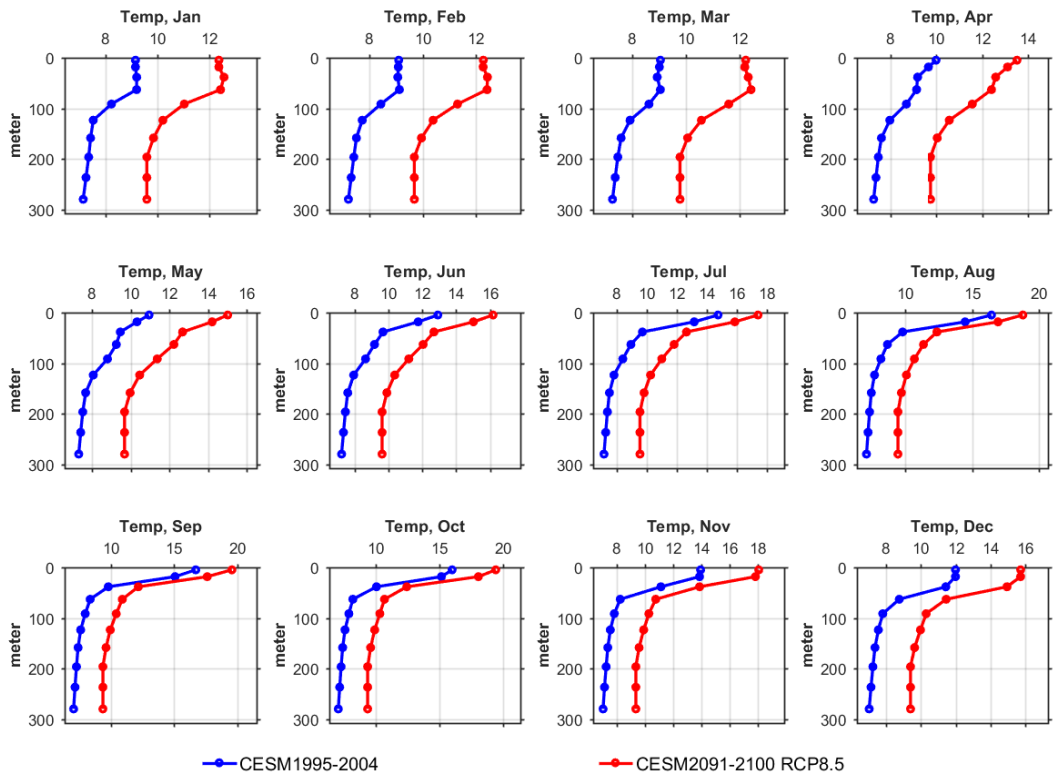

Figure 2.2. SSM Node 45 Temperature Profile Comparison

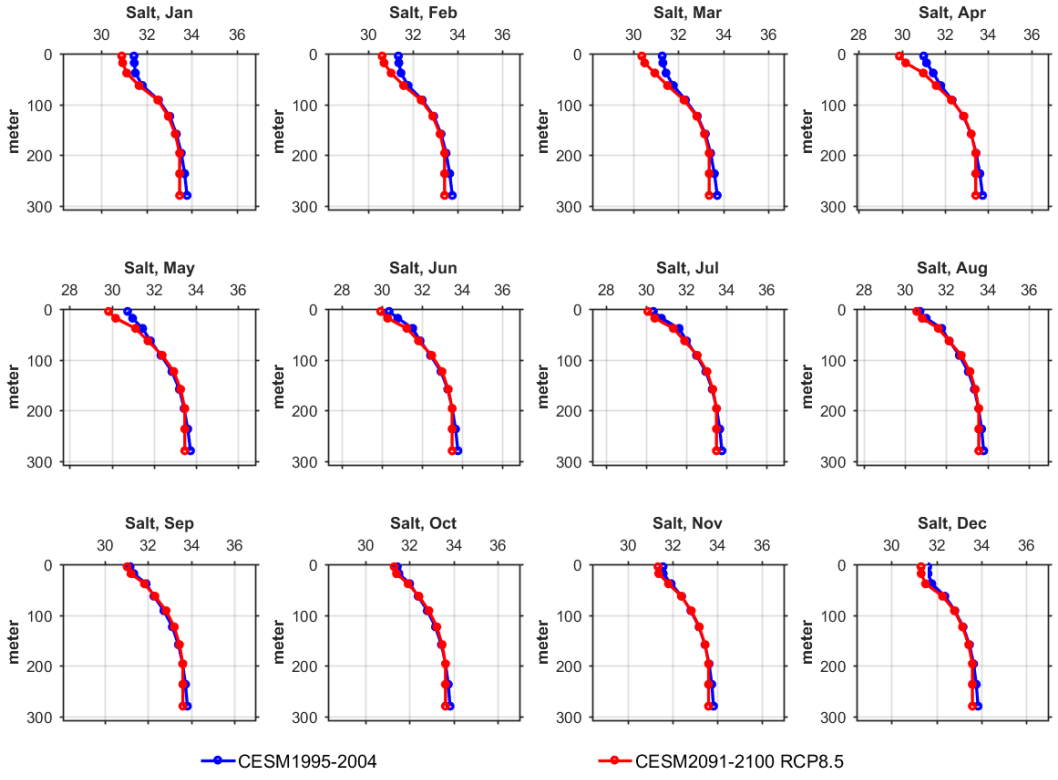

Figure 2.3. SSM Node 45 Salinity Profile Comparison

2.2.2 Water Quality

Similar to temperature and salinity, historical water quality predictions for biogeochemical parameters from the CESM for Y2000 were compared with measured data collected by DFO. This comparison served as a validation step to assess the accuracy of the CESM in predicting biogeochemistry over the Pacific Northwest continental shelf adjacent to the Salish Sea. The comparisons were conducted qualitatively (profile shape and stratification) and quantitatively by computing bias or mean error and RMSE between DFO data and CESM predictions. Unlike temperature and salinity, where bias was negligible, a positive and negative bias was found in many variables predicted by the CESM historical run. This bias was considered reasonable given that CESM does not have site-specific nearshore information on coastal zone nutrient loading and local biogeochemistry. Otherwise CESM predictions and observed data showed similarities in profile characteristics. In general, CESM results were found to underestimate dissolved organic nitrogen (DON) and phosphate (PO4) levels, and overestimate DO. The approach selected was to estimate the needed bias correction using this comparison and apply the same for both historical and future scenario runs. Detailed data verification and bias correction processes are described in Appendix A2.

Figure 2.4 through Figure 2.14 provide a comparison between historical and future scenarios for the water quality profiles at the same representative SSM OBC node as example after bias correction. The comparison shows that, across all the OBC nodes over the Pacific Northwest continental shelf, future concentrations predicted by CESM for the RCP8.5 scenario for DO are on average 28% (1.7 mg/L) lower than the historical scenario. Nutrient loads are predicted to increase slightly, with NO2-NO3, NH4, DON, and PO4 increasing by 9%, 4%, 7%, and 4% respectively.

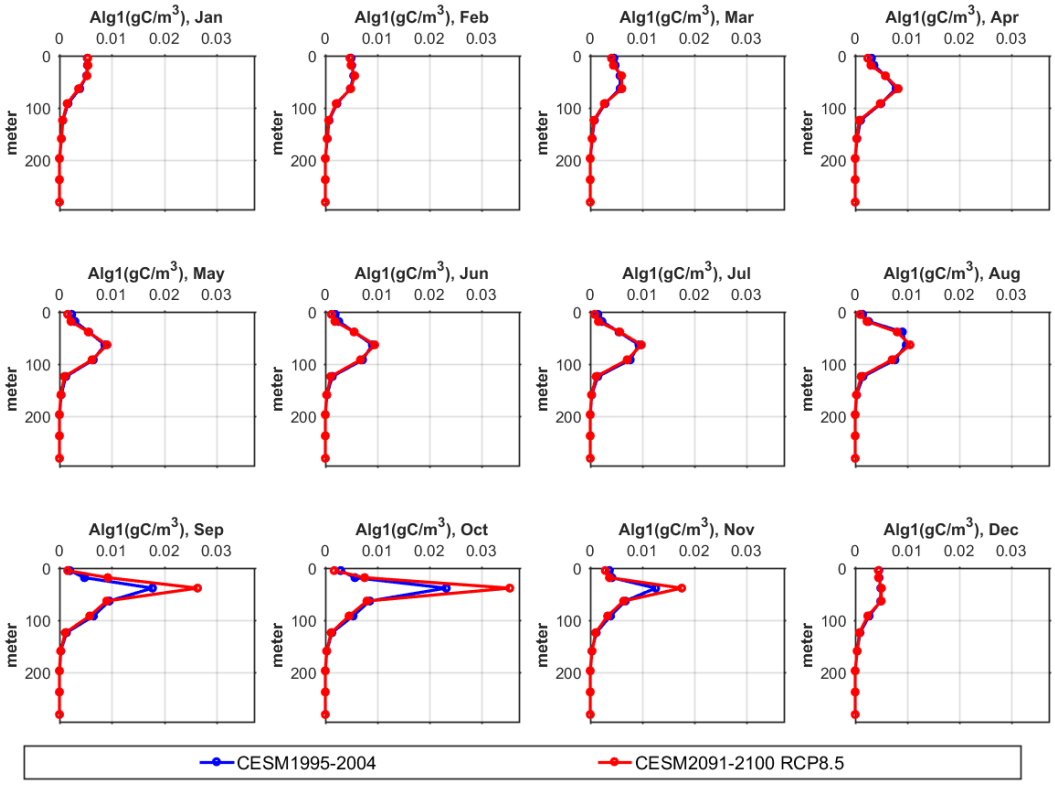

Figure 2.4. Comparison of ALG1 Profiles

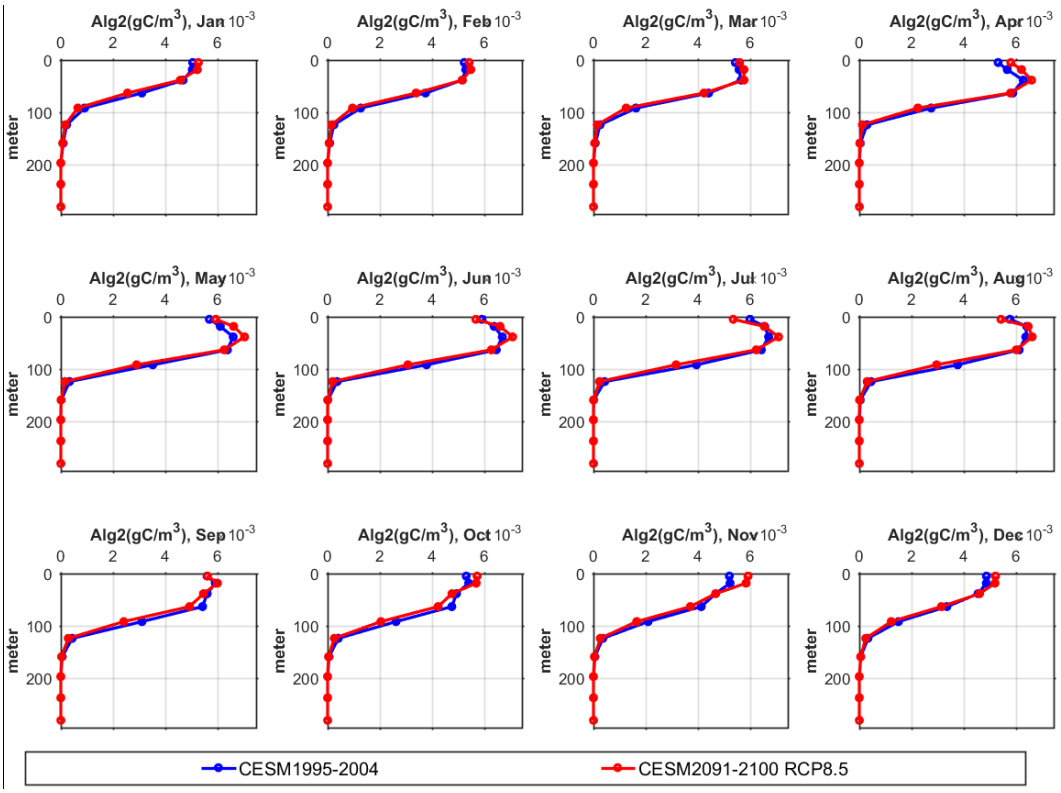

Figure 2.5. Comparison of ALG2 Profiles

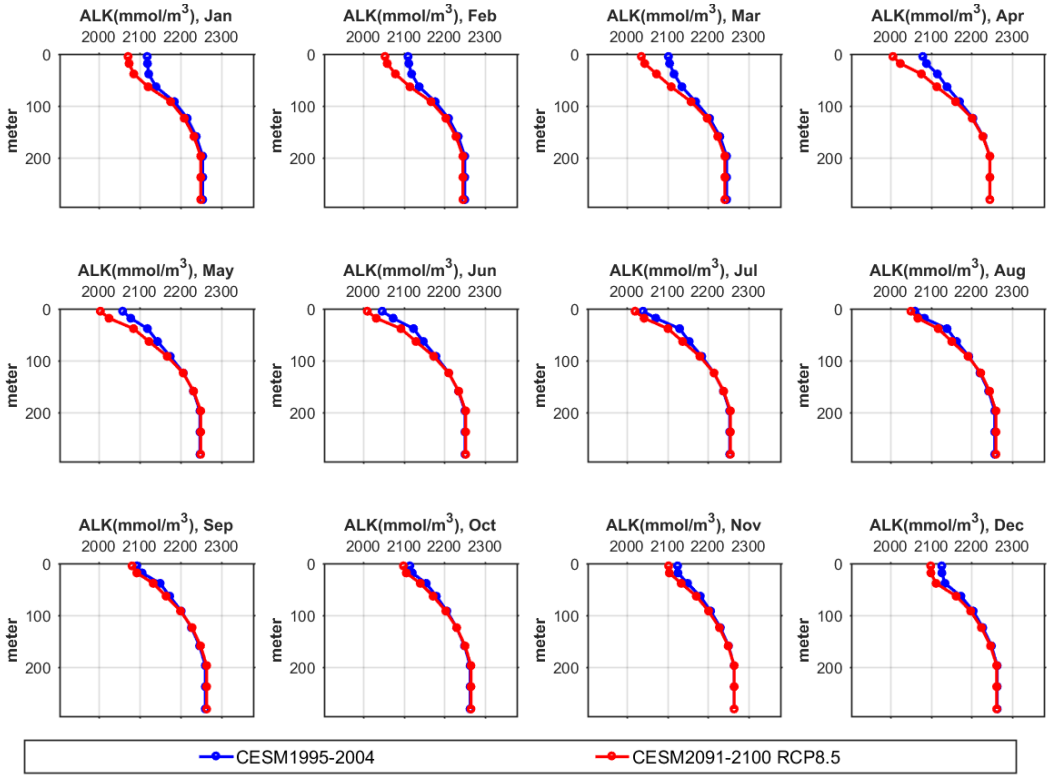

Figure 2.6. Comparison of Alkalinity Profiles

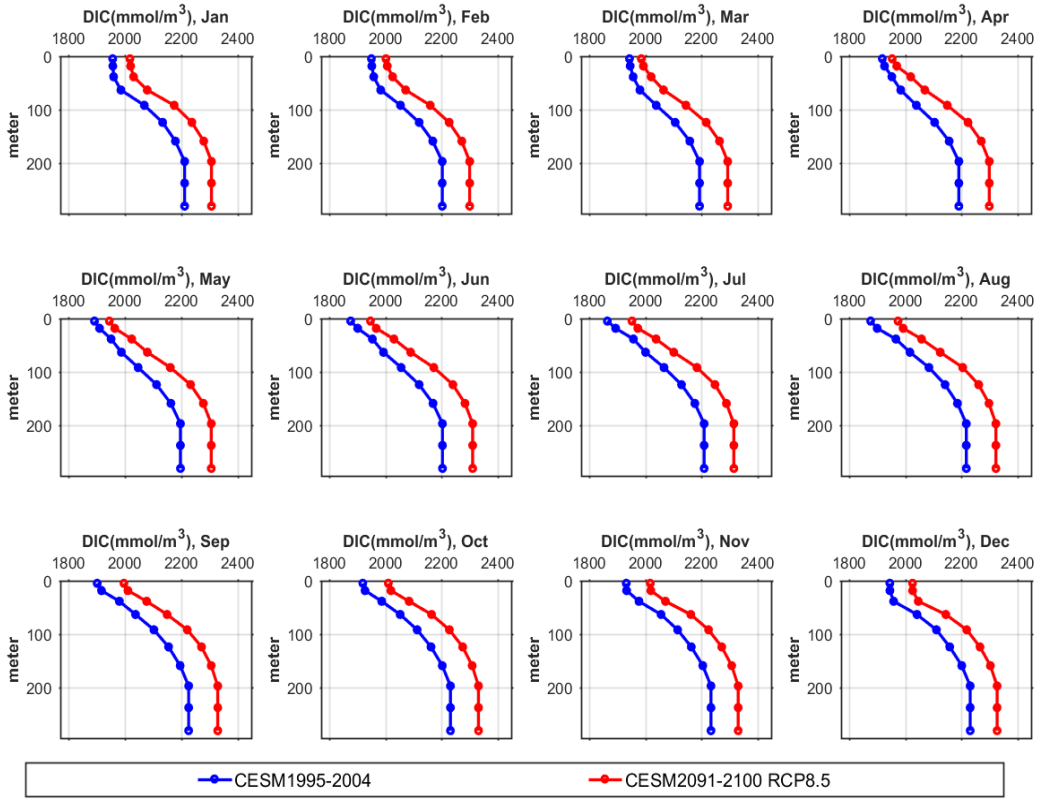

Figure 2.7. Comparison of DIC Profiles

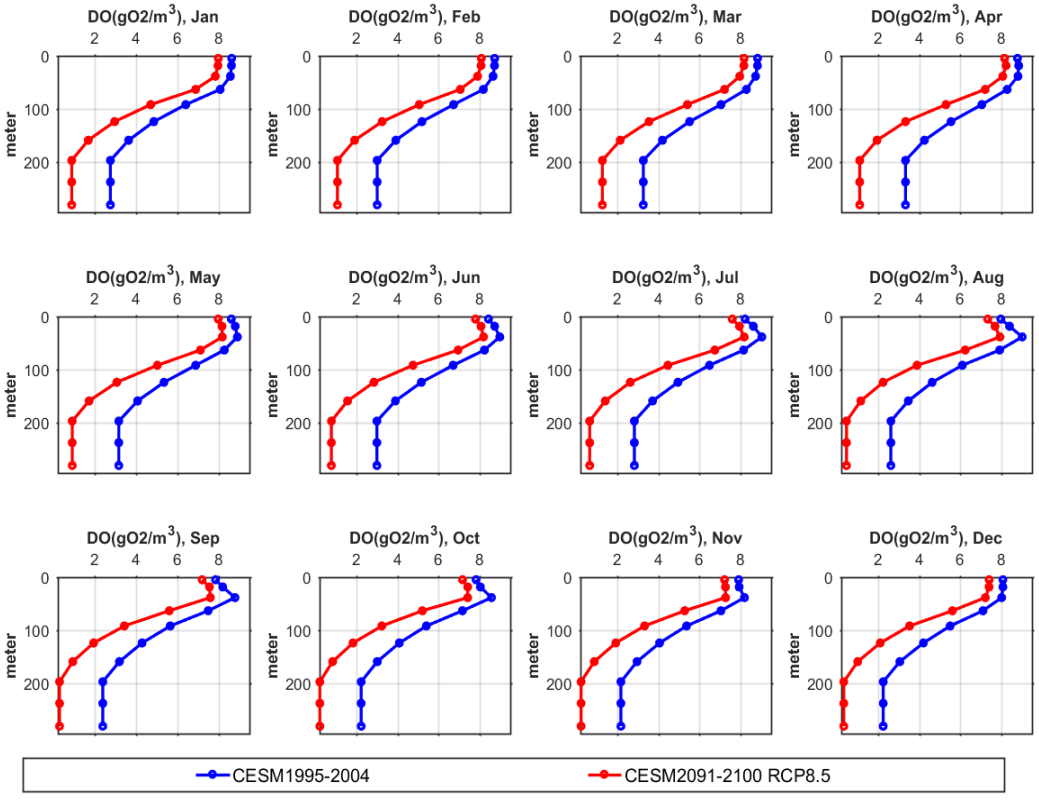

Figure 2.8. Comparison of DO Profiles

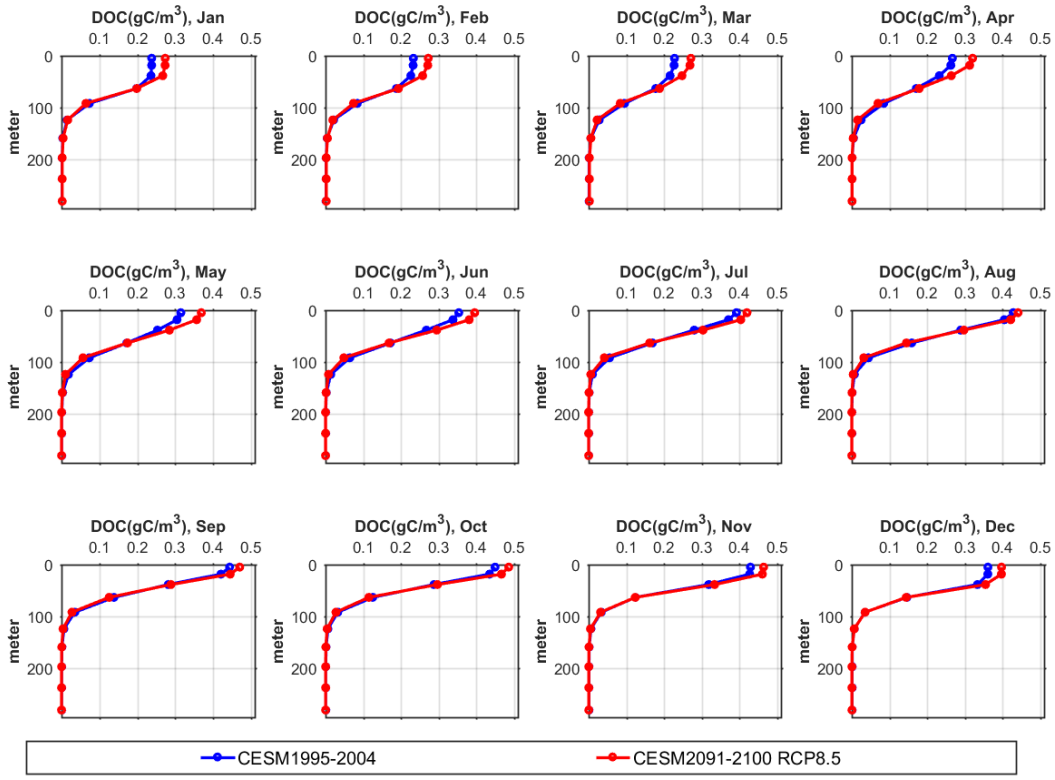

Figure 2.9. Comparison of Dissolved Organic Carbon (DOC) Profiles

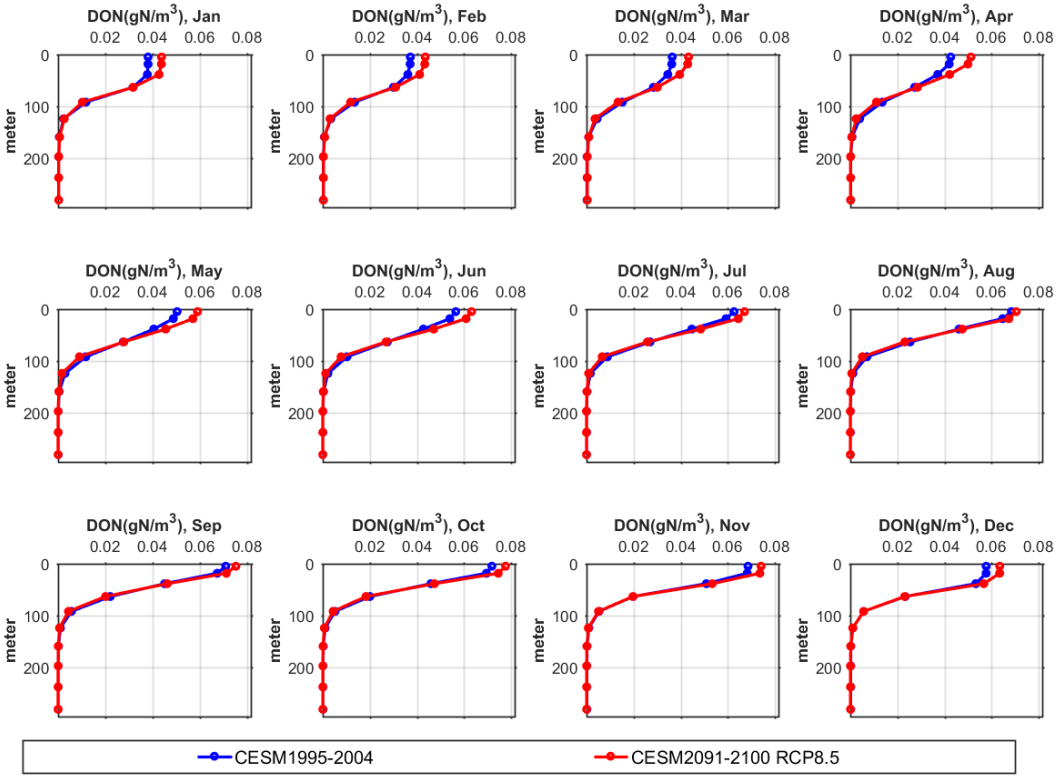

Figure 2.10. Comparison of DON Profiles

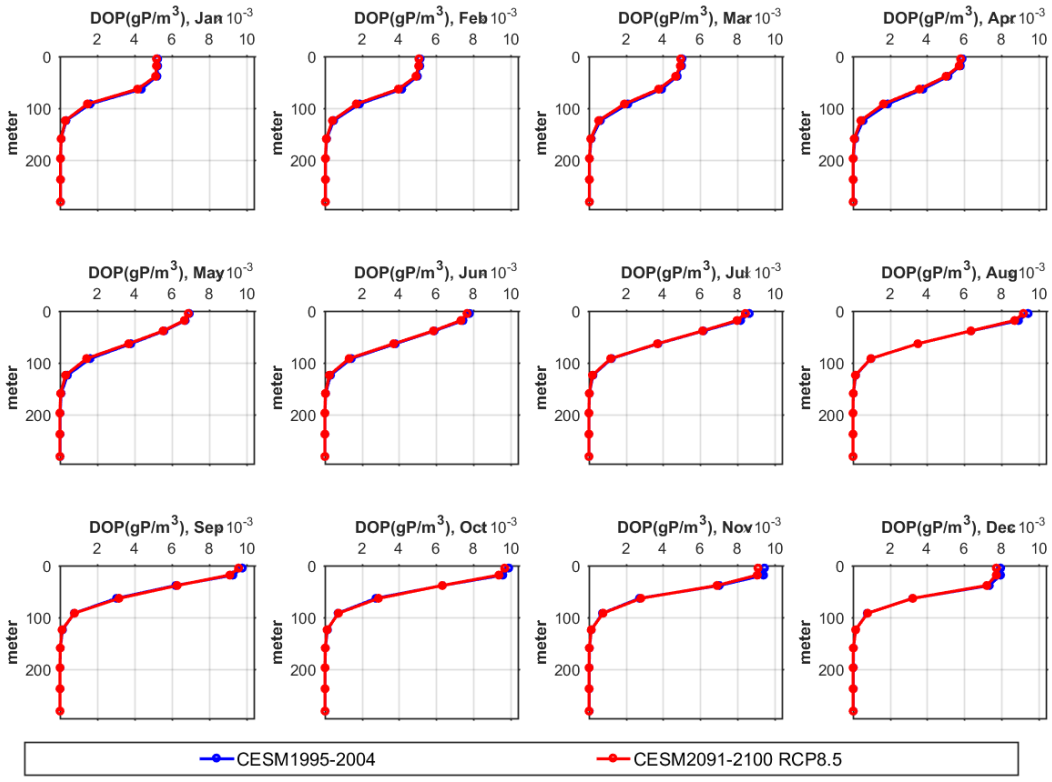

Figure 2.11. Comparison of Dissolved Organic Phosphorus Profiles

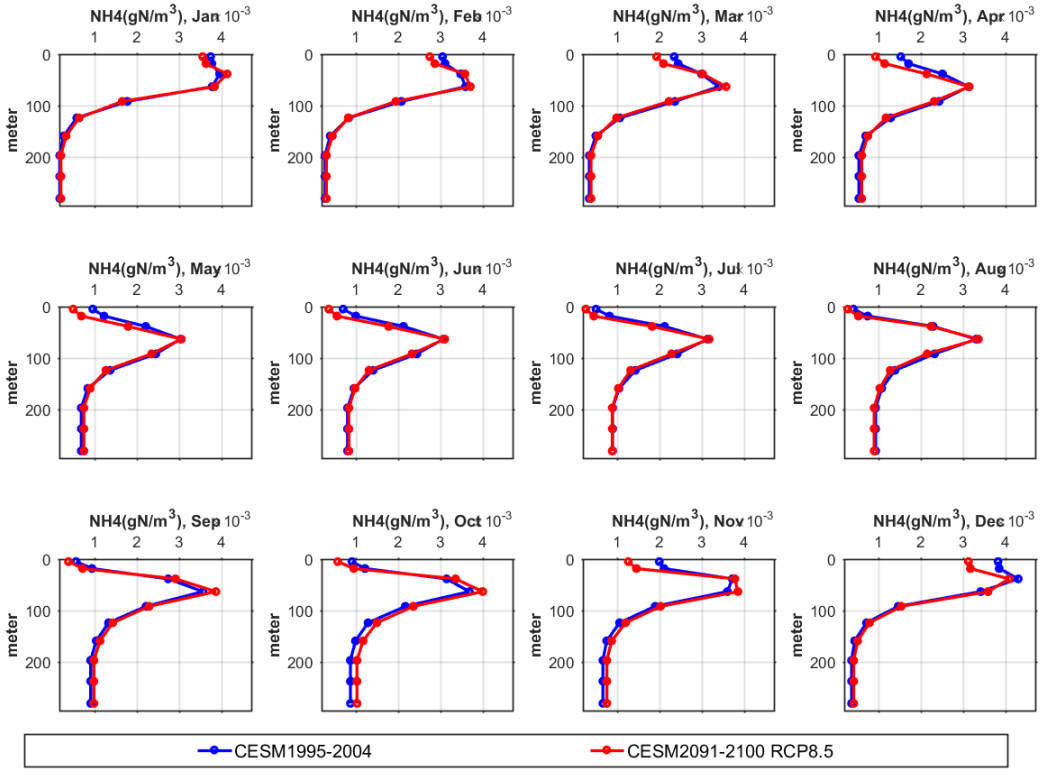

Figure 2.12. Comparison of NH4 Profiles

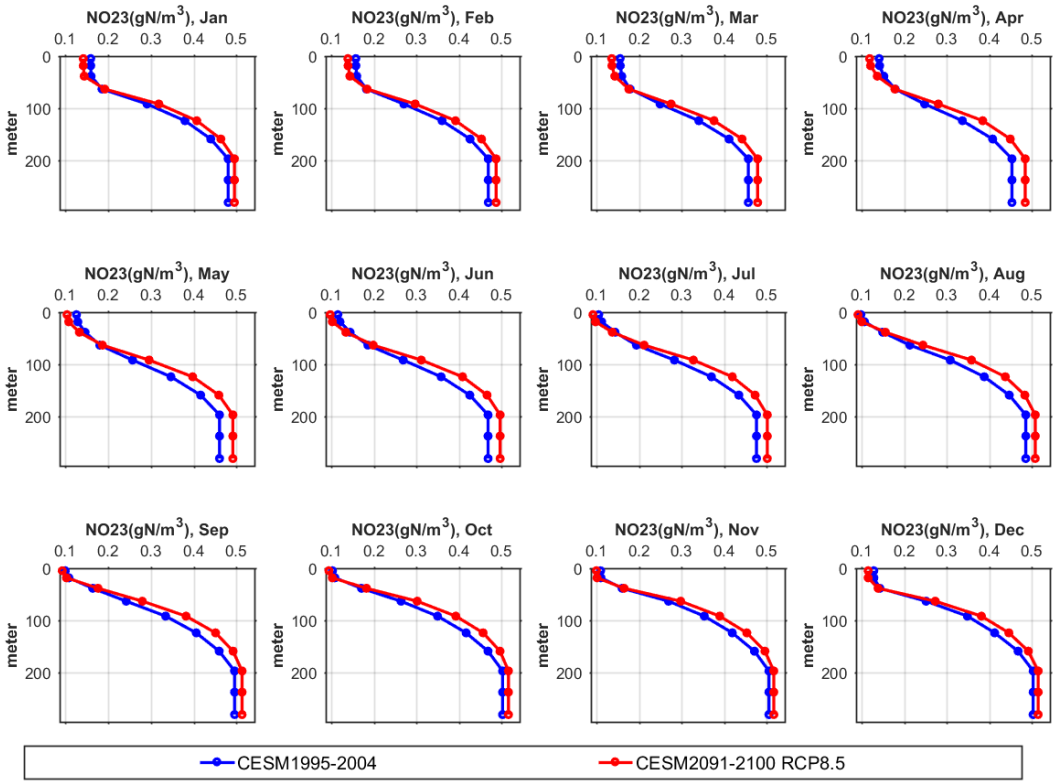

Figure 2.13. Comparison of NO2-NO3 Profiles

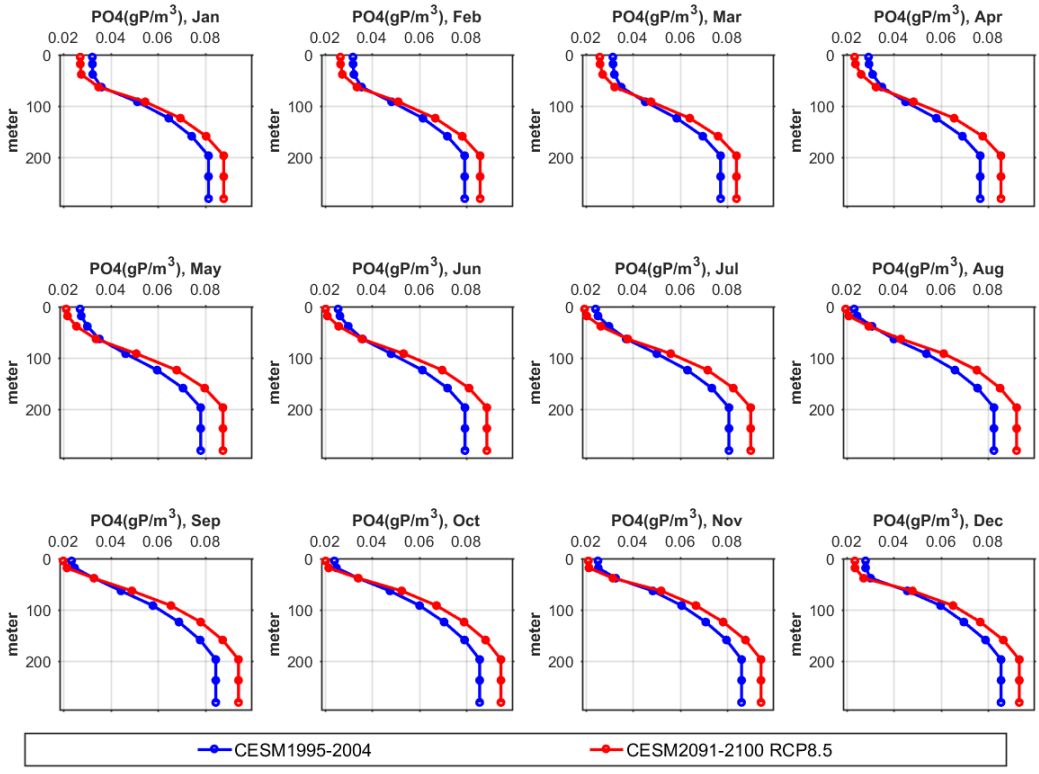

Figure 2.14. Comparison of PO4 Profiles

2.3 Future Meteorological Forcing over Salish Sea

Researchers at PNNL had previously conducted dynamic downscaling of simulations from CCSM4, including simulations of historical climate (1975-2004) and two future climate scenarios (RCP4.5 and RCP8.5) over the period 2005-2100. CCSM4 is an earlier version of CESM (Gent et al. 2011) with a spatial resolution of 0.9˚ (latitude) by 1.25 ˚ (longitude). The dynamic downscaling was conducted by Gao et al. (2014) using the WRF model version 3.2 coupled with the CLM at a finer resolution of 0.125˚ over North America. The temporal resolution of this model is 1 hour. Temperature, precipitation, and solar radiation results from this effort were bias corrected against National Aeronautics and Space Administration's Phase 2 of the North American Land Data Assimilation System, which is also at 0.125˚ resolution. Bias correction was conducted the using Bias Corrected Spatial Downscaling method (Wood et al. 2004). The meteorological variables that are available in these datasets are dew point temperature, shortwave solar radiation, longwave solar radiation, specific humidity, diffusive horizontal radiation, direct normal radiation, wind-u component, wind-v component, air temperature, and precipitation.

The spatial domain of the downscaled meteorological forcing ends at the continental United States boundary and does not cover the entire Salish Sea domain. Figure 2.15 shows WRF model nodes that fall within the SSM domain. For simplicity, the SSM model was setup to use uniform meteorological input. The metrological data from selected WRF nodes were averaged spatially to obtain representative time series for each variable for the historical and future years. The variables from WRF were converted to net heat flux, net shortwave radiation, wind speed, wind direction, precipitation, and evaporation to serve as inputs to SSM using COARE formulations described in Fairall et al. (2003).

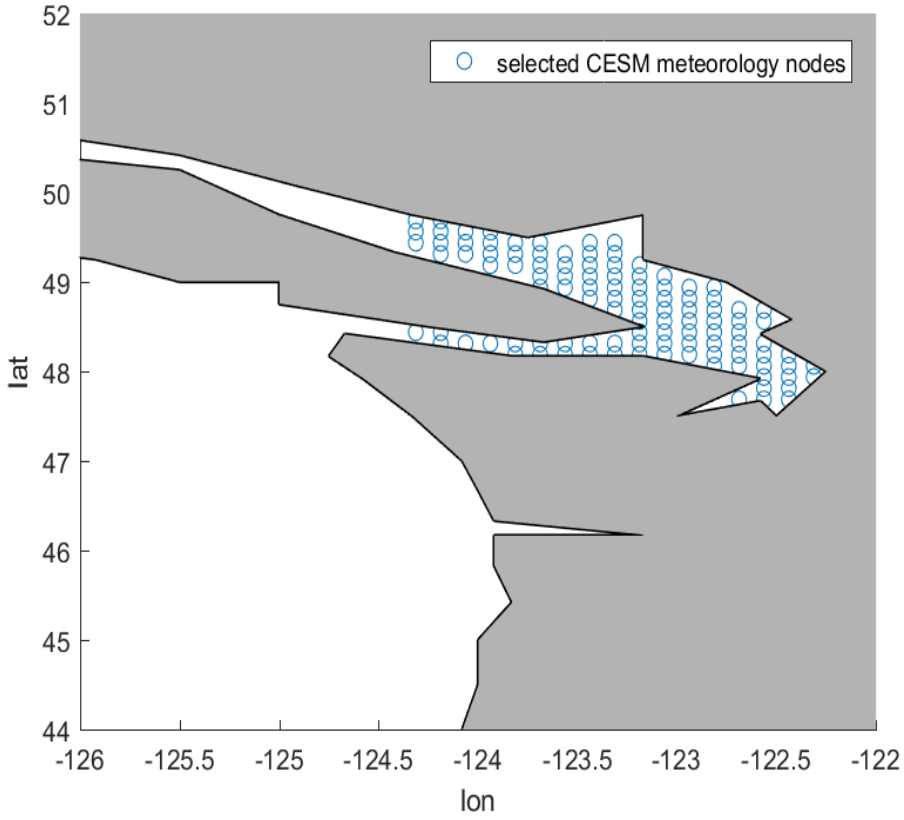

Figure 2.15. WRF Model Nodes Selected for Developing SSM Meteorological Inputs

Figure 2.16 provides a comparison of metrological variables between the historical (Y2000) and future (Y2095) conditions for the RCP8.5 emissions scenario. Air temperature is an average of 3.5˚C higher than the historical scenario, indicating a warmer atmospheric boundary over the Salish Sea. The net heat flux is the measure of heat exchange between air and water, with flux from air to water being positive. Considering that future air temperature is higher, one may expect that the net heat flux would also be higher in the future; however, the future heat flux remains at levels similar to the historical. This is because net heat flux into water is dependent on temperature difference between air and sea surface. The sea surface temperature is also higher in the future and, as a result, temperature difference and net heat flux are relatively unchanged. The wind direction and magnitude in the future are also relatively unchanged in Y2095 and RCP8.6 emissions scenario simulations.

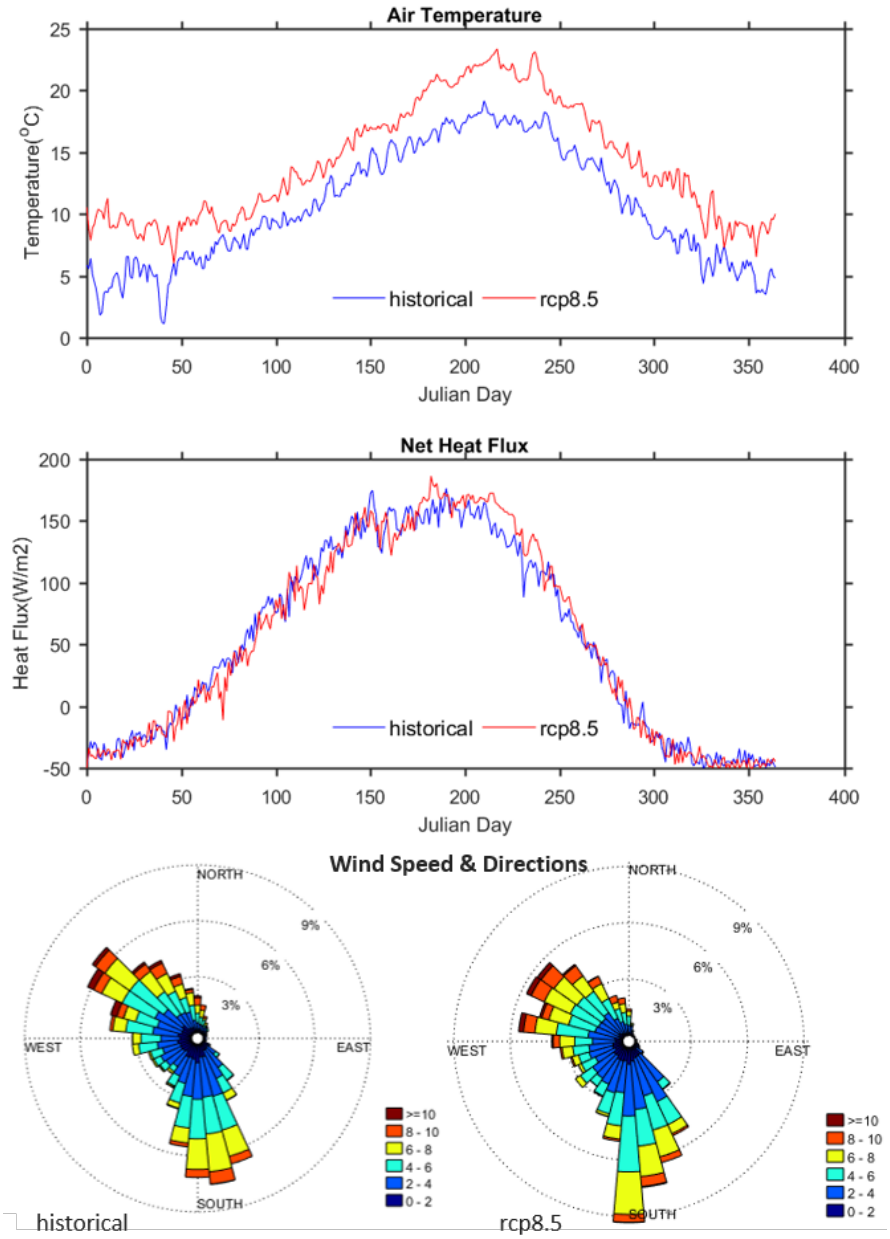

Figure 2.16. Comparison between Historical and Future Meteorological Variables

2.4 Future Hydrological Loading Estimates for the Salish Sea

Hydrological loading to the SSM includes three types of inputs: river flows from major rivers that are continuously monitored by the U.S. Geological Survey; non-point source loads computed using hydrological analysis; and wastewater treatment plant (WWTP) loads. Ecology has developed a procedure using hydrological and multiple regression analyses for the Salish Sea domain to estimate freshwater loads (Mohamedali et al. 2012). Figure 2.17 shows a total of 64 freshwater sources to the Salish Sea domain that include rivers and non-point sources. These are estimated using regressions developed from historical data from 32 gaged locations. Four rivers that lie outside the Salish Sea but within SSM domain are the Columbia, Willamette, Chehalis, and Willapa and are included. In addition, 88 U.S. WWTPs and nine Canadian WWTPs are included in the SSM inflow inputs.

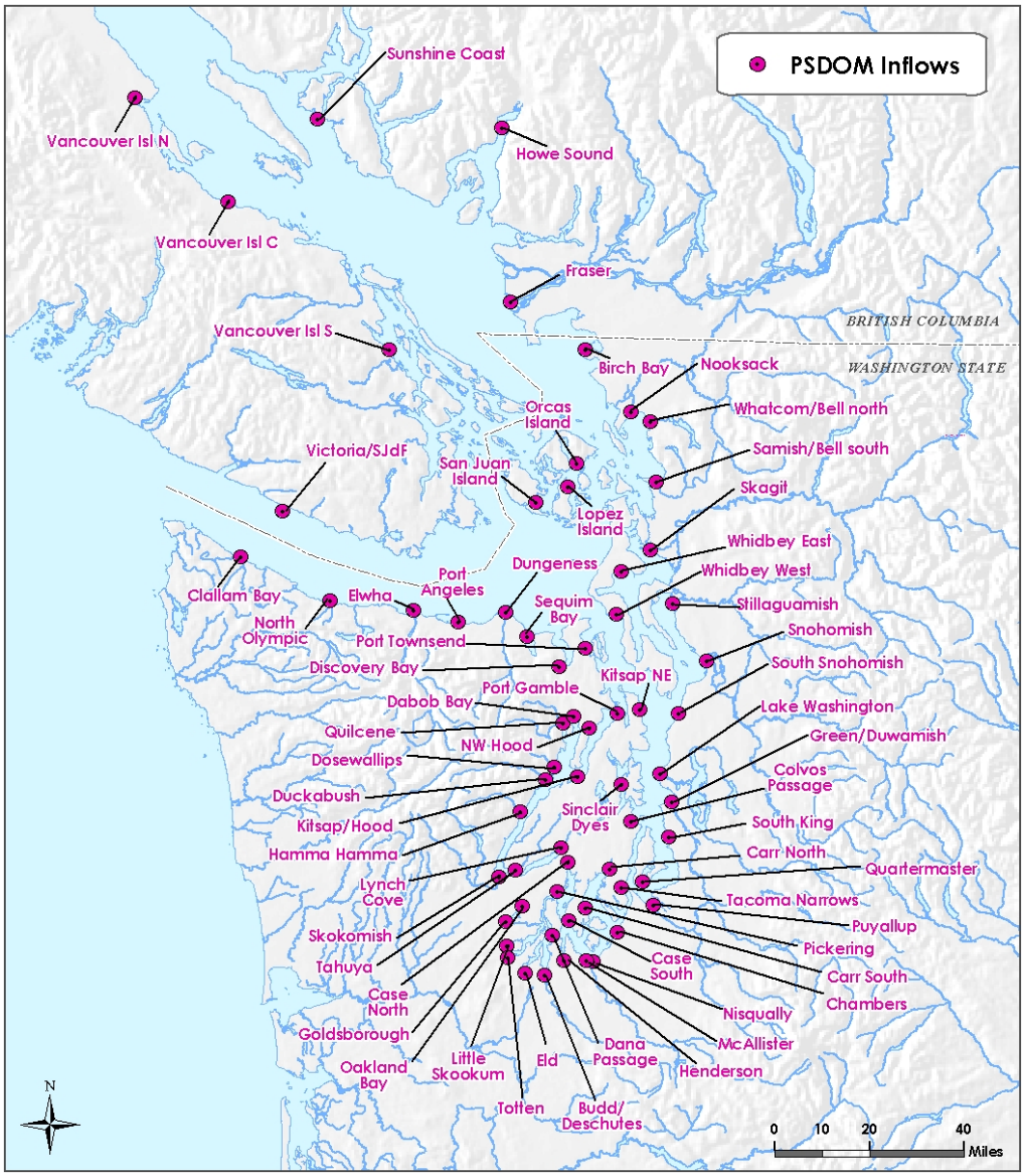

Figure 2.17. Freshwater Inflows from U.S. and Canada Included in SSM

To generate historical and future hydrological inputs to the Salish Sea, the approach was to use downscaled data products at the locations of existing gaged streams and compute the freshwater and wastewater inputs using the regression procedure for the Salish Sea developed by Ecology described in Mohamedali et al. (2012). Downscaled hydrological data products for the Pacific Northwest have been computed by organizations such as the University of Washington Climate Impacts Group and PNNL. For consistency with CESM products from the fifth assessment simulations, we selected the PNNL hydrological data product corresponding to historical and future RCP8.5 scenario future simulations that were available.

This included future flows from downscaled and bias corrected meteorological forcing described in section 2.3 through a physically based hydrological model, the Model for Scale Adaptive River Transport or MOSART (Li et al. 2013) by Hejazi et al. (2015). River temperatures associated with these flows were calculated using the MOSART heat model (Li et al. 2015). Hourly river flow and water temperature for 13 major rivers to the Salish Sea area were acquired for both the historical scenario (1995-2004) and RCP8.5 scenario (2091-2100).

Using the procedures developed by Ecology, the hydrological predictions for the 13 major rivers were extrapolated to 64 watersheds and SSM inflow inputs as follows:

1. Bias correction. Because the Hejazi et al (2015) study was at continental U.S. scale, MOSART was applied at relatively coarse resolution (one-eighth of a degree) and did not resolve the smaller watersheds within the Puget Sound region of the Salish Sea. Also, the study domain was restricted to U.S. continental watersheds and only covered parts of the Fraser River basin. Due to these reasons, the MOSART predicted flows and temperatures were bias corrected using comparison of historical predictions to observations from 1995-2004. The bias correction method used is a cumulative distribution function matching approach, as described in Brocca et al. (2011). First, the historical scenario datasets were scaled to match the distribution function of observations and then the differences between before and after bias corrected historical scenario datasets were applied to the RCP8.5 scenario datasets. Differences were applied as additive for temperature and multiplicative for flow. The flow of all 13 rivers was bias corrected using observed data; however, the temperature of only three rivers was bias corrected, since long-term temperature observations were only available at the Snohomish, Nooksack, and Cedar Rivers monitoring sites.
2. Cross-correlation. Following Roberts et al. (2014) and Mohamedali et al. (2011), we developed cross correlation to extrapolate the 13 major river flows to 32 gaged locations. We paired each of the 32 gaged watersheds with a MOSART simulated river in the historical scenario based on the strongest correlations available. Then a linear regression relationship was developed for each of the pairs. Using the linear regression coefficients and MOSART simulated river flows, the 32 gaged watersheds flows were derived for both historical and future RCP8.5 scenarios.
3. Extrapolation. Following Mohamedali et al. (2011), we extrapolated the historical scenario and RCP8.5 scenario flow predictions from the 32 gaged locations to freshwater inflows from all 64 watersheds by scaling streamflow according to watershed area and historical average annual rainfall.

River water quality was not simulated in MOSART, so the most recent Y2014 datasets for both historical and future RCP8.5 scenario were used, except for dissolved inorganic nitrogen (DIN). Coastal nearshore environment and biogeochemical response are sensitive to nutrient loads, especially nitrates (NO2+NO3) and ammonia. Future DIN loads were estimated based on watershed land-use change and

population growth using methods established in Roberts et al. (2014). The future land-use projection through 2070 is based on Oregon State University's Envision Project's "Status Quo" scenario. This scenario projected slight decreases in agriculture and forested area in the Puget Sound region, while increases in development mostly concentrated in existing urban areas. The correlation between river DIN and land-use index is used to project future DIN loads (Roberts et al. 2014).

Future WWTP flow was estimated assuming linear correlation between watershed population and WWTP flow rate. Roberts et al. (2014) collected the population projections from each county website and calculated county population growth rate. Most counties do not predict population up to Y2095, thus we assumed the population growth rate remained the same and projected population in Y2095. WWTP temperature and water quality were assumed to be unchanged.

2.4.1 Future River Flow and Temperature Predictions

Figure 2.18 illustrates bias corrected monthly average flows simulated using MOSART for historical and future scenarios. Observed data from the period 1995 to 2004 is also presented. The rainfall dominated rivers (Skokomish, Deschutes, Nisqually, Duwamish, Stillaguamish, and Cedar) are shown to peak in winter months. MOSART predicted an increase in winter flow. For rivers dominated by winter rainfall and snowmelt (Puyallup, Snohomish, Skagit, Nooksack, Dungeness, and Elwa), two peaks were noticeable, one in winter and one in spring/summer. The results showed trends indicating increased winter rainfall dominated flow and decreased spring/summer snowmelt flow. Note that MOSART does not attempt to simulate dam management on those rivers, so predicted flow change does not reflect impacts from future water management. Fraser River is a snowmelt-dominated river (peak in late spring/summer) and also the largest freshwater input into the Salish Sea. MOSART predicted a slight reduction in summer flow and an earlier snowmelt-induced peak. The overall reduction of freshwater inflow (4.7%) is likely due to the combination of summer drought and elevated evaporation rate from predicted temperature increases in the future. These results are consistent with literature on future river flows under a warmer climate.

Figure 2.19 shows predicted river temperatures based on MOSART heat model plotted as monthly averages. All 13 rivers show a trend of increased temperatures in the future. On average, yearly temperatures are predicted to increase by 3.2˚C in the future Y2095 RCP8.5 scenario in Y2095 relative to the historical scenario Y2000. On average, the August temperatures are predicted to increase by nearly 5.5˚C.

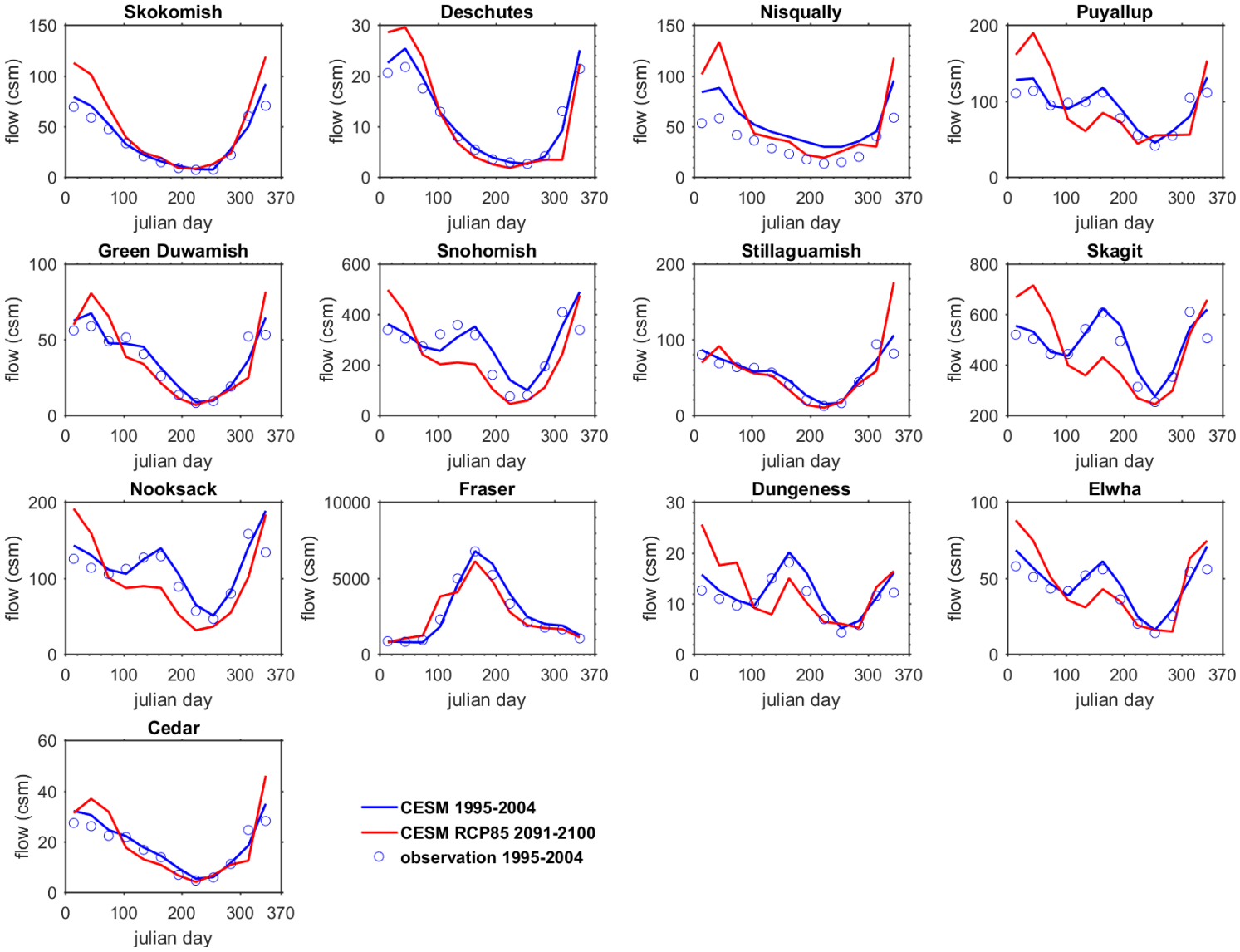

Figure 2.18. Bias-Corrected MOSART Simulated Flow Monthly Average

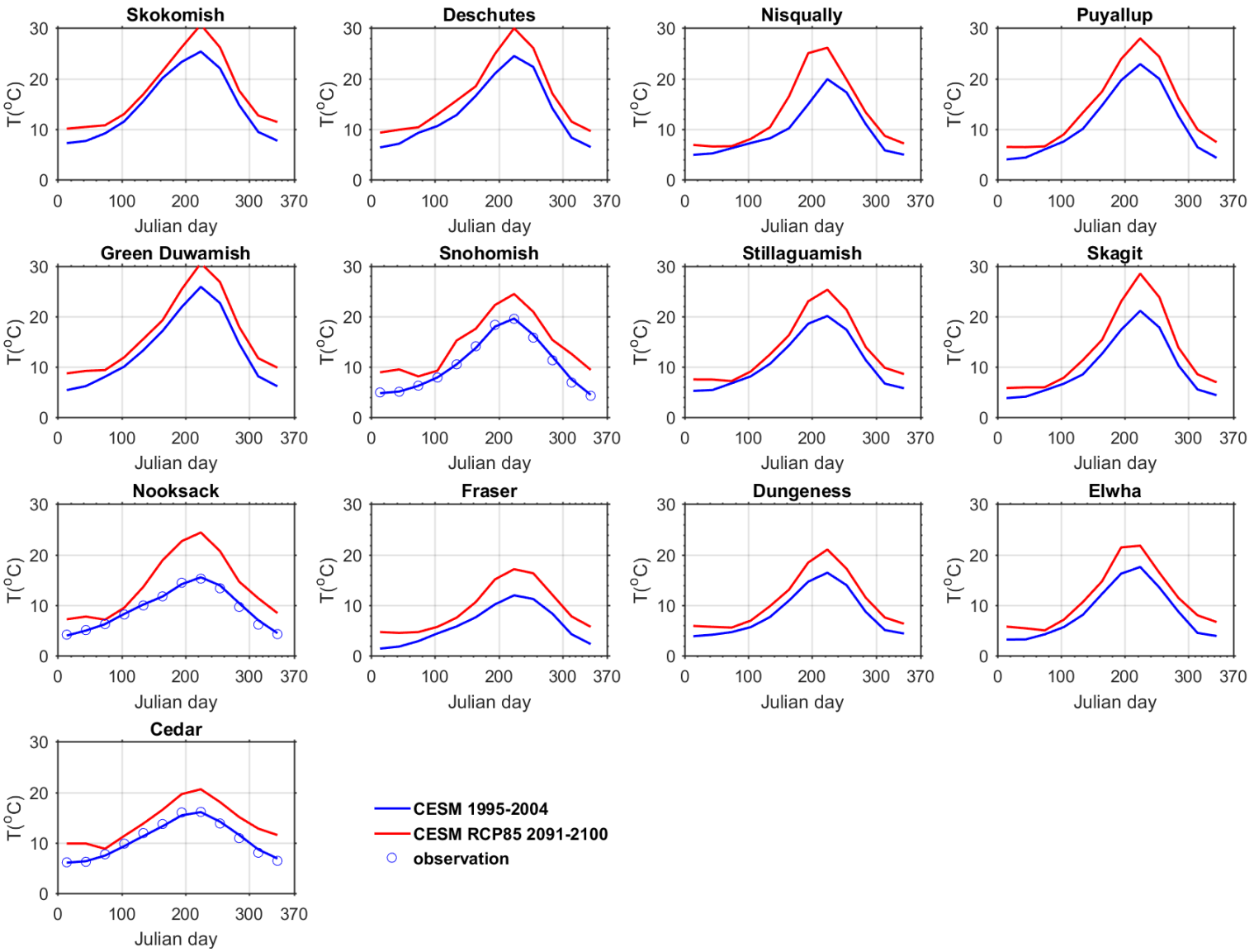

Figure 2.19. Bias-Corrected MOSART Simulated Monthly Average Temperature

2.4.2 Watershed Nutrient Loads

As mentioned above, river nitrate-nitrite load is assumed to be correlated to land-use index, which is calculated from the regional urbanization projections. Figure 2.20 shows that total nitrate-nitrite load from rivers is predicted to increase by 44% from historical to RCP8.5 scenario. Since the overall flow rates remain at the same level from historical to future, this increase in total nutrients is due to population growth and related land-use change assuming the land-use/nitrate-nitrate relationship is unchanged in the future.

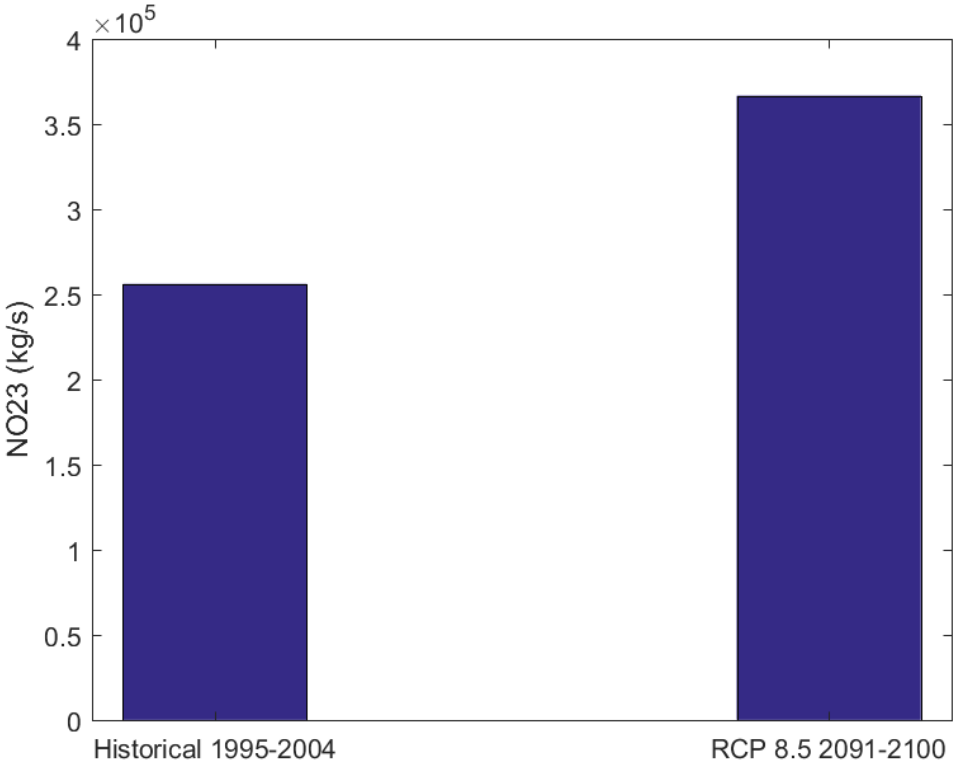

Figure 2.20. Total River Nitrate-Nitrite Load Comparison between Scenarios

2.4.3 WWTP Flow, Temperature, and Nutrient Loads

In computing future water quality variable concentrations from WWTP, the assumption was that treatment requirements and plant capacity will ensure wastewater concentrations remain within effluent limits and will not change significantly; however, the WWTP flow will increase in proportion with population growth. Total wastewater flow to the Salish Sea during the period 2091-2100 is predicted to be 2.91 times that of the historical scenario for the period 1995-2004 (see Figure 2.21). Total Nitrate-Nitrite load from WWTPs in 2091-2100 is predicted to be 2.19 times that of historical scenario (see Figure 2.22). Total nutrient loads do not increase at the same rate as total flows because the population is projected to grow more rapidly in regions with higher WWTP water quality controls.

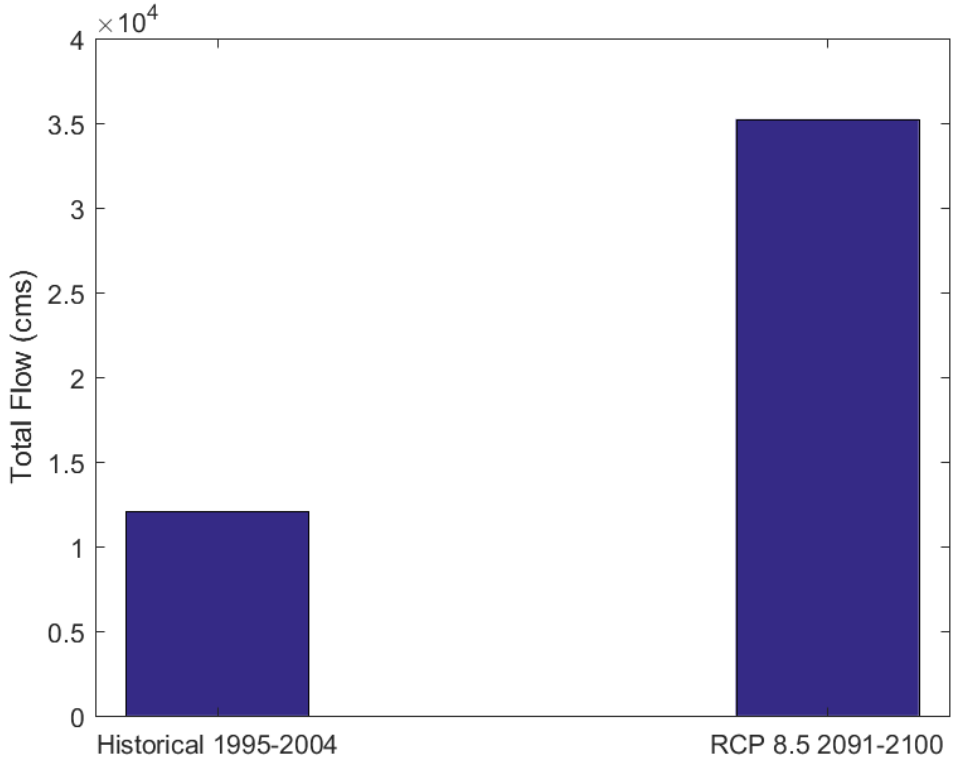

Figure 2.21. Comparison of Total Flow from WWTPs

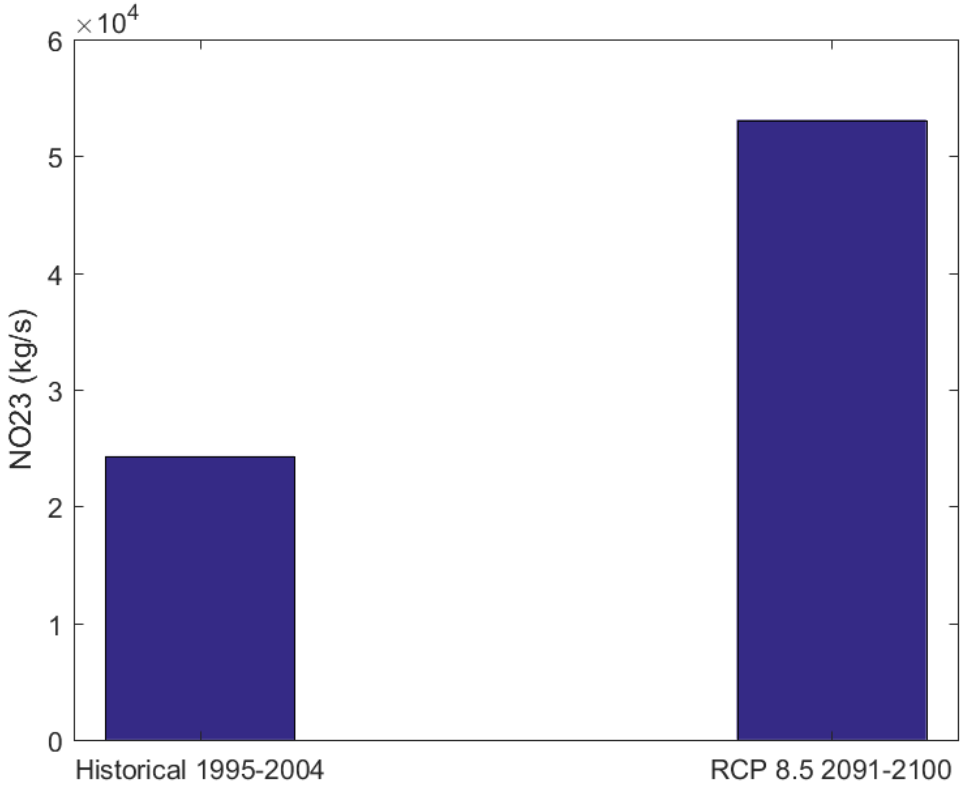

Figure 2.22. Comparison of Total Nitrate-Nitrite Load from WWTPs

2.5 Sea Level Rise

The global sea level rise trend is predicted to continue beyond the end of 21st century. There are uncertainties due to the rate and magnitude of ice sheet loss. Also, global sea level rise has different levels of impacts over different coastlines around the world. For example, due to upward movement of Pacific Northwest land, the projection in this region is less than global average. To prepare the future Salish Sea boundary conditions, taking into account relative sea level rise, we used the Sea Level Change Curve Calculator (Version 2015.46) developed by the USACE (Huber and White 2015). The Sea Level Change Curve Calculator offers multiple scenarios, as shown in Figure 2.23 for Neah Bay, Washington, at the entrance to the Salish Sea via Strait of Juan de Fuca. These scenarios were designed to describe conditions for decision-making and planning instead of predicting the future. For this study, with the goal of developing a worst-case impact estimate, the highest sea level change estimate was chosen from the National Oceanic and Atmospheric Administration (NOAA) high-rate scenario, which shows 1.5 meters relative sea level rise at Neah Bay. This value was applied at the 87 SSM boundary nodes for the future scenarios.

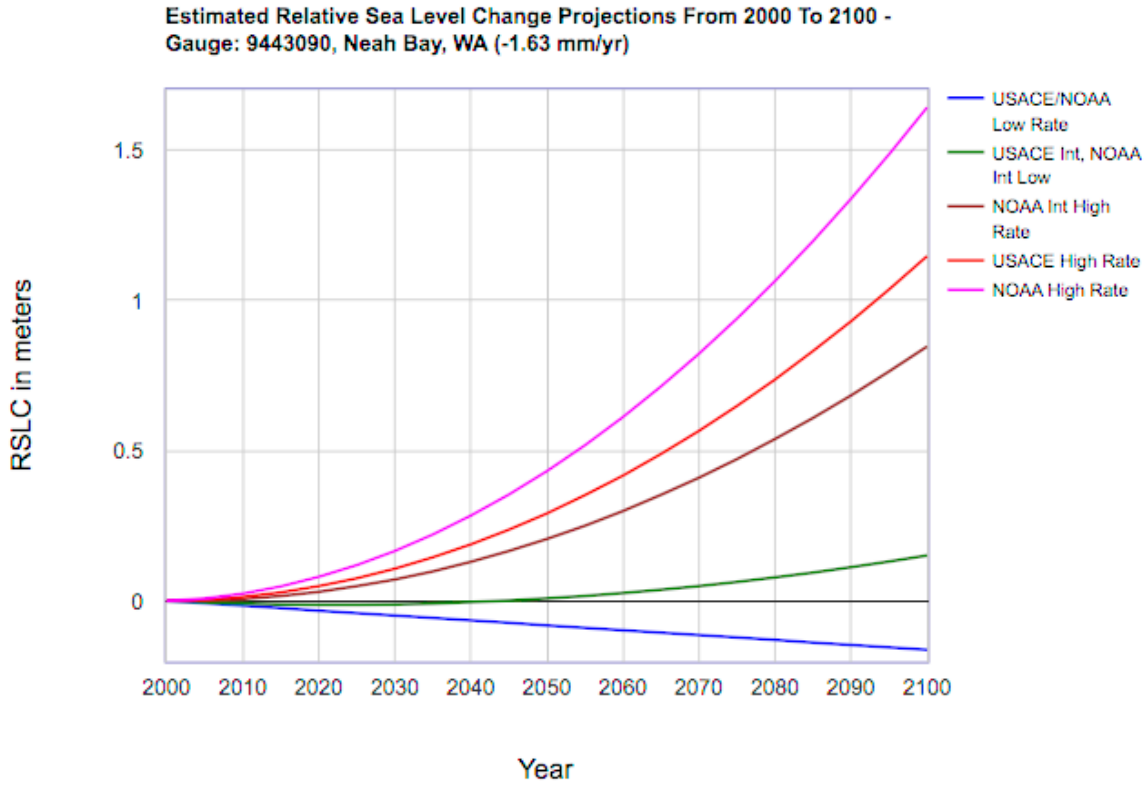

Figure 2.23. Sea Level Rise Scenario Options for Neah Bay

2.6 Summary of Future Climate Inputs

Inputs to the SSM corresponding to the future climate scenario RCP8.5 based on CESM simulations are summarized in Figure 2.24 and Figure 2.25. In general, as a result of global warming, the temperatures over the continental shelf, air and sea surface, and river discharges are all warmer by ≈2–4ºC. The sea level at the continental shelf is estimated to rise by as much as 1.5 m. Although future

wastewater flow magnitudes are higher, the freshwater inflow from gaged rivers and nonpoint source runoff is predicted to be lower by ≈4.4%. Ocean chemistry is predicted to change as well. In addition to thermal stress as described earlier, the Salish Sea is also expected to experience a higher concentration of nutrient loads from ocean boundary, river mouths and WWTPs. The incoming estuarine exchange flow from the Pacific Ocean is predicted to be lower in DO by 1.7 mg/L for the RCP8.5 scenario. The effects of these changes to oceanic, meteorological, and hydrological loads to the Salish Sea as a result of projected climate change and sea level rise is assessed in the sections following the SSM calibration.

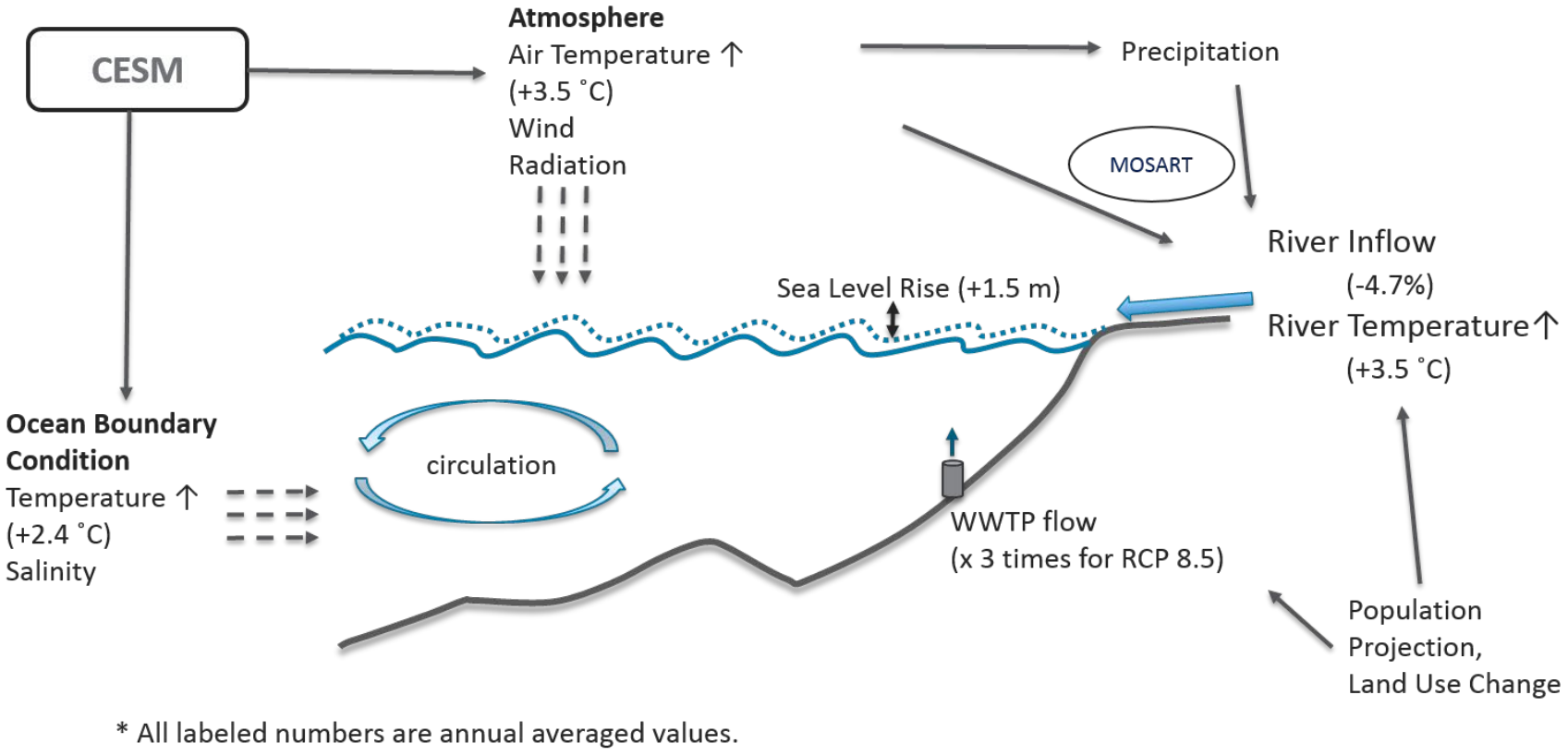

Figure 2.24. Summary of Projected Changes to SSM Inputs for Temperature, Salinities, and Flows for Future Year 2095, RCP 8.5 Scenario

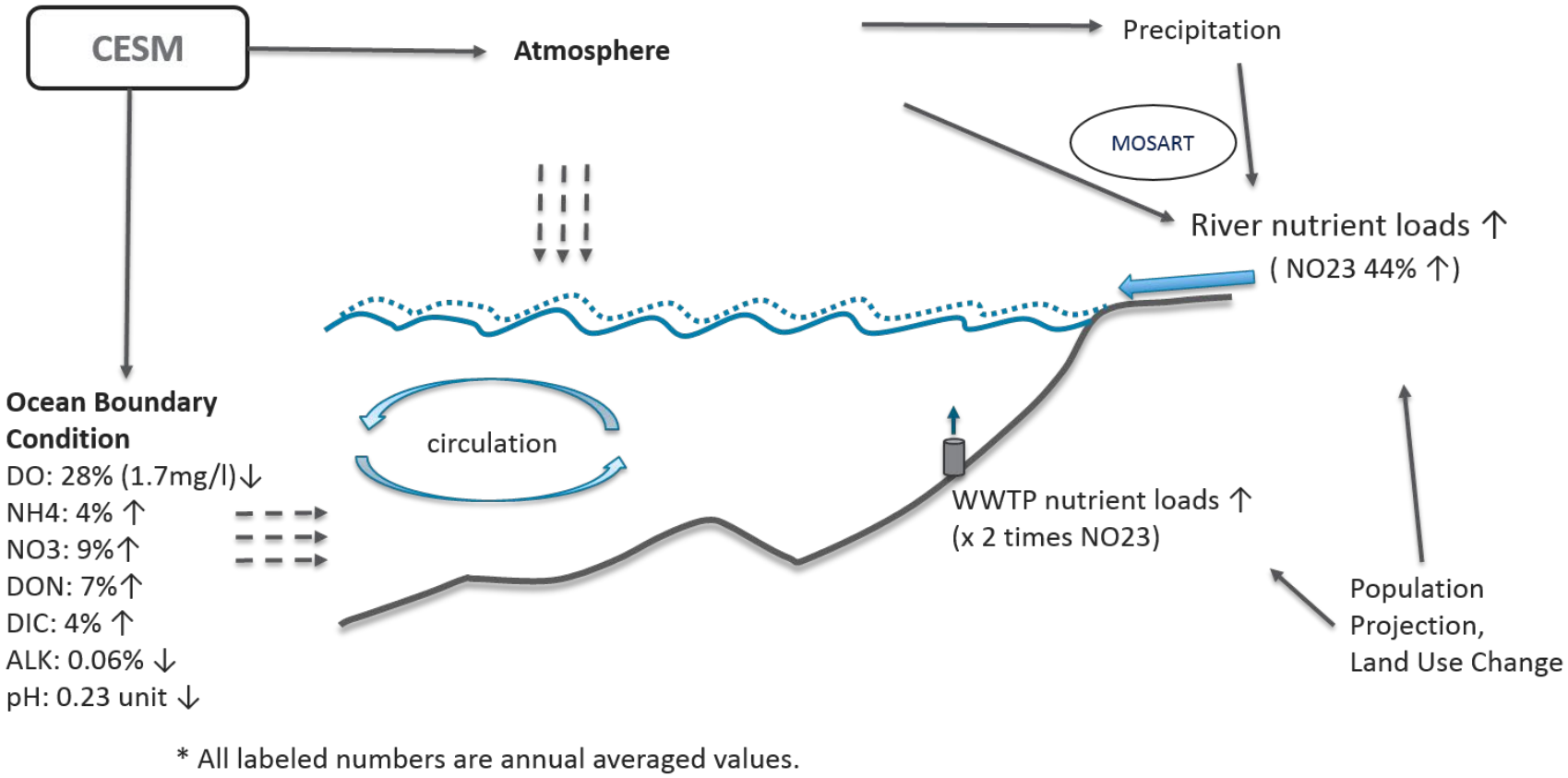

Figure 2.25. Summary of Projected Changes to SSM Inputs for Water Quality Variables for Future Year 2095, RCP 8.5 Scenario

3.0 Baseline Calibration for Year 2014

In this section, we describe improvements to the SSM that were incorporated as part of this project and the calibration of the updated model using data from Y2014. The base model for this project consisted of the Khangaonkar (2012) version with the addition of sediment diagenesis and carbonate chemistry (pH) state variables (Pelletier et al. (2017a and 2017b) and Bianucci et al. (2017)). This project added two improvements: expansion of the model domain and improvements to the heat-flux computation in the intertidal shallow environment.

3.1 Salish Sea Model Improvements

3.1.1 Expansion of Model Grid to Continental Shelf

The original SSM grid terminated at the entrances to the Salish Sea at the north end of the Georgia Strait near Campbell River, British Columbia, and the west end of the Strait of Juan De Fuca at Neah Bay, Washington. These ocean boundaries were moved farther out to the open ocean to minimize the impact on the estuarine plume and mixing zones near the entrances. That expanded SSM domain encompassed Vancouver Island and extended approximately 168 km west of the continental shelf boundary. Willapa River, Chehalis River, and Columbia River discharges to the shelf were included. The results confirmed the magnitude of generated exchange through the Strait of Juan De Fuca ($\approx 130 m^3/s$ based on 2006 data) and its role as the primary Salish Sea estuarine exchange pathway, but also showed that Johnstone Strait at the north end of Georgia Strait could be significant as well (Khangaonkar et al. 2017).

Subsequently, as part of this project, the exact configuration and placement of the ocean boundary were revisited. For various anticipated applications of the SSM, the ocean boundary forcing would need to be specified based on monitoring data, or global scale model predictions, interpolated to the local boundary. For this project, for simulation of historical and future climate response, the ocean boundary would need input from the CESM. Following numerous tests, it was determined that the model performance was at its best when grid configuration terminated at the edge of the continental shelf (200–300 m depths) and did not cross over (> 2 km depths). This helped limit the large pressure gradient error and resulting mixing that would otherwise occur across the shelf break. Figure 3.1 shows the expanded domain model grid that was used in the final calibration.

3.1.2 Intertidal Zone Temperature Simulation Capability

The original FVCOM (v2.7) model code does not have the capability of simulating temperature in the intertidal zone. The model simulates wetting and drying to ensure model stability but requires temperature to be turned off to function without unrecoverable errors. In FVCOM, dry cells are isolated from hydrodynamic calculation when the water falls below a prescribed depth (e.g., 0.05 m). Although the dry cells remain inactive from an advection perspective, they remain active for the heat flux and diffusion computations resulting in extremely high or low temperatures from the small amount of stagnant water in dry cells. To allow for a successful temperature simulation in the intertidal zone for this project, temperature prediction on dry cells was first bounded within prescribed high and low cutoff limits to prevent the code from crashing.

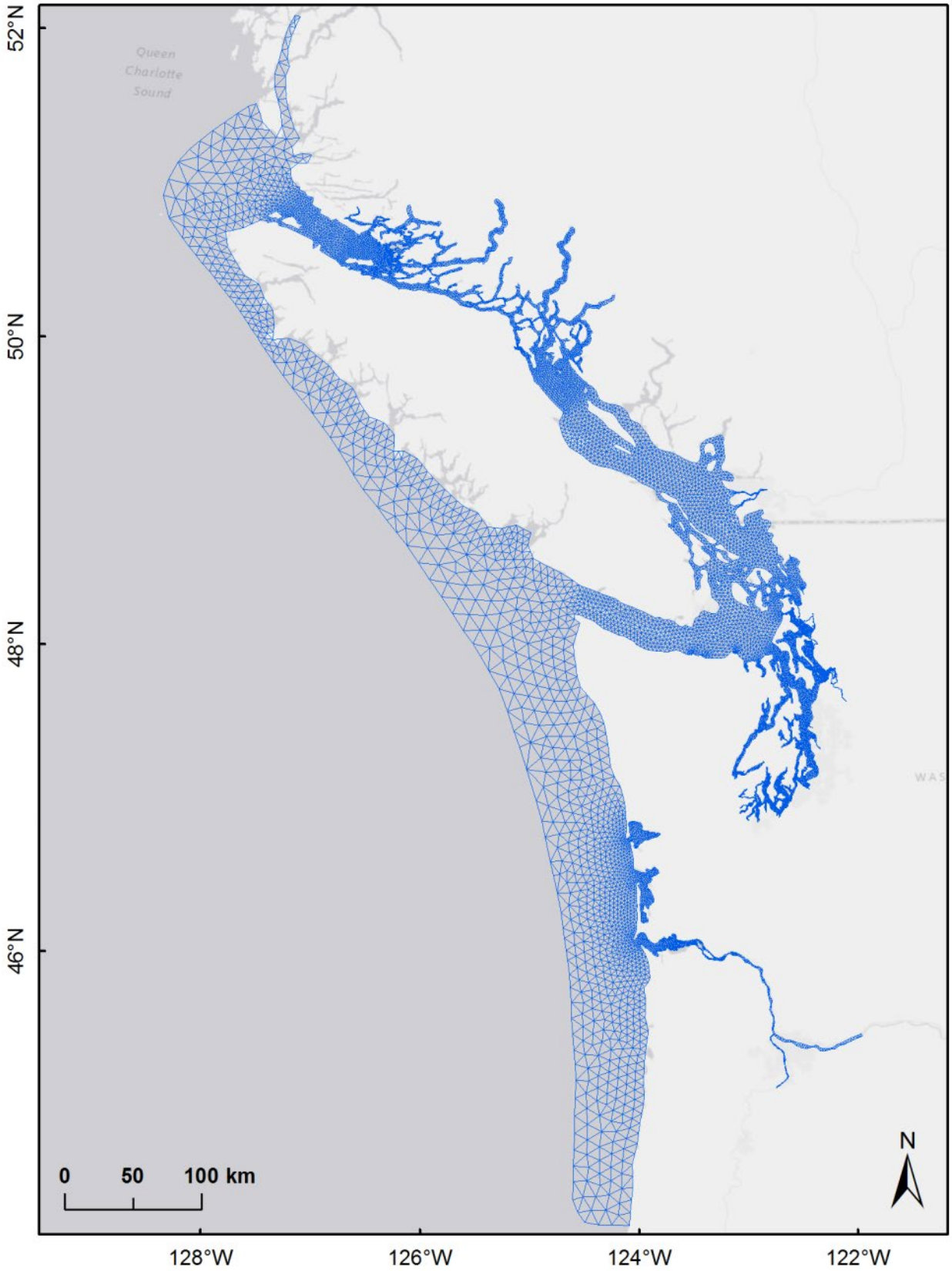

Figure 3.1. Computational Grid Constructed Using Triangular Finite Volume Elements

The second modification was related to the distribution of shortwave solar radiation through the water depth in the intertidal zone. FVCOM uses net heat flux as the input parameter. Typically, it is received as a direct output from a meteorological model (e.g., WRF model). FVCOM first separates shortwave solar radiation from net heat flux and reintroduces it to the water column layers using an attenuation function. The remainder of heat flux is delivered to the water column through the water surface layer. The exponential functions that attenuate light through the water column were designed for waters with bed elevations lower than mean sea level. The computations failed to account for conditions when the domain extends up into the estuarine intertidal zone above the mean sea level resulting in lower heat flux and lower than observed temperatures. Following numerous tests, the code was modified such that short wave solar radiation is now allowed to enter the water column fully, uniformly distributed for user selected prescribed shallow depths defined by the user (e.g., 3 m). The code transitions smoothly from the shallow region to original heat flux calculations beyond a prescribed cutoff depth (e.g., 10 m).

3.2 Hydrodynamic Model Setup (2014)

The hydrodynamic component of the SSM was developed using the FVCOM model framework (Chen et al. 2003) and has been discussed in detail previously (Khangaonkar et al. 2017; Khangaonkar 2012, Khangaonkar et al. 2011a). The model solves Reynolds-averaged Navier Stokes equations for turbulent flows with the Boussinesq approximation in an integral form by computing fluxes between non-overlapping horizontal triangular control volumes. The model simulates water-surface elevation, velocity, temperature, salinity, sediment, and water quality constituents forced by river inflows, tides, and meteorological drivers such as wind and solar radiation.

Available bathymetry from the Cascadia grid employed in tsunami propagation research by the DFO was used to construct the model grid through the Discovery Islands and Johnstone Strait for this assessment. The shelf model grid was developed using bathymetry of the Advanced Circulation model of Eastern North Pacific database (Spargo et al. 2004). The resulting model grid shown in Figure 3.1 has 16,012 nodes and 25,019 triangular elements with a vertical configuration of 10 sigma-stretched layers using a power-law function with an exponent P-Sigma of 1.5 with more layer density near the surface. The selection of 10 sigma layers after numerous sensitivity tests was deliberate, taking into consideration the grid resolution, bathymetry, circulation characteristics of the Salish Sea, and the limits imposed by the pressure gradient error criterion associated with the sigma coordinate system (Mellor et al. 1994). This required smoothing the bathymetry to minimize hydrostatic inconsistency associated with the use of the sigma coordinate system with steep bathymetric gradients and basin-specific vertical distortion to eliminate volume error due to smoothing. The associated slope-limiting ratio dH/H = 0.2 was required where H is the local depth and dH is the change in water depth between adjacent nodes. The model employs the Smagorinsky scheme for horizontal mixing (Smagorinsky 1963) and the Mellor-Yamada level 2.5 turbulent closure scheme for vertical mixing (Mellor and Yamada 1982) with a low background mixing of 1×10^{-6} m^2/s. The bottom friction was the quadratic law with the drag coefficient determined by the logarithmic bottom layer as a function of bottom roughness that was set at 1 mm uniform over the entire domain.

The model setup and validation presented here is based on Y2014 data and uses similar procedures as those described in Khangaonkar (2012) for specification of river loads and boundary conditions. The model is forced with daily values of freshwater inflow from a total of 19 major gauged rivers, 46 ungauged streams estimated through hydrological analysis, and 100 wastewater flows that were included

as described in section 2.0 based on Mohamedali et al. (2012). Approximately 24% of this inflow is from watersheds that drain into Puget Sound south of Admiralty Inlet, 10% discharge into the U.S. side of the Strait of Juan de Fuca and the Strait of Georgia, and 67% from watersheds that drain into the Strait of Georgia and the Strait of Juan de Fuca in Canadian reaches including Fraser River. Fraser River alone contributes 46% of the total flow to the Salish Sea. Figure 3.2 shows the distribution of freshwater inflows to the various sub-basins within the Salish Sea based on Y2014 data. Flow values are presented in m^3/s and percentages are relative to total estimated freshwater inflow to the Salish Sea of 6.92E+03 m^3/s.

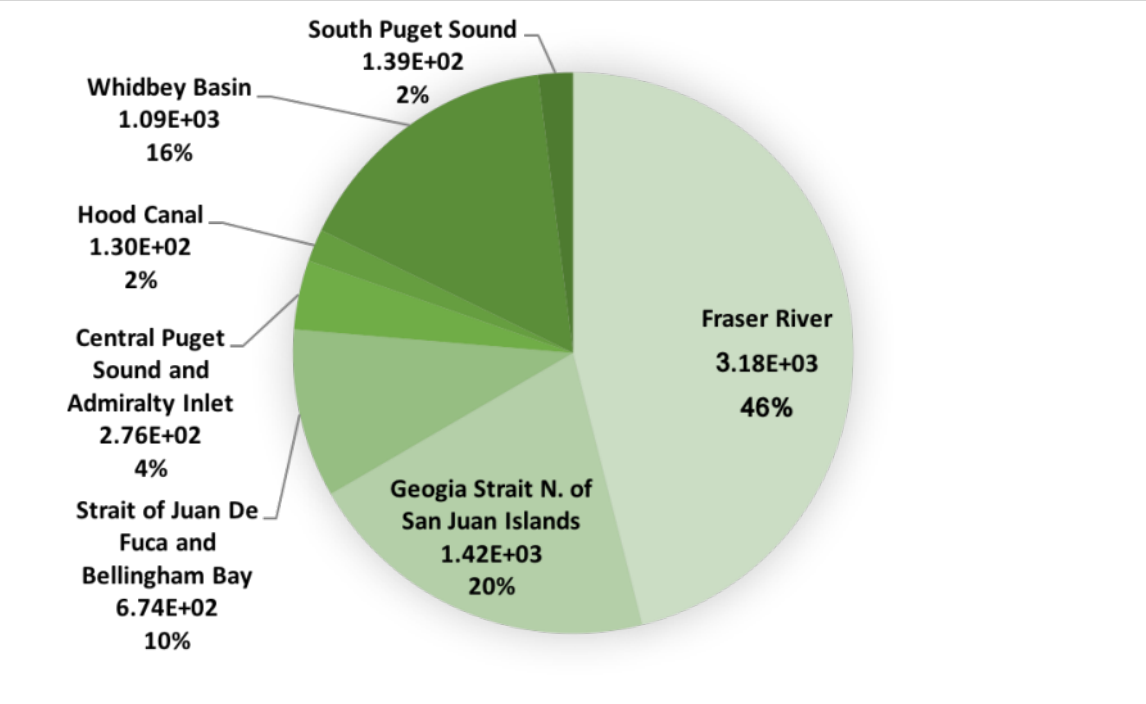

Figure 3.2. Distribution of Freshwater Discharge to Major Salish Sea Basins

The model is forced with wind and heat flux at the water surface. Meteorological inputs were obtained from WRF reanalysis data generated by the University of Washington. Tidal forcing at the open boundary was based on tidal constituents (S2, M2, N2, K2, K1, P1, O1, Q1, M4, and M6) from the Eastern North Pacific model (Spargo et al. 2004). Temperature and salinity profiles were extracted from quarterly monitoring data collected from various locations over the continental shelf by DFO and interpolated to the model ocean boundary in time and space. Figure 3.3 shows the locations of DFO stations that were used in preparation of the open ocean boundary conditions.

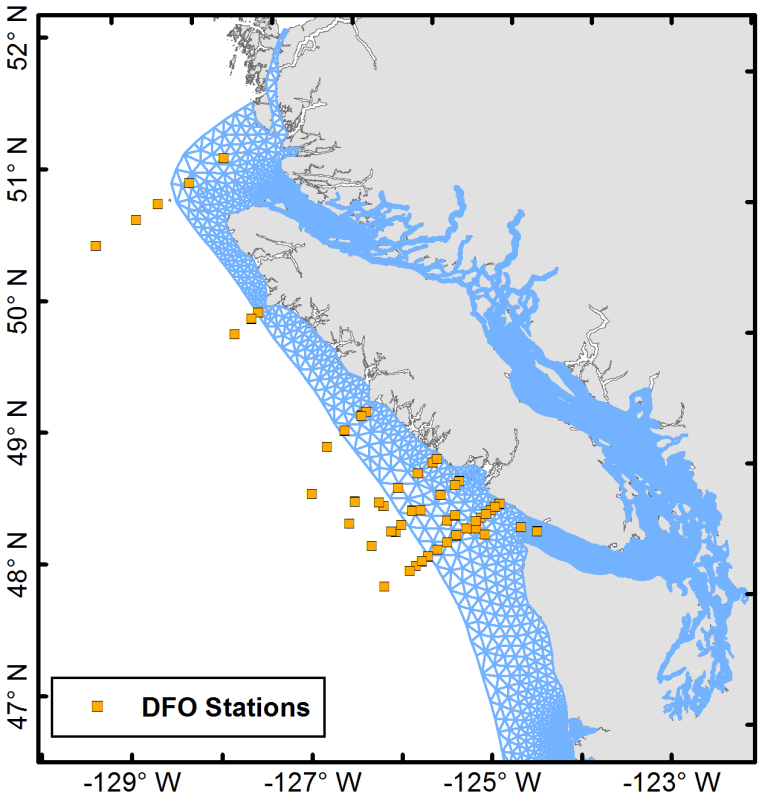

Figure 3.3. DFO Water Quality Monitoring Stations

3.3 Hydrodynamic Model Calibration (2014)

The SSM has been calibrated previously for years X, Y, and Z (cite). This project affords an opportunity for model validation, where performance of the predictive tool is reconfirmed through comparison with data from a separate year (Y2014 in this case). Typically, this requires the model to be applied without changing the model (calibration) parameters such as friction, turbulence parametrization, etc. This was also the case for this model application for Y2014 conditions; however, the changes to the model grid and location of the boundary required iterative runs to fine tune the procedures for conversion of the monitoring data to suitable boundary conditions at the edge of the continental shelf. Similarly, specification of heat load from WRF model output required an adjustment to accommodate the change from a 6-hour interval used in prior calibration efforts to an hourly interval for 2014. Model parameters were otherwise unchanged from Khangaonkar et al. (2012) values.

The error statistics of water surface elevation, salinity, and temperature were computed at nine tide stations (X-Tide stations, Flater 1996) and 24 water quality stations maintained by Ecology shown in Figure 3.4.

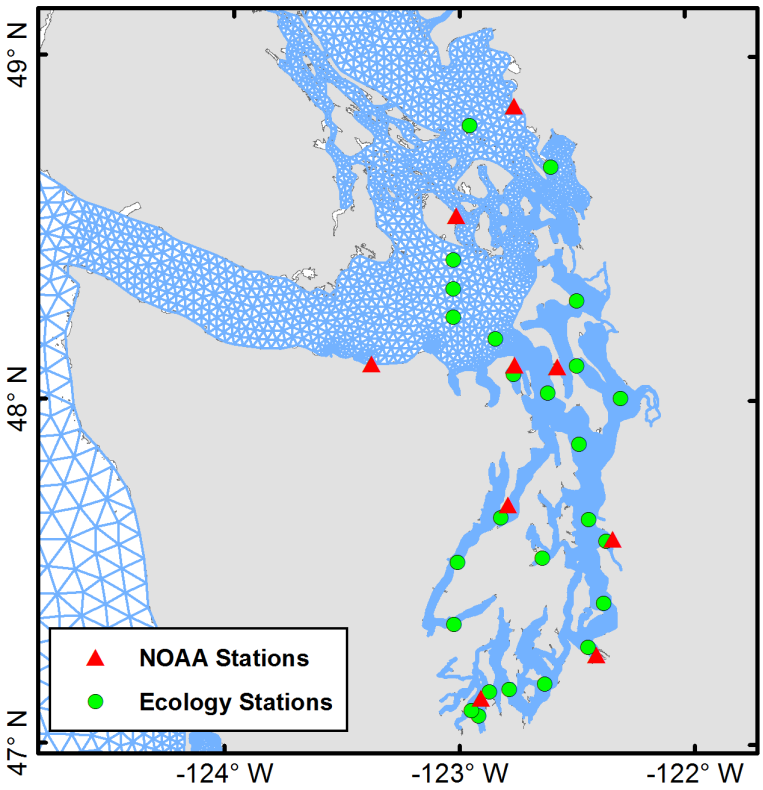

Figure 3.4. Monthly Monitoring Data from Ecology and Tide Predictions Using NOAA Algorithms

Model performance was evaluated using error statistics such as absolute mean error or mean error to assess bias and RMSE. The absolute mean error and RMSE of time series with N elements are defined as

$$AME = \frac{1}{N}\sum|(X_{\mathrm{mdl}} - X_{\mathrm{obs}})| \tag{1}$$

$$RMSE = \sqrt{\frac{\sum(X_{\mathrm{mdl}} - X_{\mathrm{obs}})^2}{N}} \tag{2}$$

To assess model skill, we computed the Willmott Skill Score, or WSS (Willmott, 1982), defined as

$$WSS = 1 - \frac{\sum(X_{\mathrm{mdl}} - X_{\mathrm{obs}})^2}{\sum(|X_{\mathrm{mdl}} - \overline{X_{\mathrm{obs}}}| + |X_{\mathrm{obs}} - \overline{X_{\mathrm{obs}}}|)^2} \tag{3}$$

where X_{mdl} and X_{obs} are the values from the model and observations, and an overbar represents a time average. The WSS is a measure of the level of agreement between the observed and modeled values, with a value of 1 indicating perfect agreement and a value of 0 indicating no agreement.

The Salish Sea portion of the domain (west of Strait of Juan De Fuca and south of Discovery Islands) was unchanged and specification and configuration of the river and wastewater loads were consistent with the prior calibration. Therefore, the scope of this validation effort was limited to demonstrating that tidal elevations and salinity and temperature profiles were reproduced within the Salish Sea at a reasonable level of accuracy. Overall validation results for water surface levels, temperature, and salinity in the form of error statistics at all stations were found to be of good quality with relative water surface elevation errors of less than 10% at most stations within the Puget Sound. Figure 3.5 (a) and (b) show representative sea surface temperature and salinity contour plots from spring, summer, fall, and winter months. Domain-wide temperature RMSE is 0.76ºC (less than 1ºC performance target) with a bias of -0.27 ºC.

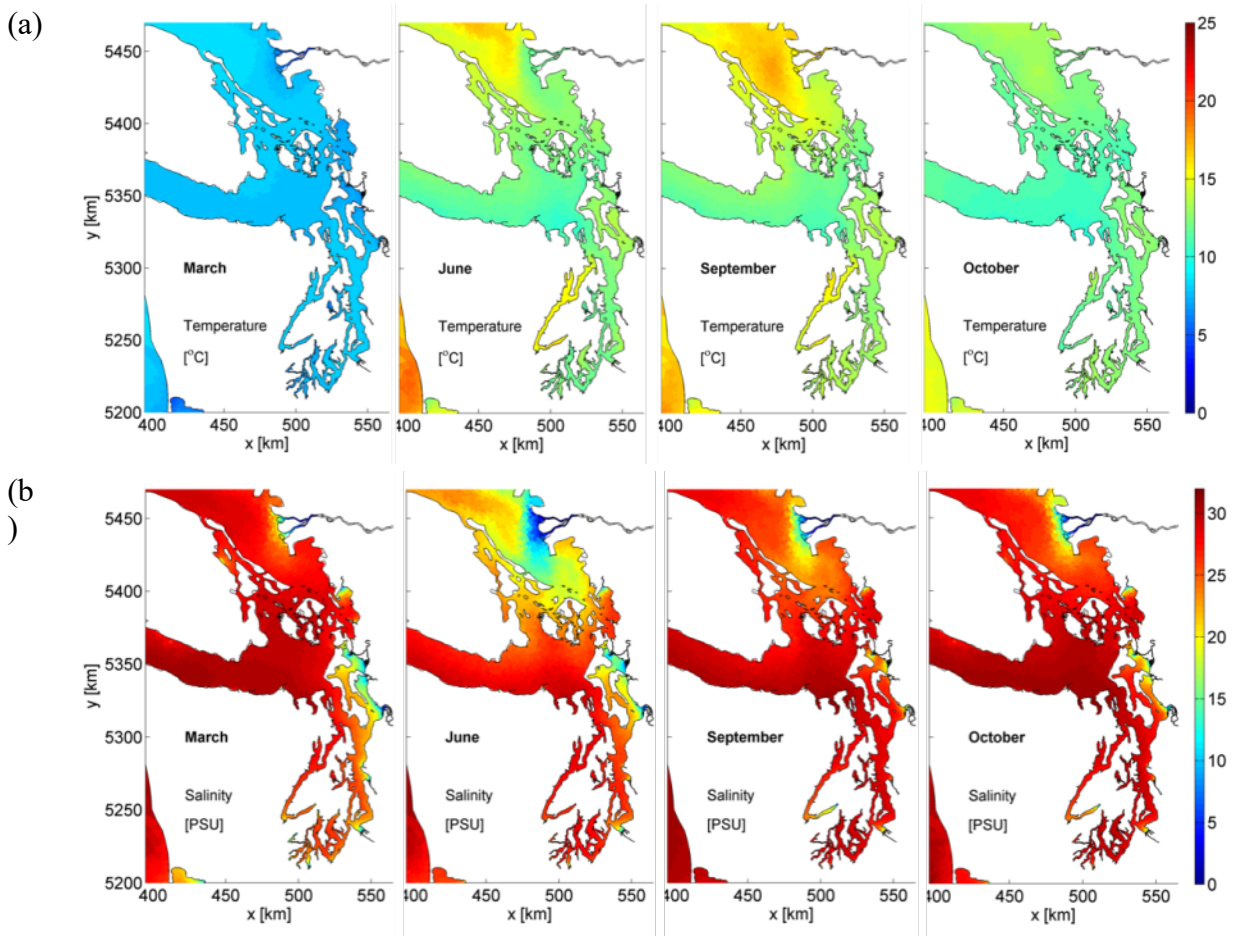

Figure 3.5. (a) Sea Surface Temperature and (b) Salinity Contour Plots

The domain-wide salinity error is 0.97 ppt with a bias of -0.12 ppt. Model skill scores calculated for temperature and salinity were also high with WSS values of 0.95 and 0.84 respectively (see Table 3.1). The 2014 hydrodynamic calibration improved over prior efforts by providing reduction in domain-wide root mean square errors for temperature, salinity, and water surface elevations relative to prior results (Khangaonkar et al. 2012) from Year 2006.

The influence of the Fraser River plume on temperature and salinity is noticeable. Also visible are sea surface temperatures in the Georgia Strait and Hood Canal regions warm up earlier than other sub-basins.

Table 3.1. SSM Overall Error Statistics and Skill Scores for Major Constituents for Y2014

	ME (Bias)			RMSE			WSS		
	Max	Min	Ave	Max	Min	Ave	Max	Min	Ave
T (ºC)	0.49	-1.84	**-0.28**	1.97	0.54	**0.76**	0.98	0.86	**0.96**
S (ppt)	0.21	-1.06	**-0.12**	2.37	0.37	**0.97**	0.9	0.52	**0.84**
DO (mg/L)	1.0	-0.66	**-0.24**	1.59	0.6	**0.99**	0.95	0.23	**0.90**
Nitrate NO3+NO2 (µ mol/L)	6.1	-4.52	**0.96**	10.16	3.67	**6.49**	0.97	0.63	**0.90**
Chlorophyll a (µ mol/L)	3.63	-4.84	**0.83**	19.39	2.49	**4.37**	0.89	0.35	**0.69**
Ammonium NH4 (µ mol/L)	0.69	-1.45	**0.29**	2.24	0.4	**1.16**	0.88	0.33	**0.69**
Phosphate PO4 (µ mol/L)	-0.21	-1.48	**-0.67**	1.48	0.45	**0.93**	0.88	0.28	**0.57**
pH	0.44	0.06	**0.12**	0.49	0.16	**0.21**	0.68	0.37	**0.60**

ME = Mean error (bias)
AME = Absolute mean error
RMSE = Root mean square error
WSS = Willmott Skill Score (1982)
Max = Maximum value of site specific error statistic among 21 Puget Sound Stations
Min = Minimum value of site specific error statistic among 21 Puget Sound Stations
Ave = Global error statistic considering data and model results from all stations

3.4 Biogeochemical Model Setup (2014)

The biogeochemical component of SSM is based on CE-QUAL-ICM, a three-dimensional, time-variable model that was developed by the USACE for simulating water quality (Cerco and Cole 1994). CE-QUAL-ICM was originally developed as the eutrophication model for the Chesapeake Bay and has been applied to several lakes and estuaries (e.g., Bunch et al. 2000; Cerco et al. 2000 and 2004; Cerco 2000; Tillman et al. 2004). For application to the Salish Sea, an "offline" approach of coupling a FVCOM hydrodynamic solution to CE-QUAL-ICM developed by Kim and Khangaonkar (2011b) was used. The water quality calculations in this mode are conducted using a previously computed hydrodynamic solution in FVCOM framework and biogeochemical calculations using CE-QUAL-ICM kinetics over the same finite volume mesh. Khangaonkar et al. (2012) demonstrated that annual biogeochemical cycles of nutrient balance, phytoplankton bloom(s), and DO in the Puget Sound region of the Salish Sea could be reproduced successfully using FVCOM-ICM with significant gains in computational efficiency associated with the use of a larger time step for the offline biogeochemical model. Typical applications of the SSM at this resolution involve hydrodynamic solution stored at 1-hour intervals and interpolated for use at the biogeochemical model time step that is typically a factor 20 times larger than the external mode time step (2 s) of the hydrodynamic model.

For this effort, we included 18 state variables: two species of phytoplankton (diatoms P1 and dinoflagellates P2), labile and refractory DOC and particulate organic carbon, ammonium (NH_4), nitrate

(NO_3+NO_2), labile and refractory dissolved organic nitrogen and particulate organic nitrogen, phosphate (PO_4), DO, DIC, and TA. Figure 3.6 provides a schematic representation of the biogeochemical model consisting of phytoplankton production and excretion, predation on phytoplankton by zooplankton, dissolution of particulate carbon, heterotrophic respiration, denitrification, and settling. Model formulation and CE-QUAL-ICM kinetics are described extensively in Cerco et al. (1994, 2000, and 2004) and are summarized in Appendix B.

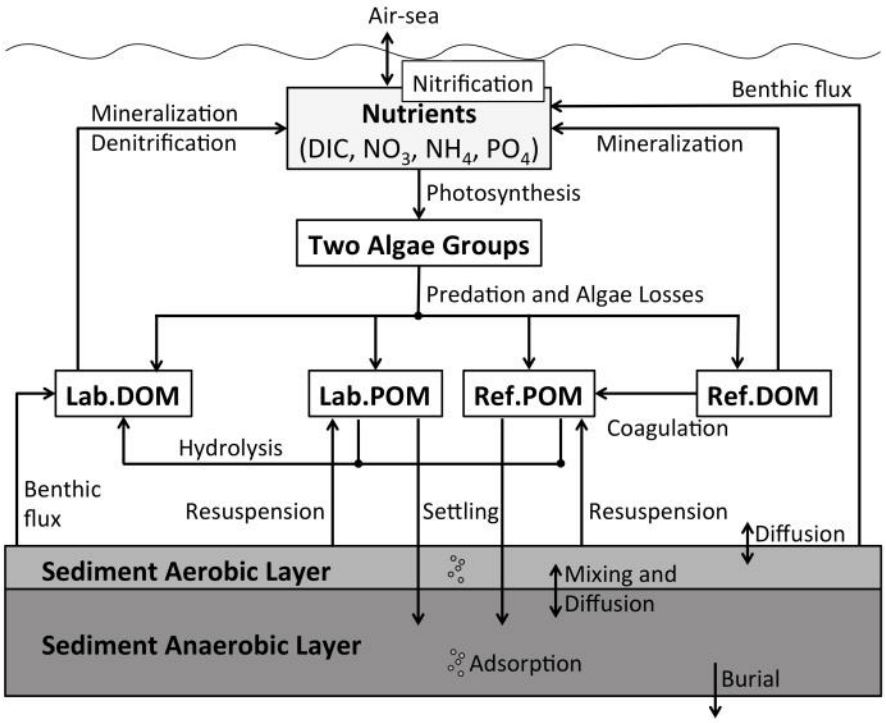

Figure 3.6. FVCOM-ICM Biogeochemical Process Configuration

Prior SSM calibration efforts and studies used constant and uniform values; benthic sediment fluxes were specified for DO, ammonium, nitrate and nitrite, and phosphate based on field measurements. While this approach allowed a reasonable domain-wide calibration, the model could not simulate a satisfactory response to changes in nutrient loads or algae growth and sedimentation which showed strong variations within Salish Sea sub-basins. Reproduction of observed hypoxia and low DO levels (< 2 mg/L) in some sub-basins such as South Puget Sound and Hood Canal could not be achieved simultaneously with relatively healthy near-bed DO levels (4 - 6 mg/L) in most other sub-basins. In a subsequent assessment, sediment fluxes in SSM were linearly scaled in proportion to nitrogen loading from watershed inflows, marine point sources, and atmospheric deposition. This was based on the expectation that higher loads would cause additional phytoplankton growth, higher particulate deposition to the sediments, and higher exchanges of nitrogen and oxygen. This significantly improved model performance underlining the need and importance of a coupled sediment diagenesis module.

Sediment diagenesis is where biogeochemical processes transform the nutrients delivered to the sediments from particles settling from the water column and release a portion of the nutrients back into the water column. The process also consumes oxygen and is referred to as SOD. A portion of the nutrients are buried and permanently lost. Sediment diagenesis flux models range from simple empirical

relationships (Fennel et al. 2006) to complex process simulations with time-varying state variables (Boudreau 1997). Di Toro et al. (1990 and 2001) developed a sediment flux and SOD model that has gained wide adoption in estuarine modeling frameworks such as those of Cerco and Cole (1995), Chapra (1997), and Martin and Wool (2013). Di Toro's approach (2001) calculates SOD and the release of nitrogen and phosphorus from the sediments as functions of the downward flux of carbon, nitrogen, and phosphorus from the water column.

The biogeochemical component of the SSM (FVCOM-ICM) was coupled with the two-layer sediment diagenesis model of Di Toro (2001). Detailed description of the sediment diagenesis model configuration, processes, equations, and subsequent incorporation in to the SSM have been described previously by Pelletier et al. (2017a) and Bianucci et al. (2017 in press). This is a two-layer sediment model with a thin aerobic layer of variable thickness above a thicker (≈10 cm) anaerobic layer. The model integrates four processes: (i) deposition of particulate organic carbon (C) and nitrogen (N) collectively referred to as particulate organic matter from the water column into the sediment; (ii) decomposition of particulate organic matter in the sediment, producing dissolved forms of C and N in the sediment pore water (diagenesis); (iii) reaction of the solutes formed by diagenesis and (a) transport between a thin aerobic layer at the surface of the sediment and a thicker anaerobic layer below the aerobic layer, or (b) released as gases (methane and nitrogen gas); and (iv) return of solute forms of C and N to the overlying water, and transfer of DO from the overlying water into the sediment to supply the oxidation of solutes (dissolved organic C and ammonium) in the aerobic sediment layer. The FVCOM-ICM sediment diagenesis code was tested for accuracy against standalone steady-state and dynamic tests in simplified geometric settings using tools developed by Mississippi State University (Martin 2002; Ecology 2013).

The setup of the biogeochemical component of the SSM, including river loads and ocean boundary conditions, were developed for using most recent available data from Y2014. This includes daily concentrations of nutrient and water quality constituent loads from a total of 19 major gauged rivers, 46 ungauged streams, and 100 wastewater flows estimated using a combination of hydrological and multiple regression analyses (Mohamedali et al. 2012). Ocean boundary values for nutrients, DO, and algal biomass were also from quarterly monitoring data collected from various locations over the continental shelf by DFO (see Figure 3.3) and interpolated to the model ocean boundary in time and space.

3.5 Biogeochemical Model Calibration (2014)

Table 3.2 provides a list of major biogeochemical model parameters used in the validation along with ranges of values found in the literature (Bowie et al. 1985; Cerco and Cole 1994; Bunch et al. 2000; Cerco et al. 2000; Tillman et al. 2004). The domain-wide calibration of the model along with reproduction of hypoxia and low DO levels in sub-basins such as the Lynch Cove region of Hood Canal was completed as part of this effort. While most parameter values are unchanged from those previously presented in Khangaonkar et al. (2012) and Bianucci et al. (2017 in press), key changes during recalibration following activation of the sediment diagenesis kinetics included adjustments of maximum photosynthetic rates of diatoms and dinoflagellates, associated algal settling velocities, reaeration formulation, and the rates of total and net sedimentation rates associated with sediment diagenesis modeling. The algal nutrient ratios have been kept static at the Redfield ratios (106:16:1 for C/N/P). Similarly, static carbon-to-chlorophyll ratios based on measured data were used with a base ratio of 37 for diatoms and 50 for dinoflagellates. Due to a lack of sufficient primary production data in Puget Sound, the maximum photosynthetic rate for diatoms and dinoflagellates was set at a constant spatially uniform

value of 350 g C g-1Chl d-1 at the upper end of the typical literature range (200–350 g C g-1 Chl d-1). The Puget Sound region of the Salish Sea is nutrients-limited and the system was not sensitive to further increase in maximum photosynthetic rates. The effect of zooplankton grazing is included through a first-order predation term with rates of 1 d-1 and 0.5 d-1 for diatoms and dinoflagellates respectively.

Table 3.2. Major Biogeochemical Model Parameters

Symbol	Value	Unit	Literature Range	Definition
***Algae parameters (*inputs/algae.dat)**				
PM1	350	g C g^{-1} Chl d^{-1}	200 – 350	Maximum photosynthetic rate of diatom
PM2	350	g C g^{-1} Chl d^{-1}	200 – 350	Maximum photosynthetic rate of dinoflagellates
BM1	0.1	d^{-1}	0.01 – 0.1	Basal metabolic rate of diatom
BM2	0.1	d^{-1}	0.01 – 0.1	Basal metabolic rate of dinoflagellates
BPR1	1.0	d^{-1}	0.05 – 1.0	Base predation rate of diatom
BPR2	0.5	d^{-1}	0.05 – 1.0	Base predation rate of dinoflagellates
ANC1	0.175	g N g-1 C		Nitrogen-to-carbon ratio for diatoms
CCHL1	37	g C g^{-1} Chl	30 – 143	Carbon-to-chlorophyll ratio for diatoms
KHN1	0.06	g N m^{-3}	0.003 – 0.923	Half-saturation conc. for nitrogen uptake by diatoms
KHP1	0.02	g P m^{-3}	0.001 – 0.163	Half-saturation conc. for phosphorus uptake by diatoms
ALPHMN1	12.	g C g^{-1} Chl (E m^{-2})$^{-1}$		Initial slope of PvsI curve for algal group diatom
TMP1	12	ºC	up to 35	Optimal temperature for growth of diatom
ANC2	0.175	g N g-1 C		Nitrogen-to-carbon ratio for dinoflagellates
CCHL2	50	g C g^{-1} Chl	30 – 143	Carbon-to-chlorophyll ratio for dinoflagellates
KHN2	0.06	g N m^{-3}	0.005 – 0.589	Half-saturation conc. for nitrogen uptake by dinoflagellates
KHP2	0.02	g P m^{-3}	0.0003 – 0.195	Half-saturation conc. for phosphorus uptake by dinoflagellates
ALPHMN2	12	g C g^{-1} Chl (E m^{-2})$^{-1}$		Initial slope of PvsI curve for algal group 2 dinoflagellate
TMP2	18	ºC	up to 35	Optimal temperature for growth of dinoflagellates
Mineralization constants				
KHONT	3.0	g O_2 m^{-3}	-	Half-saturation conc. of DO required for nitrification
KHNNT	0.5	g N m^{-3}	-	Half-saturation conc. of NH4 required for nitrification
KHODOC	0.5	g O_2 m^{-3}	-	Half-saturation conc. of DO required for oxic respiration
KHNDN	0.1	g N m^{-3}	-	Half-saturation conc. of nitrate required for denitrification
AOCR	2.37	g O_2 g^{-1}C	-	Oxygen-to-carbon mass ratio in production and respiration

Symbol	Value	Unit	Literature Range	Definition
AONT	4.33	g O_2 g^{-1} N	-	Oxygen consumed per mass ammonium nitrified
KTNT1	0.0045	$°C^{-2}$	-	Effect of sub-optimal temperature on nitrification
KTNT2	0.0045	$°C^{-2}$	-	Effect of super-optimal temperature on nitrification
TMNT	30	ºC	25 – 35	Optimal temperature for nitrification
AANOX	0.5		0-1	Ratio of denitrification to oxic carbon respiration rate
ANDC	0.933	g N g^{-1} C	0.933	Mass nitrate-nitrogen reduced per mass DOC
Kr		fn[a.(b.W)^C}	a=0.251, b=1, c=2	Reaeration coefficient as a function of wind speed
SS	0.25	m d^{-1}		Fixed solids settling rate
WSLAB	5	m d^{-1}		Labile particulate organic solids settling rate
WSREF	5			Refractory particulate organic matter settling rate
WS1	0.4	m d^{-1}	0 – 30.	Settling velocity of diatom
WS2	0.2	m d^{-1}	0 – 30.	Settling velocity of dinoflagellates
NT_m	0.4	g N m^{-3} d^{-1}	0.01 – 0.7	Maximum nitrification rate

To initiate quicker response to light availability and initiate spring bloom earlier than in prior versions, the initial slope of production versus irradiance relationship was increased to 12. Settling rates specified were 0.4 and 0.2 m day−1, and optimum temperatures for algae growth were 12ºC and 18ºC for diatoms and dinoflagellates respectively and are unchanged from prior calibration efforts. However, reaeration coefficient Kr, which is computed as a function of wind speed [$Kr = a\ (b\ W)^c$], was updated to values a=0.251, b=1, and c=2.0 to match Wanninkhof (2014) updated gas exchange wind speed relationship parameterization.

Parameter values for sediment diagenesis processes were set to default values recommended by DiToro (2001) and Testa et al. (2013). The most significant iterative adjustment was related to net settling rates of suspended organic sediments in the bottom layer of the water column. A net settling rate of 5 m d-1 was used for organic suspended sediments WSSLAB and WSSREF (see Table 3.2) respectively, which ensured that particulate organic matter reached the bottom layer of the water column within a short period of less than two weeks on average. Capture of organic matter by the sediment layer is controlled by net sedimentation rate that is the difference between the settling and resuspension rates. The net sedimentation rates for labile and refractory organic sediments were adjusted as part of calibration to 1 m d-1 and the net settling rates for diatoms and dinoflagellates were set to 0.2 m d-1 and 0.075 m d-1. The settling velocities used in the SSM are generally within the range of the literature (e.g., EPA 1985).

Another previous improvement to the model incorporated into this validation was the addition of carbonate system to the water column through inclusion of TA and DIC (Bianucci et al. 2017 in press; Pelletier et al. 2017b). The model simulates TA increases due to primary production, remineralization of labile and refractory DON, water column denitrification, and sediment fluxes of NH4. Regenerated primary production, water column nitrification, and sediment fluxes of NO3 reduce TA. Similarly, the model simulates the increase in DIC through remineralization of labile and refractory DOC, water column denitrification, phytoplankton losses by predation, basal metabolism and photorespiration, and sediment

fluxes. Primary production and water column nitrification processes consume DIC. Air-sea exchange of CO2 is included, coupled to reaeration coefficient that can either increase or decrease DIC depending on whether the surface partial pressure of CO2 (pCO2) is lower or higher than the atmospheric pCO2. Seawater pCO2 and carbonate system constants such as the solubility of CO2 (K0) were computed using equations and approach in the CO2SYS software by Lewis and Wallace (1998). The dissociation constants for carbonic acid (K1, K2) and bisulfate ion (KSO4) were based on formulations of formulations by Lueker et al. (2000) and Dickson (1990) and borate-to-salinity ratio of Uppstrom (1974) was used consistent with recent observational studies (e.g., Takahashi et al. 2014; Fassbender et al. 2016). River gage and wastewater discharge monitoring data from 2014 were used to derive regressions for pH, DIC, and TA as a function of river flow and used to specify loading. The ocean boundary conditions at the continental shelf for TA and DIC were calculated as regressions of salinity (S), and temperature (T) and DO based on Ianson et al. personal communication): DIC = –17.51 * T – 0.95 * DO + 2440.62; TA = 470.13 + 52.85 * S if S < 33.85 and TA = –4932.6 + 212.44 * S if 33.85 ≤ S ≤ 34.65 (where DIC, TA, and DO are given in μmol/kg, T in ºC and S in psu).

The importance of exchange flow from the Pacific Ocean and its dominating influence on basin-wide variability in stratification and temperature response has been discussed previously (Khangaonkar et al. 2011 and 2017). This tidally averaged inflow ($143x10^3 m^3/s$ in 2014) enters the Salish Sea through the Strait of Juan De Fuca through layers below the depth of zero motion and carries with it dissolved inorganic nutrients including nitrate (NO3+NO2), phosphate (PO4), and ammonia. Incoming bottom layer phosphate concentrations are typically low (1.9 -2.3 μ mol/L). However incoming bottom layer nitrate concentrations are relatively high (29.2 – 33.4 μ mol/L) and are the prominent food source consumed by algae in this nitrogen-limited system. The incoming DO levels are also low, varying between 2.7–4.5 mg/L. This incoming flux of nutrients and DO is distributed with tidally averaged flows to Georgia Strait ($59x10^3 m^3/s$ via Haro Strait passage east of San Juan Islands) and to Puget Sound ($16x10^3 m^3/s$ via Admiralty Inlet), and a large fraction is returned back out to the Pacific Ocean as part of surface layer outflow. Similar inflows but of a smaller magnitude system ($9x10^3 m^3/s$) also occur through the north boundary of the Georgia Strait through passages around Discovery Islands (Discovery Passage and pathways around Cortes Island).

Figure 3.7 presents an example comparison of surface and bottom layer predictions of chlorophyll *a*, DO, and nitrate concentrations with monthly monitoring data from an inner Salish Sea / Puget Sound Station of East Basin (EAP003, near Vashon Island). The upper layer occupies 3% of the water column, represents Salish Sea outflow plume of brackish water, and includes influence of nutrient depletion due to primary production. The bottom layer, which occupies the lower 15% of the water column in SSM, is representative of incoming nutrients and DO. Chlorophyll *a* plot shows a combined effect of spring bloom of diatoms followed by a die-off/predation-induced reduction and then a late summer bloom attributed to dinoflagellate growth. There is very little algal activity in the winter months of December, January, and February due to low temperatures and limited light availability. The surface layer nitrate concentrations show a decline and recovery corresponding to algal growth and die-off. As shown in Figure 3.6, surface nitrate concentrations are depleted to near-zero levels during most of the spring-summer period. In many stations within the Salish Sea bottom layer, concentrations are also indirectly affected by surface biological activity. The incoming bottom layer concentrations drop as a result of strong vertical mixing over the Admiralty Inlet sill and are further reduced through reflux flow mixing in the central Puget Sound region. Nearly 60-66% of surface outflow headed out to the Pacific Ocean from

Puget Sound is refluxed back to mix with bottom layer inflow (Ebbesmeyer and Barnes 1980; Khangaonkar et al. 2017).

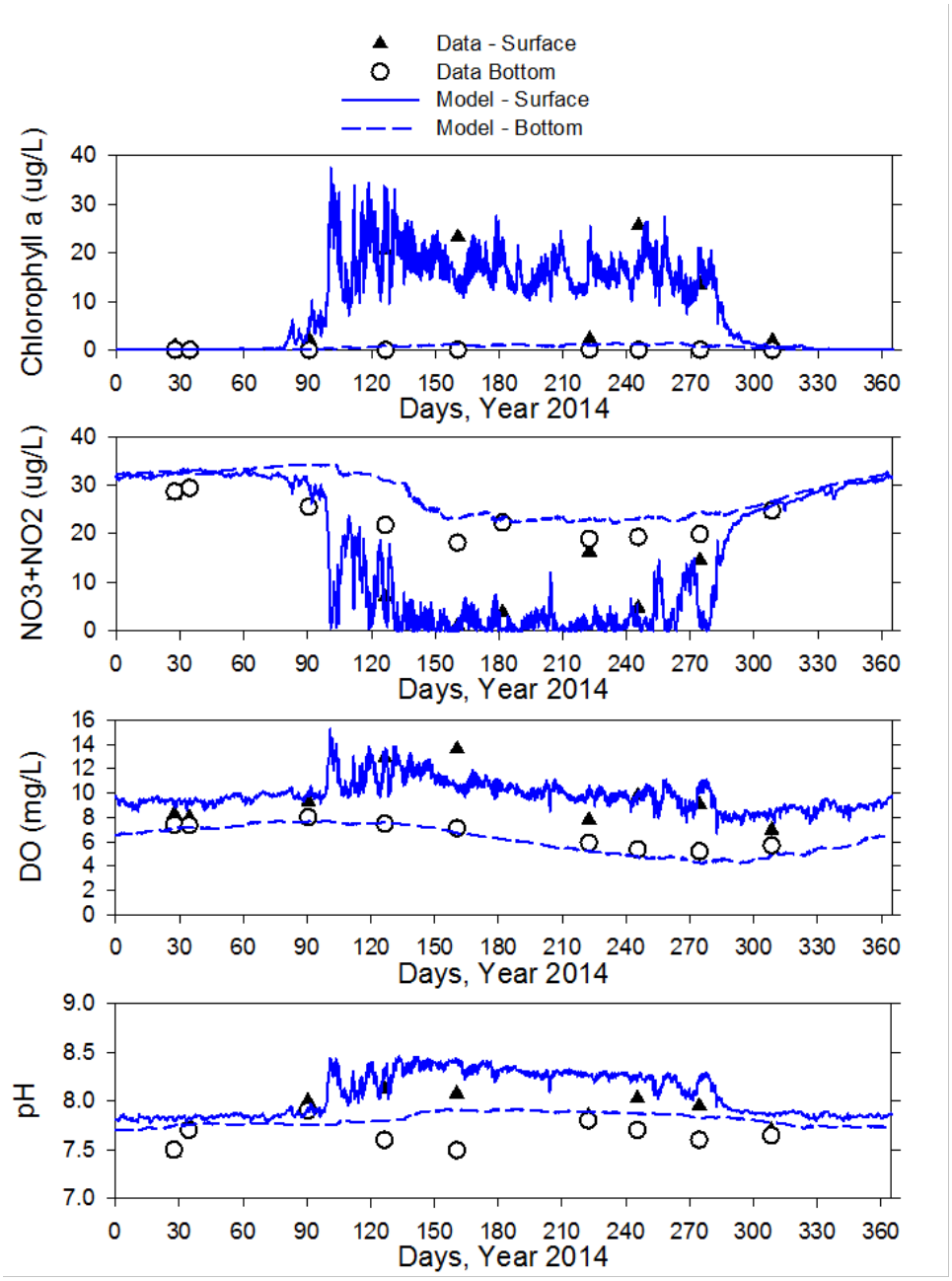

Figure 3.7. Time Series of Model Results and Observed Data from Surface and Bottom Layers

DO levels in winter and spring increase as a result of reaeration and algal growth. The surface DO levels show two peaks corresponding to spring and late summer algal blooms. However, water column below the euphotic zone and bottom layers experiences a steady drawdown of DO resulting from a combination of respiration, decay, mineralization, and SOD due to settling of detritus and organic matter of algal origin. Lowest DO levels are observed during September, October, and November months just prior to culmination of algal biological activity. Effect of biological activity on pH is seen in the form of

≈0.5-unit separation between surface and bottom layers. During peak growth period, consumption of DIC results in a sharp increase in pH relative to incoming bottom layer waters. At this East Basin station, pH results show a bias of 0.11 units and further tuning and improvement in pH is predicted with data from new monitoring programs focused on ocean acidification in the future.

Figure 3.8 shows progression of DO concentrations from Neah Bay station at the entrance to Salish Sea via Strait of Juan de Fuca. The incoming water bottom layer water that enters Salish Sea through the Strait of Juan de Fuca is low in DO (≈2–4 mg/L). This water passes through the Strait of Juan de Fuca, which is a region of high mixing with features similar to a coastal plain estuary. The bottom layer concentrations increase due to mixing with oxygen-rich surface layer as the bottom layer water travels towards Georgia Strait and Puget Sound.

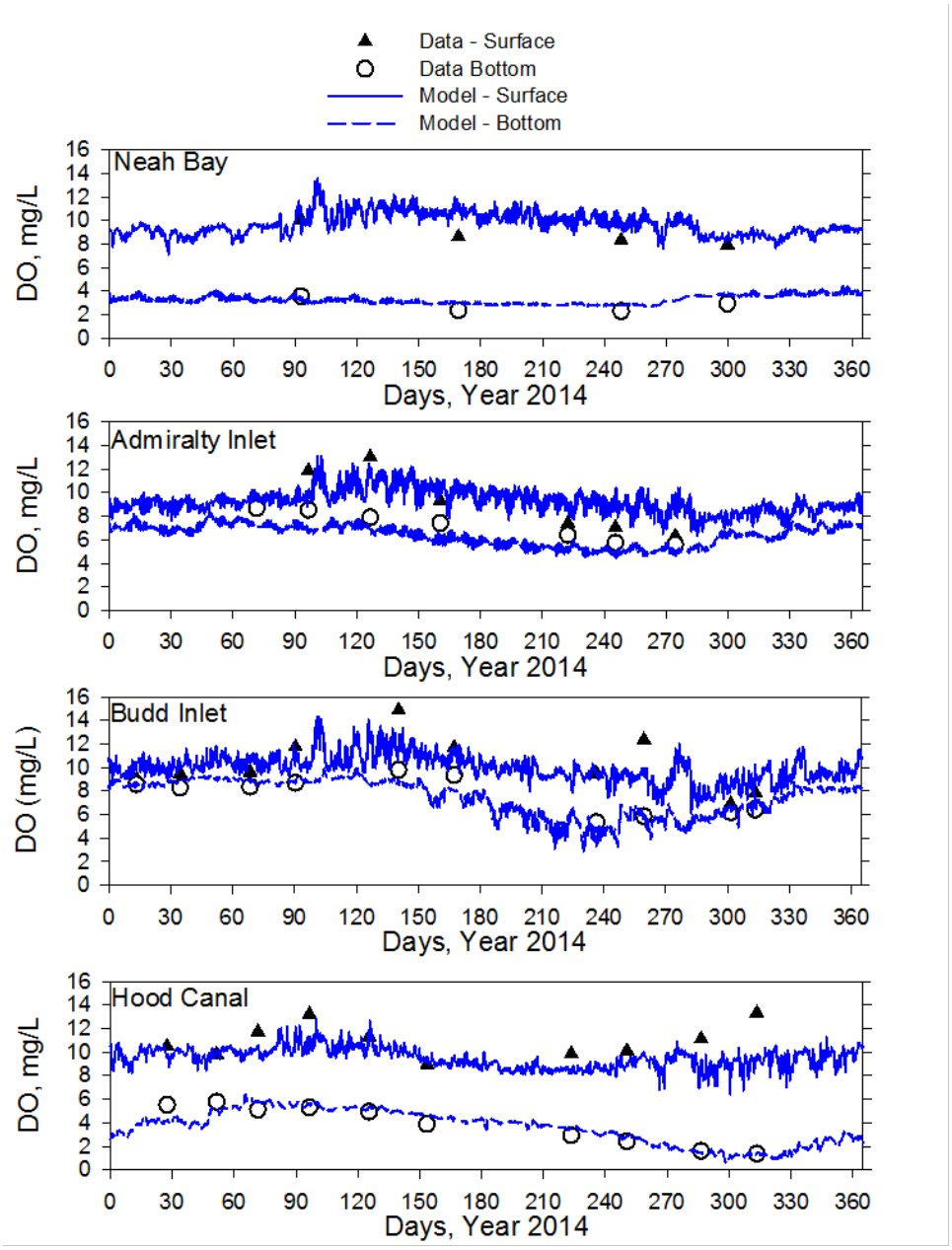

Figure 3.8. Time Series Data Showing Progressive Change in Bottom and Surface Layer DO

In the early part of the year, the bottom layer concentrations increase further to over 8 mg/L with mixing over Admiralty Inlet sill. The DO levels then begin to drop during the summer especially in the lower layers. This is most evident in basins with higher residence times such as Budd Inlet/South Sound and Hood Canal. The effect of DO consumption by water column respiration/mineralization and sediment organic matter decay is most evident in the Lynch Cove region of Hood Canal where DO concentrations drop to hypoxic levels (< 2 mg/L).

Table 3.1 includes model error statistics mean error, RMSE, and WSS values for characterization of model skill for all parameters. Model skill is the highest for temperature, salinity, nitrate, and DO. Detailed calibration to ammonia values was not attempted as concentrations were typically very low

relative to dominant nitrate concentrations. Similarly, a detailed calibration for phosphate was not attempted as the model currently does not include inorganic suspended solids and partitioning of phosphate between dissolved and particulate phase was not considered. Further improvement of pH kinetics is feasible but not attempted beyond the results presented mostly due to lack of data for alkalinity and DIC, monitoring that is currently in progress.

The ability of the model to accurately reproduce spatial variability within the Salish Sea, including hypoxia and low DO levels in selected sub-basins such as Hood Canal, Penn Cove, and inlets within South Puget Sound represents significant advancement over prior versions. The sediment diagenesis module allows for coupling of sediment water interactions and enables direct accounting of the impacts of nutrient pollution on water/sediment quality from biological growth and subsequent sedimentation and decay of organic matter. The carbonate chemistry module allows model application for ocean acidification assessments. Model validation and sensitivity tests presented in this paper are based on Year 2014 data sets and were mostly comparable to data from other years (2006, 2007, 2008) previously examined and are considered representative of the system. Significant improvement in DO calibration was achieved relative to 2012 effort with a Salish Sea-wide RMSE of < 1 mg/L.

4.0 Simulation of Historical and Future Conditions

This section describes the SSM simulation using the calibrated model for two scenarios—historical (Y2000) and future RCP8.5 scenario (Y2095)—and evaluates the Salish Sea response to the RCP8.5 scenario. Due to the complex geomorphology, estuarine circulation, and nearshore biogeochemical processes, the Salish Sea response to climate change was expected to be different from that of the outer ocean. We analyzed (1) Salish Sea-wide changes in hydrodynamic processes affecting temperature, salinity, and overall circulation and (2) Salish Sea-wide changes in biogeochemical processes affecting water quality and algal lifecycles. The SSM model for historical and future scenarios was forced with boundary conditions derived from CESM simulations as described in section 2.0. The model simulation results are presented below.

4.1 Salish Sea Estuary-Scale Hydrodynamics Response

4.1.1 Estuarine Circulation

The Salish Sea water quality benefits from the natural presence of a strong estuarine two-layer circulation and relatively rapid water renewal and exchange with the Pacific Ocean. The Strait of Juan de Fuca is the primary pathway through which Pacific Ocean water enters the Salish Sea. The strength of the total tidally averaged inflow from Pacific Ocean to Salish Sea is nearly 10–20 times the corresponding average freshwater river inflows (Sutherland et al. 2011; Khangaonkar et al. 2017). Thus, it is important to understand how climate change and sea level rise will affect Salish Sea-wide circulation.

Sea level rise increases the exchange flow transection area and has a potential of increasing the exchange flow between the Pacific Ocean and Salish Sea; however, the model results show that the overall circulation is unaffected (Figure 4.1). Tidally averaged, bottom layer flows at the Strait of Juan de Fuca and Haro Strait experience slight reductions but are small in terms of percentage, and bottom layer flows of Admiralty Inlet remain the same. A possible explanation for the overall unaffected estuarine circulation is that the effect of sea level rise may be counteracted by reduction of salinity gradient at the Salish Sea-Pacific Ocean interface. These results imply that exchange flows to the Salish Sea in the future will have similar amounts compared to present day.

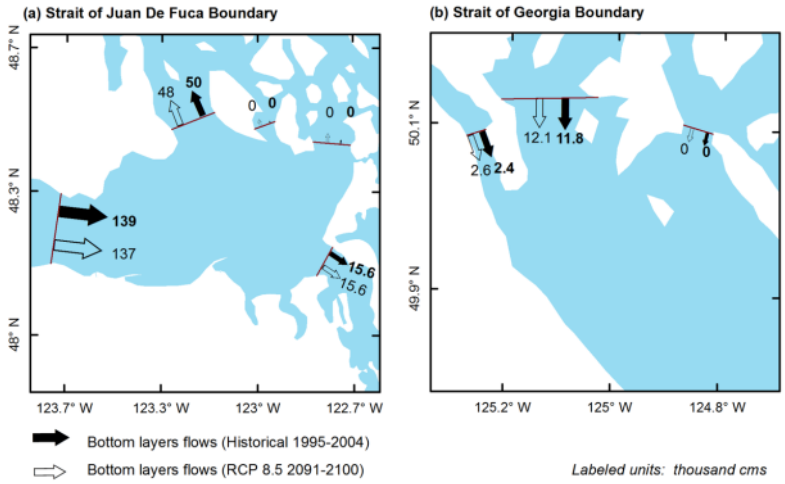

Figure 4.1. Tidally Averaged Bottom Layer Flows for Historical and Future Scenarios

4.1.2 Temperature Increases

The Salish Sea maintains relatively low temperatures (annual mean ≈10˚C) and most marine life in the system are cold-water species that are sensitive to temperature shifts. As expected, with higher future annual average air temperatures (ΔT ≈3.5˚C), higher ocean boundary temperatures (ΔT ≈2.4˚C), and higher tributary inflow temperatures (ΔT ≈3.5˚C), and with circulation strength relatively unchanged, the temperatures in the Salish Sea were correspondingly higher.

Figure 4.2(a) shows a characteristic spatial pattern of sea surface temperatures over the SSM domain from the historical Y2000 simulation, averaged over the yearlong simulation period. This historical simulation also represents existing conditions under current climate where the Salish Sea surface temperatures are consistently lower than those over the continental shelf. This is primarily due to the effect of circulation that results in mixing the cooler waters of the bottom layer with the warmer surface waters. The same pattern holds in the future and is particularly noticeable in Figure 4.2(b), which shows annual mean temperature from the RCP8.5 simulation. Despite significantly higher temperatures in the future, the mixing and circulation within the Salish Sea appears to provide a cooling effect for the surface layers. The bottom layers will be correspondingly warmer. Figure 4.2(c) shows the increase in the annual mean sea surface temperature in future RCP8.5 scenario relative to the historical scenario. Overall warming of the Salish Sea is predicted in the future dominated by global ocean warming (ΔT ≈2.4˚C) at the boundary. A Salish Sea surface temperature ΔT ≈2.15˚C and bottom temperature ΔT ≈1.90˚C is predicted in the future Y2095 RCP8.5 scenario relative to historical conditions.

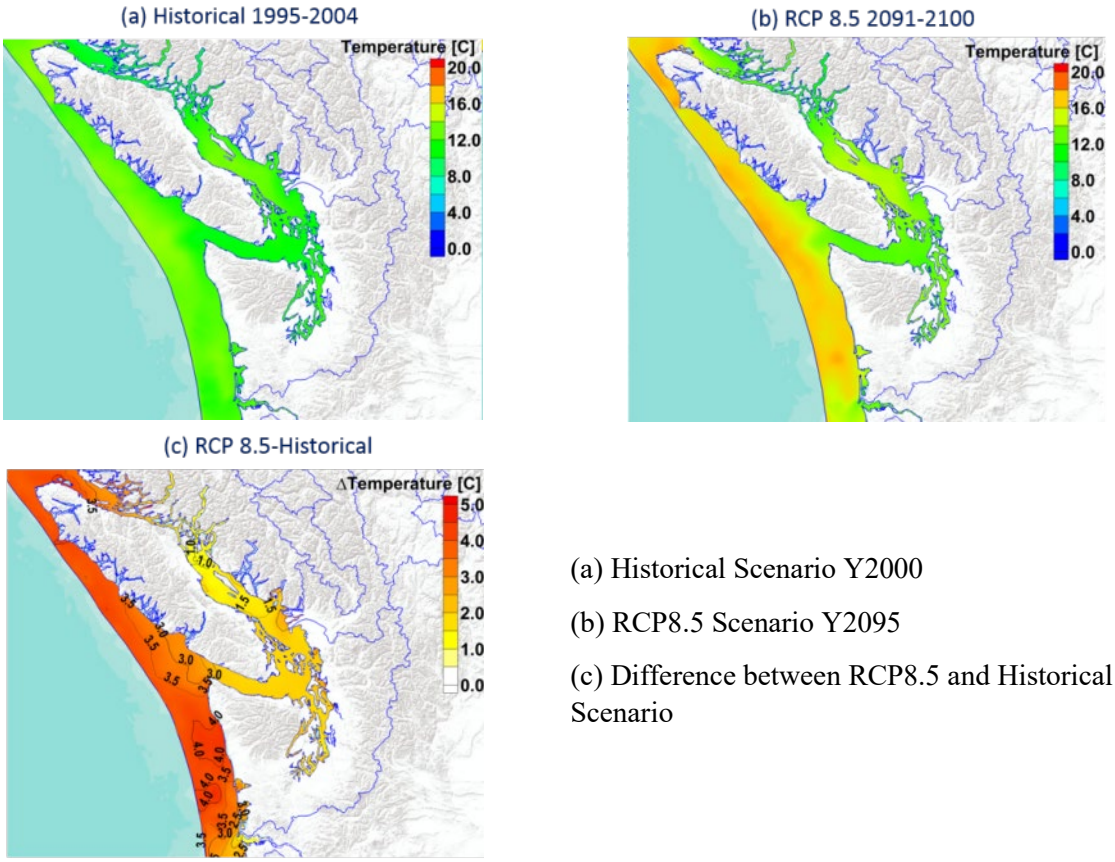

(a) Historical Scenario Y2000

(b) RCP8.5 Scenario Y2095

(c) Difference between RCP8.5 and Historical Scenario

Figure 4.2. Simulated Salish Sea Annual Mean Surface Temperature

Water quality standards for the protection of aquatic life in marine waters of Washington State are listed in Table 4-1 below based on their use classification.

Table 4.1. Aquatic Life Temperature Criteria in Marine Water

Category	Highest 1-DMax
Extraordinary quality	13°C (55.4°F)
Excellent quality	16°C (60.8°F)
Good quality	19°C (66.2°F)
Fair quality	22°C (71.6°F)

When temperatures exceed the above criteria, either naturally or through anthropogenic impacts, the habitat is considered under thermal stress. Thermal stress tolerance varies among species over the range shown in Table 4.1. As a qualitative assessment of the change in thermal exposure as a result of climate change, areas in the Salish Sea with surface temperature greater than 18˚C on a typical summer day (August 13) were plotted for the historical and future RCP8.5 scenarios. As shown in Figure 4.3, in the historical scenario, greater than 18˚C thermal stress only exists in the Snohomish River Estuary and the southeast end of Hood Canal. However, in the future Y2095 RCP8.5 scenario, thermal stress of greater than 18˚C is observed in almost the entire Hood Canal as well as in Samish River Estuary, Snohomish River Estuary, Skagit River Estuary, and the south end of Holmes Harbor. A large thermal stress zone

also forms in the Strait of Georgia, which is partially shown in Figure 4.3. More detailed analysis of estuary future temperature change and the consequences are provided in the next section.

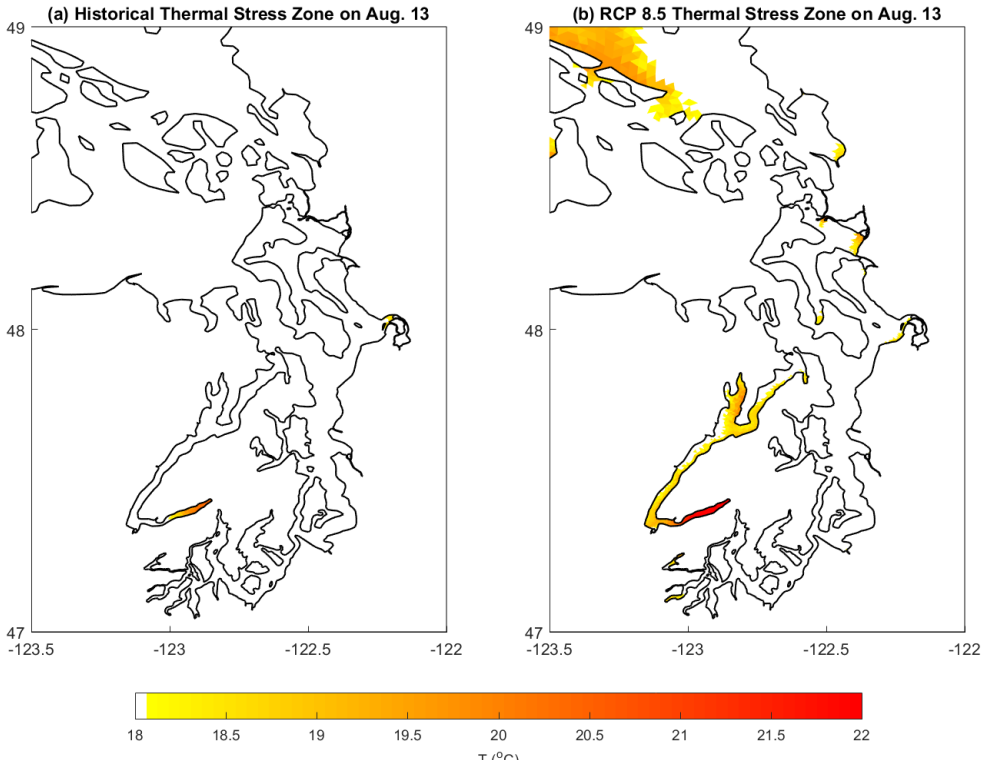

Figure 4.3. Surface Thermal Stress Zones between Historical and Future RCP8.5 Scenarios

Figure 4.4 provides a statistical summary of domain-wide temperatures for the historical and future RCP8.5 scenarios. The Salish Sea-wide mean temperature rises from 10.46˚C (historical) to 12.23˚C (RCP8.5), with a net $\Delta T \approx 1.77$˚C, which is slightly smaller than the net temperature increases at the OBC.

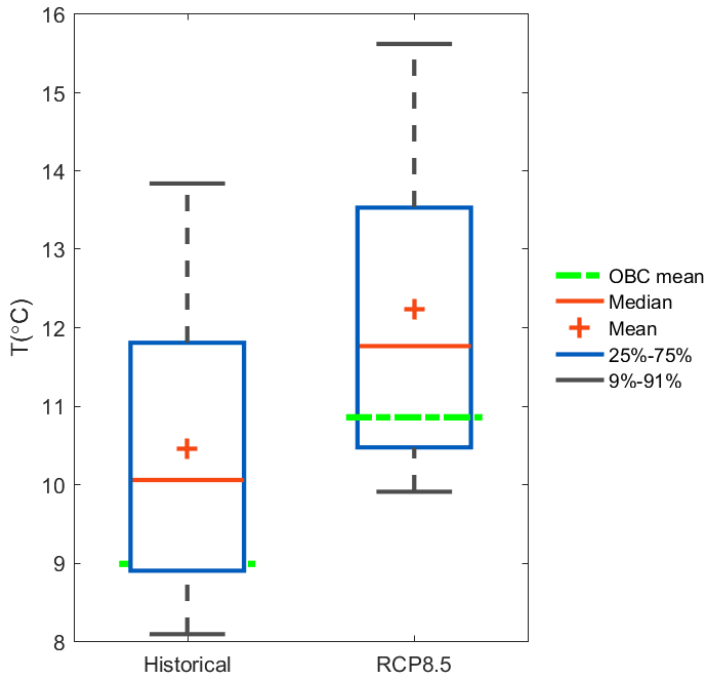

Figure 4.4. Hourly Temperature Statistics between Historical and Future RCP8.5 Scenarios

4.1.3 Salinity Change

Figure 4.5(a) shows the spatial distribution of simulated sea surface salinity in the historical scenario. Annual mean surface salinity varies from ≈30 ppt over the continental shelf to brackish levels inside of Salish Sea to ≈20–30 ppt in Puget Sound and Georgia Basins. The effects of large freshwater discharges from the Columbia River over the continental shelf, Fraser River in Georgia Basin, and Skagit River in Puget Sound are noticeable. Examination of results from Figure 4.5(b) shows that the spatial patterns and salinity magnitudes in the future Y2095 RCP8.5 scenario are not significantly different. The total freshwater discharge input for the future simulation was ≈4.7% lower and the circulation and exchange flows were shown to be of similar magnitudes. As a result, as shown in Figure 4.5(c), the small increase in salinity in the future Y2095 RCP8.5 scenario relative to historical levels is not noticeable at this scale except near the larger river plumes.

Figure 4.6 provides a statistical summary of domain-wide salinity for the historical and future RCP8.5 scenarios. The Salish Sea-wide mean salinity rises from 25.47 ppt (historical) to 25.84. ppt (RCP8.5), with a net change in salinity $\Delta S \approx 0.36$ ppt driven by a combination sea level rise and reduced freshwater flows estimated in this simulation.

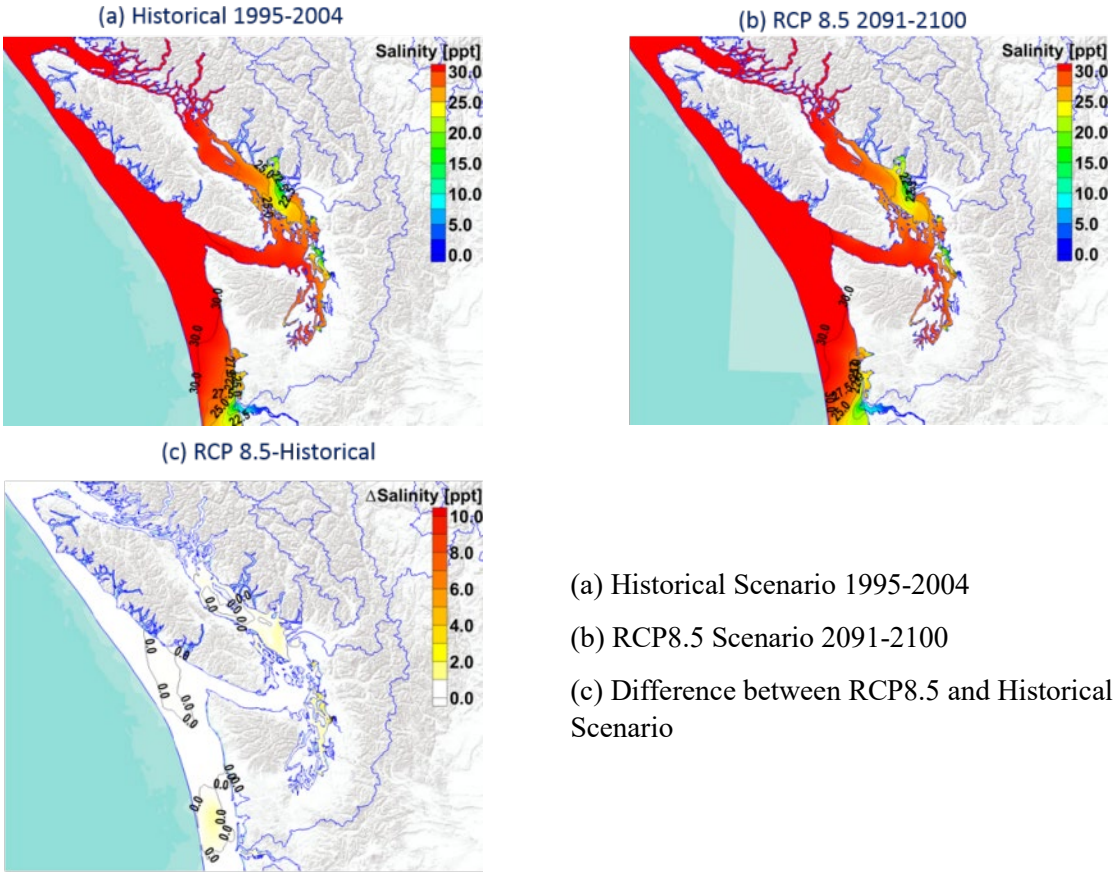

(a) Historical Scenario 1995-2004

(b) RCP8.5 Scenario 2091-2100

(c) Difference between RCP8.5 and Historical Scenario

Figure 4.5. Simulated Salish Sea Annual Mean Sea Surface Salinity

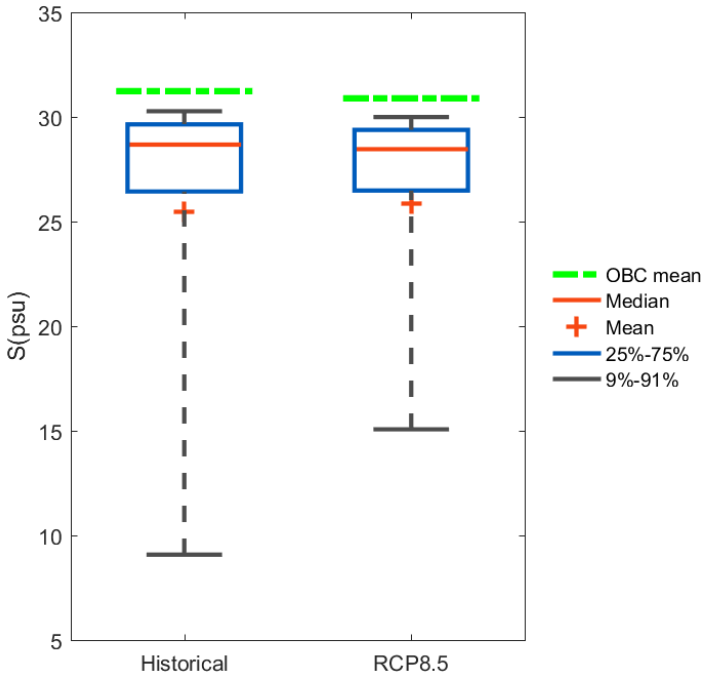

Figure 4.6. Hourly Salinity Statistics between Historical and future RCP8.5 Scenarios

4.2 Salish Sea Estuary Scale Water Quality Response

4.2.1 Nutrient Loads and Consumption

Nitrates are the primary source of food for algae in the Salish Sea, which is a nitrogen-limited system. Nitrates of oceanic origin enter the Salish Sea through the bottom layer tidal exchange inflow and account for ≈99% of the nitrate load, estimate based on Y2014 data (Khangaonkar et al. 2017 under review). A fraction of this bottom layer nitrate enters the euphotic zone through diffusion and mixing and is consumed by algal growth. In the Salish Sea, the euphotic zone is typically restricted to the upper 30 m of the water column. Also consumed is the direct nutrient load to the euphotic zone from land-based sources such as rivers and WWTPs. The outflow layer, which may vary from upper 20 m in sub-basins such as Hood Canal to as deep as ≈100 m in the Strait of Juan de Fuca, includes nutrients that are left over in the 30 m euphotic zone and those not consumed immediately below the euphotic zone. Although lower in magnitude relative to incoming nutrient load, results from Y2014 simulations using SSM show that nearly 98% of nutrients that flow out of the Salish Sea are of oceanic origin, consistent with the findings previously reported by Davis et al. (2014). In spite of a copious supply of nutrients from the ocean, in the highly stratified environment of the Salish Sea the rate of nutrient diffusion to euphotic zone is lower than the consumption rate by algal growth during the peak growing seasons. As a result, nitrate concentrations in most sub-basins are depleted to near-zero levels in spring and summer months.

As shown in Figure 4.7, nutrient loads from oceanic- and land-based sources are expected to increase in the future Y2095 RCP8.5 scenario relative to historical levels. A 9% higher concentration of nitrates in the tidally averaged estuarine inflow from the Pacific Ocean, 44% increase in nitrate loads from rivers, and near doubling of wastewater inflows results in higher availability of nitrates in the euphotic zone. A corresponding increase in algal biomass is predicted in the future. The upper panel of Figure 4.7 shows a comparison of time series of nitrate mass in the euphotic zone for the historical and future RCP8.5 simulations. Average nitrate mass in the euphotic zone is predicted to be ≈12% higher in the future. The lower panel shows simulated algal biomass for the historical and future RCP8.5 scenarios. An increase in algal biomass of 23% is predicted in the future for the RCP8.5 scenario.

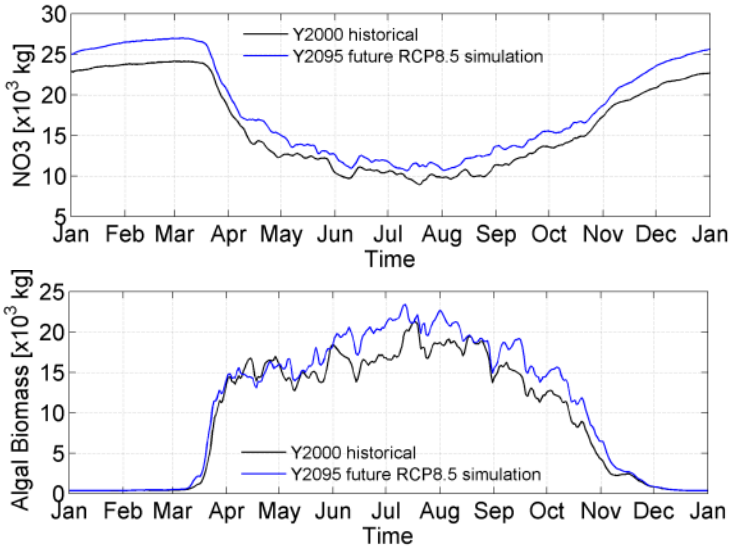

Figure 4.7. Mass of Nitrate (NO3+NO2) and Algal Biomass in Salish Sea Euphotic Zone

4.2.2 Algal Species Shifts

Harmful algal blooms are one of the major water quality concerns in the Salish Sea and occur when hazardous species quickly grow and accumulate in a water system. Although most algal species are innocuous, there are a few types that produce toxins, which can accumulate as they move up the food chain and threaten humans and wildlife. For example, in 2015 the states of Washington, Oregon, and California had to shut down shellfish and crab harvesting due to harmful algal blooms. As described in the previous section, numerous sub-basins within the Salish Sea experience strong summer algal blooms resulting in depletion of nitrates in the euphotic zone to near zero levels. Increase of land-based nutrient loads to the euphotic zone in such nutrient-limited conditions, accompanied by higher sea surface temperatures as predicted for the future Y2095 scenario, could lead to eutrophic conditions suitable for harmful algal blooms, and is therefore a serious concern.

In the SSM, algal species are grouped into two dominant categories: diatom (ALG1) and dinoflagellates (ALG2). Under typical present Salish Sea conditions, diatoms start to bloom in early spring and reach peak concentrations in May with temperatures in the range of 8–12°C. As temperatures increase further, diatoms will decline with predation by zooplankton and dinoflagellates will bloom as temperatures approach 18°C and beyond. The dinoflagellates reach peak biomass in August coinciding with peak sea surface temperatures in the Salish Sea.

Hydrodynamic model simulation results for the RCP8.5 scenario showed that annual mean temperatures within the Salish Sea would be higher ($\Delta T \approx 2.15^{\circ}C$). This results in temperatures increasing rapidly out of the preferred growth range of 8–12°C for diatoms. Dinoflagellates benefit from higher temperatures in their preferred growth range (18–24˚C) over a longer duration before the onset of fall and reduced light availability. Figure 4.8 provides time series plots of total algal biomass concentration associated with diatoms and dinoflagellates based on simulations for the historical and future RCP8.5 scenarios. As shown in the figure, diatom concentrations in the future simulation drop off rapidly after May (≈ day 150) relative to historical simulation. Conversely the dinoflagellates concentrations in the future are predicted to be over 2 times higher and occur over a longer duration. Annual average concentration of dinoflagellates in the future Y2095 RCP8.5 scenario increases by 196% relative to historical simulation. The diatom concentrations are predicted to reduce by 14% in the future simulation.

Shifts of algal species may cause complex cascading ecosystem changes, including increasing the potential for harmful algal blooms; however, the ecological aspects of modeling those complex interactions is beyond the scope of this work. In combination with higher temperatures and increased nutrient loads for the RCP8.5 scenario, the total algal biomass in Salish Sea is predicted to increase by ≈23% relative to the historical scenario. Figure 4.9 and Figure 4.10 provide comparisons of Salish Sea-wide diatom (ALG1) and dinoflagellate (ALG2) concentration statistics between historical and future RCP8.5 scenario simulations. This result must be treated with caution due to the inherent simplification of complex biogeochemical interactions into mathematical formulations. The result suggests a shift towards ecological species that favor higher temperature and that climate change has the potential to drive significant ecological changes especially during the warmest times of the year.

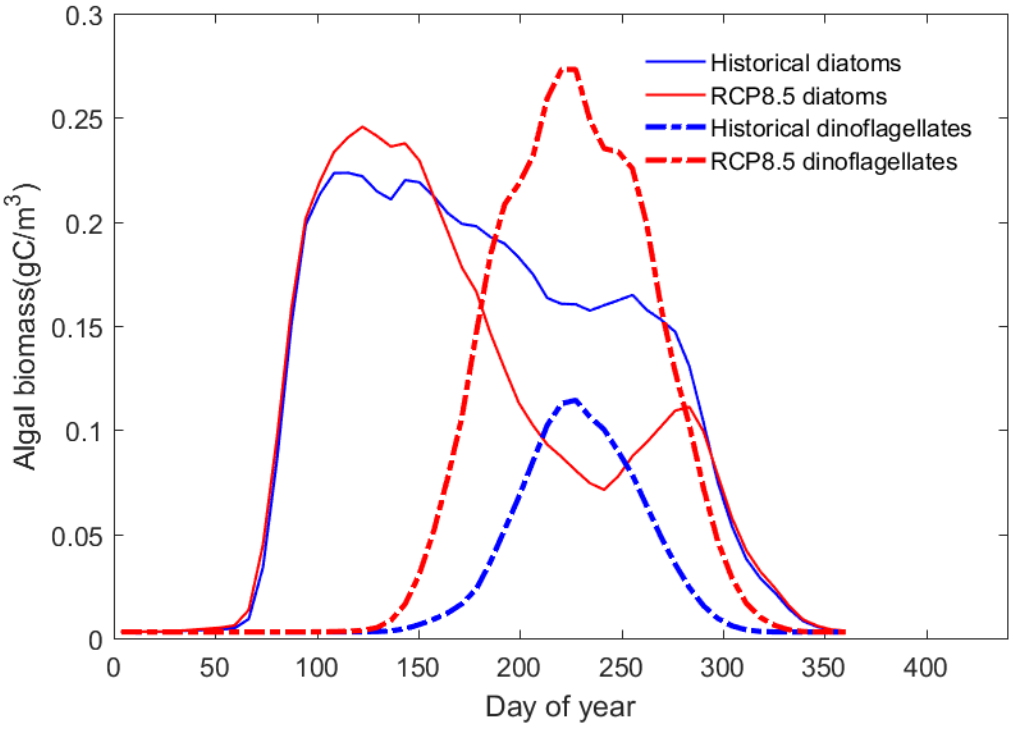

Figure 4.8. Algal Biomass Concentration for Diatoms and Dinoflagellates

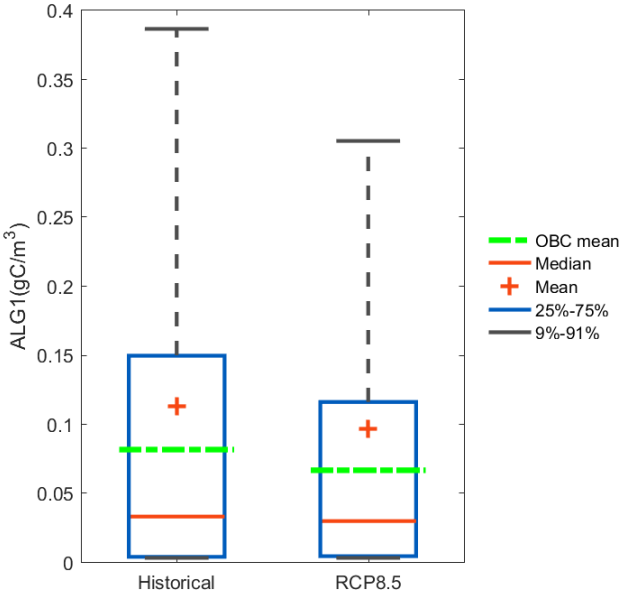

Figure 4.9. Comparison of Diatom (ALG1) Concentration Statistics

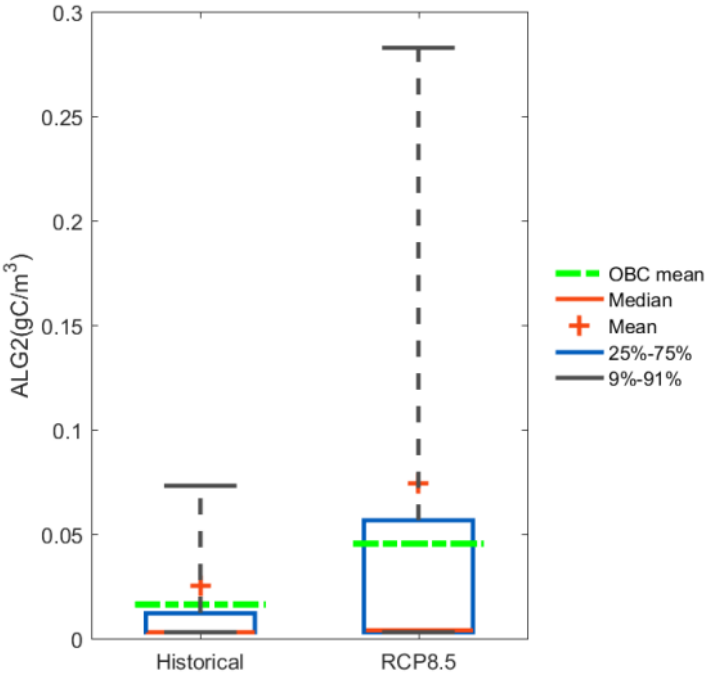

Figure 4.10. Comparison of Diatom (ALG2) Concentration Statistics

4.2.3 Dissolved Oxygen Depletion

Nutrient pollution from rivers, nonpoint source runoff, and nearly 100 wastewater sources has long been recognized as a potential threat to the ecological health of the Salish Sea, where evidence of low DO levels and hypoxia (DO concentrations <2 mg/L) exists in some basins (e.g., Barnes and Collias 1958; Stockner et al. 1979; Harrison et al. 1994; Newton et al. 1995; Embrey and Inkpen 1997; PSAT 2007 ; Albertson et al. 2002 and 2007; Paulson et al. 2006 ; Mohamedali et al. 2011; and Roberts et al. 2008 and 2014). Ecology conducts monthly monitoring of water quality variables including temperature, salinity, DO, pH, nutrients, turbidity, and chlorophyll *a* at more than 26 sites within Puget Sound. DFO conducts quarterly monitoring of a similar set of water quality variables at more than 34 stations in Canadian waters and on the continental shelf. Analysis of these data from 2000 to 2009 shows a decreasing trend in DO in the bottom waters of the Salish Sea in both U.S. and Canadian regions (Albertson et al. 2002), but it is not evident whether these trends are due to increasing nutrient pollution or long-term changes in global ocean chemistry. Recent assessment of hypoxia and sensitivity to nutrient pollution in the Salish Sea by Khangaonkar et al. (2017 under review) using SSM successfully reproduced the large region of hypoxia in Hood Canal that extends over 30–40 km during its peak. The model results showed that the hypoxia was primarily due to the existence of a two-layer classic fjord-type circulation and a nearly stagnant deep bottom layer that occupies nearly 60% of the water column. Occurrence of hypoxia was also reproduced in other sub-basins such as Penn Cove in Whidbey Basin, East Sound in Orcas Island, and south Puget Sound.

In addition to future nutrient load increases (Figure 4.7), a 28% reduction ($\Delta DO \approx 1.7$ mg/L) in DO concentrations in the estuarine inflow from the Pacific Ocean is predicted to impact Salish Sea near-bed DO levels throughout the domain. Similarly, increased algal biomass in future scenario simulations would likely result in increased settling of organic matter, resulting in higher SOD and sediment nutrient fluxes to the water column from the sediment diagenesis processes. The discussion of hypoxia and DO depletion

therefore focuses on near-bed DO levels occupying bottom 15% of the water column (The surface layer DO levels in general are at healthy concentrations due to a combination of reaeration and photosynthesis and reach supersaturation levels during peak algal growth periods.)

Figure 4.11 through Figure 4.13 show the spatial and temporal patterns of Salish Sea bottom DO for the historical Y2000 scenario, future Y2095 RCP8.5 scenario, and the relative change in DO levels between the two scenarios. Consistent with predictions for temperature and salinity, for both historical and future scenarios, the Salish Sea bottom DO levels are notably higher than those over the continental shelf. This is also attributed to estuarine circulation and mixing of high DO surface waters with incoming low DO waters entering the Salish Sea via estuarine exchange flow through the bottom layers. Figure 4.11 shows that in the present or historical Y2000 conditions, low DO levels occur during the fall months as a result of upwelling over the continental shelf. The results presented in Figure 4.121 show that in the future Y2095 RCP8.5 scenario, driven by the overall reduction in Pacific Ocean DO (ΔDO $\approx$1.7 mg/L), the majority of the continental shelf is at hypoxic DO levels < 2 mg/L. Under present conditions, the DO levels over the continental shelf typically vary between $\approx$ 2-4 mg/L. Figure 4.13 shows that the largest DO depletions are associated with the effect of predicted changes at the Pacific Ocean boundary and a somewhat muted response inside the Salish Sea domain due the benefit of estuarine circulation and mixing. The bottom DO levels inside Salish Sea are higher than those over the continental shelf and the bottom layer inflow from the Pacific Ocean.

Figure 4.11 to Figure 4.13 were plotted at a regional scale to highlight the difference in DO response inside the Salish Sea relative to the continental shelf that is primarily driven by future boundary conditions. To assess the effects of climate change on regions that were already hypoxic in the historical or present conditions, we zoomed in the plotting scale and compared the change in hypoxic zones during typical periods of DO depletion in late summer (September 1). Figure 4.14(a) shows contour plots of regions of hypoxia within the Salish Sea with only DO levels less than 2 mg/L plotted in the historical scenario. In this Y2000 scenario representative of present conditions, known regions of hypoxia such as Lynch Cove in Hood Canal, Budd Inlet, Penn Cove in the Whidbey Basin, and East Sound in the San Juan Islands are reproduced.

Figure 4.14(b) shows that in the future Y2095 RCP8.5 simulation, hypoxia zones have expanded. Nearly all of Hood Canal sub-basin, from Dabob Bay to Lynch Cove, is shown to be at hypoxic levels. New hypoxia zones are shown to form in the inner bays (e.g., North Bay and Henderson Bay in the South Sound, Discovery Bay, and Livingston Bay). The model also predicted hypoxic conditions in Bellingham Bay near the Nooksack River mouth, Samish River mouth, and Port Susan Bay; however, some of these results are in locations that are known tide flats or intertidal regions where the model may not be accurate. All intertidal regions have been simulated with a smoothed minimum depth of $\approx$5 m as a simplification.

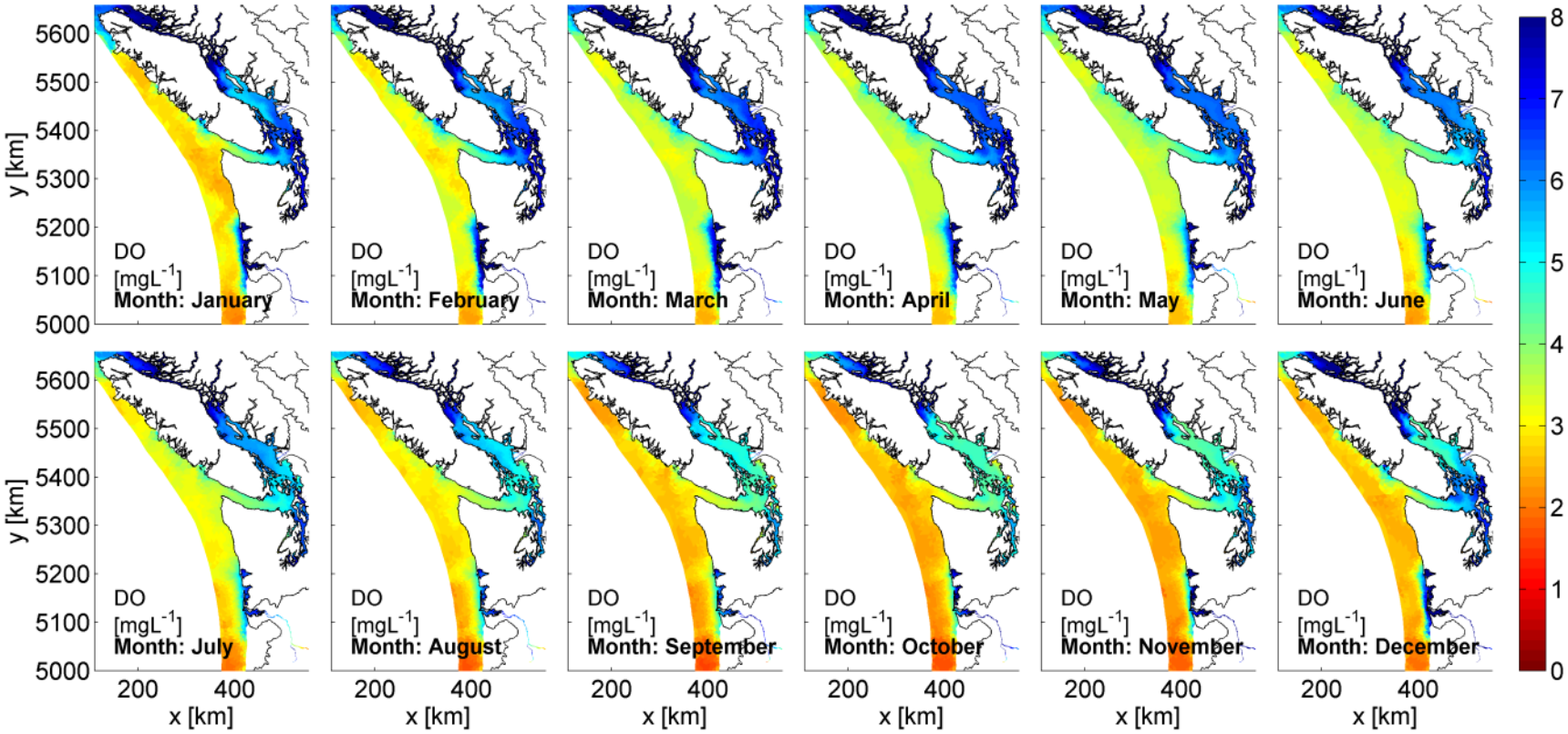

Figure 4.11. Monthly Average Bottom DO for Historical Scenario

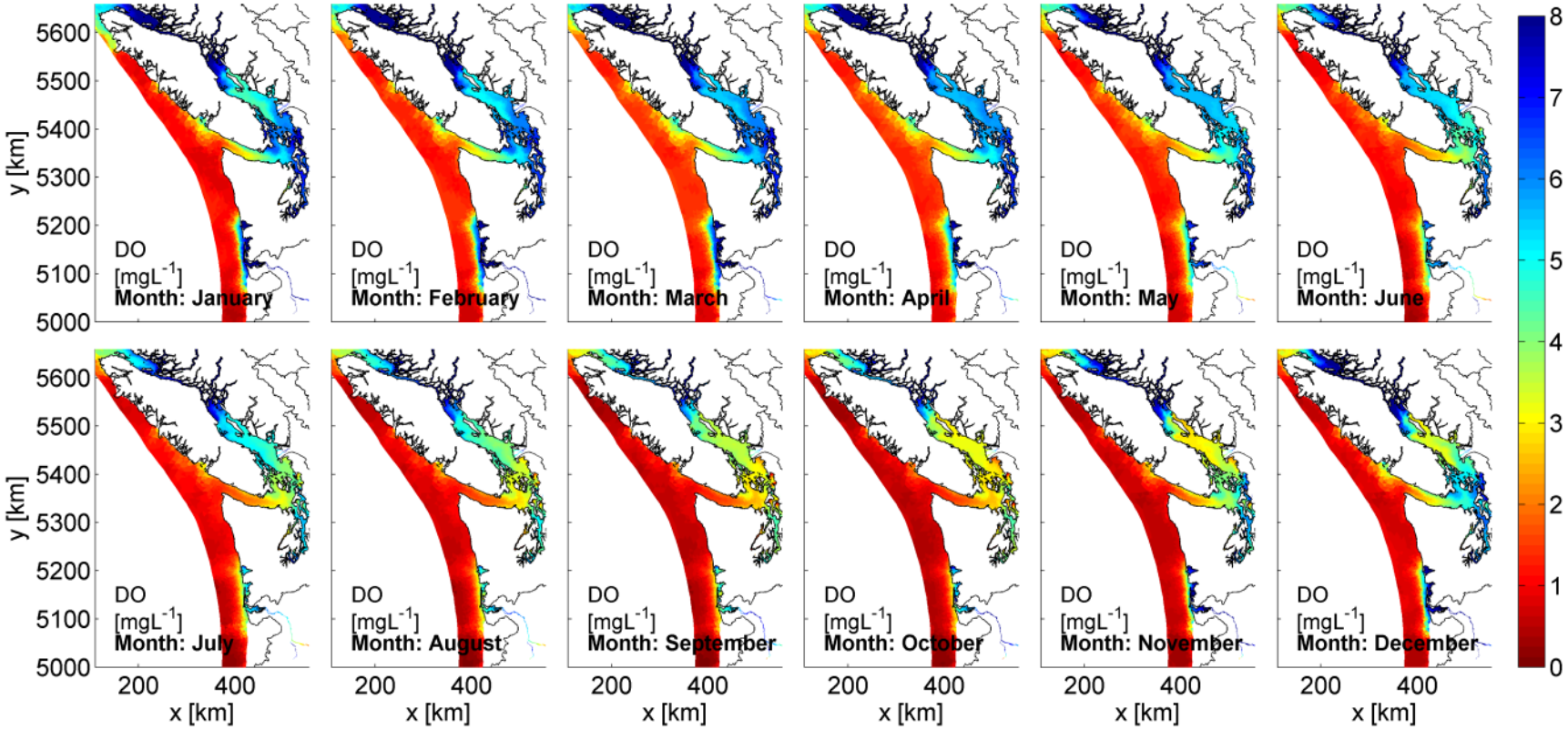

Figure 4.12. Monthly Average Bottom DO for RCP8.5 Scenario

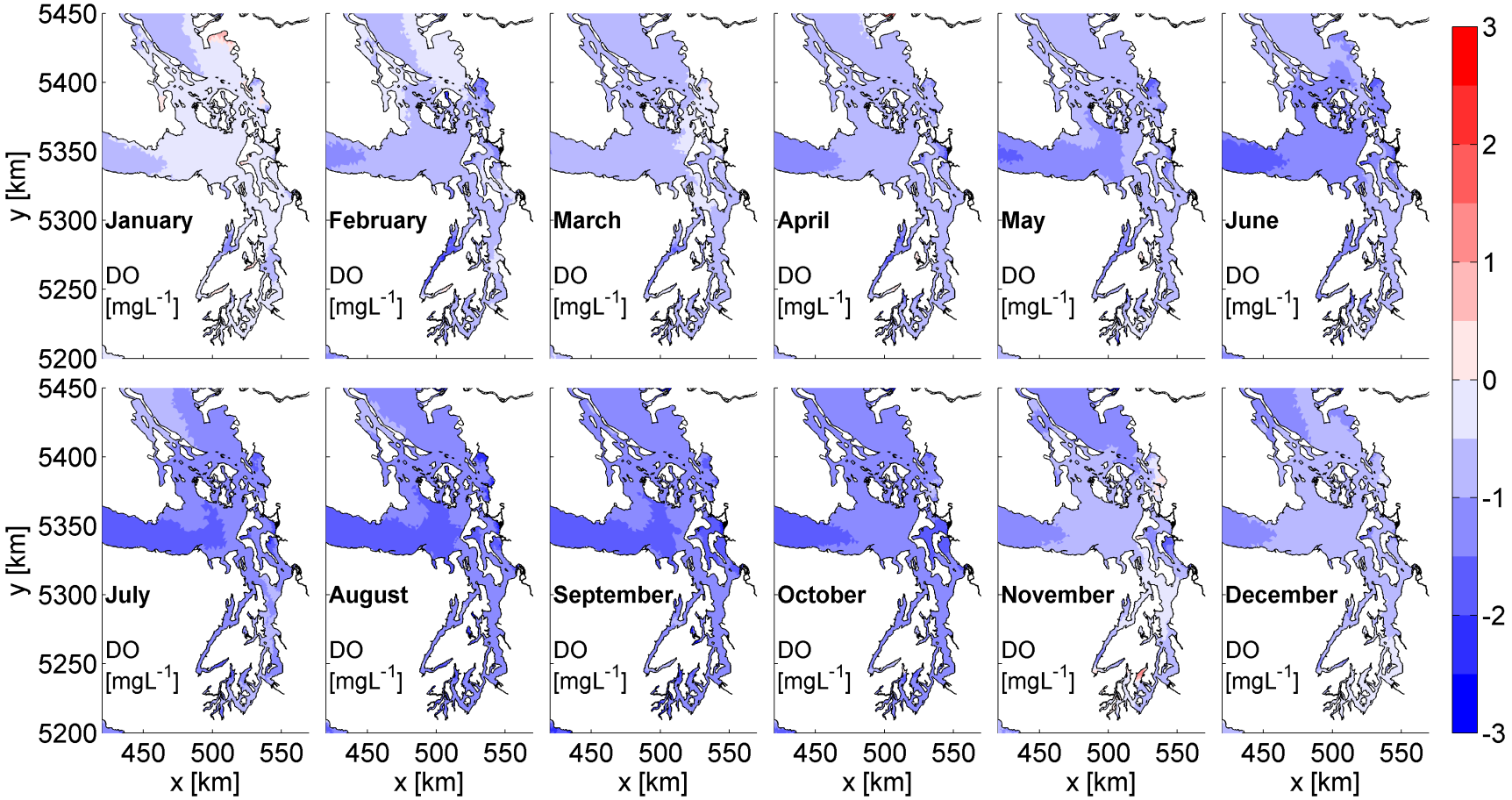

Figure 4.13. Monthly Average Bottom DO Differences between Scenarios

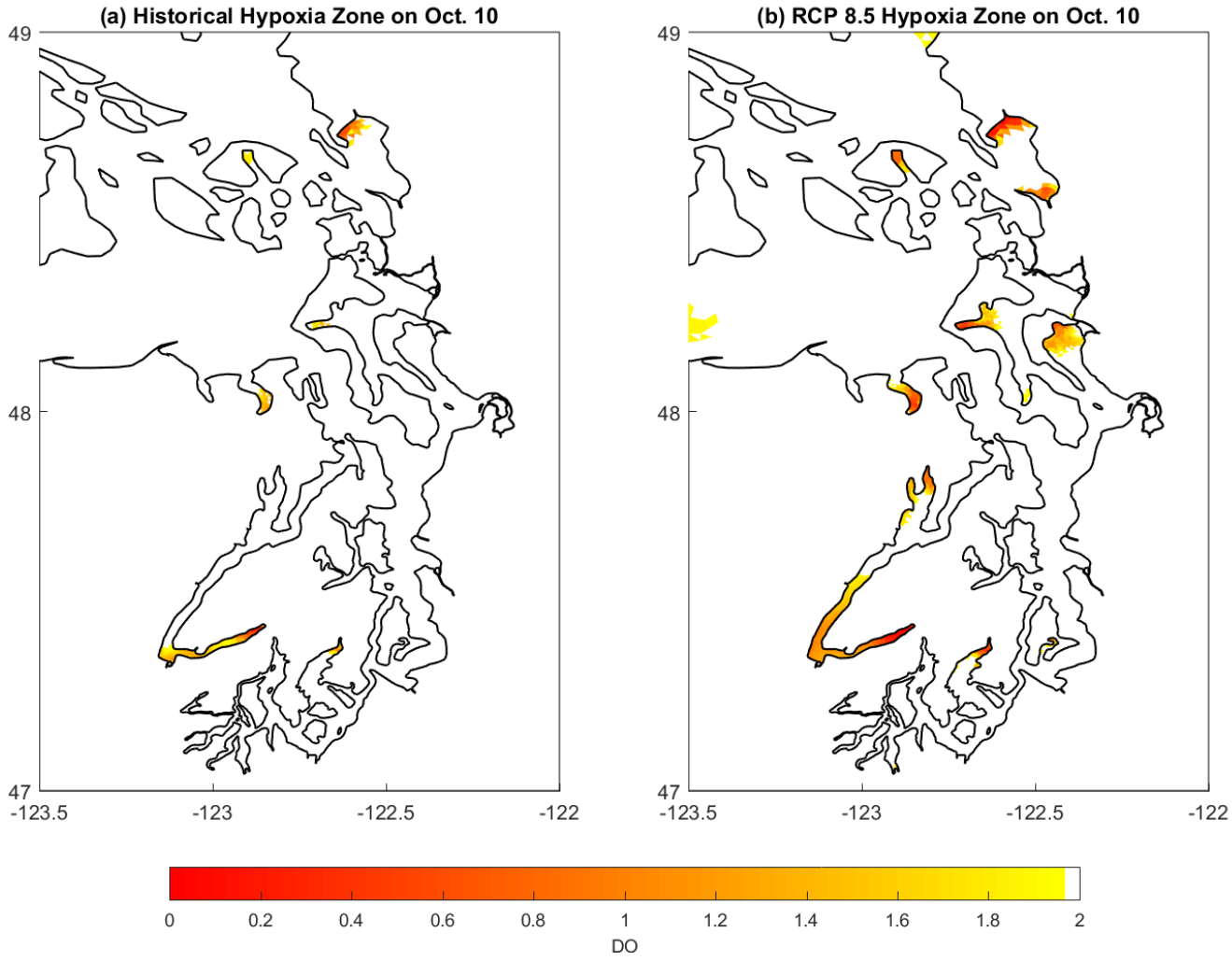

Figure 4.14. Comparison of Bottom Hypoxia Zones between Scenarios

To further examine the duration of exposure, a time series of low DO area within the Salish Sea (with DO levels < 2 mg/L) was plotted. Duration of exposure was computed as area under the curve. Total hypoxic area peaks at ≈121 km^2 in October and represents less than 1% of the total Salish Sea surface area (blue line in Figure 4.15) for historical conditions. (This hypoxia area computation did not include model predictions from nearshore intertidal regions that were set to a depth of 5 m). The total hypoxic area predicted by the RCP8.5 simulation is 2553 km^2. This is a 21-fold expansion of the hypoxic zone and corresponds to a coverage of ≈16% of the Salish Sea area.

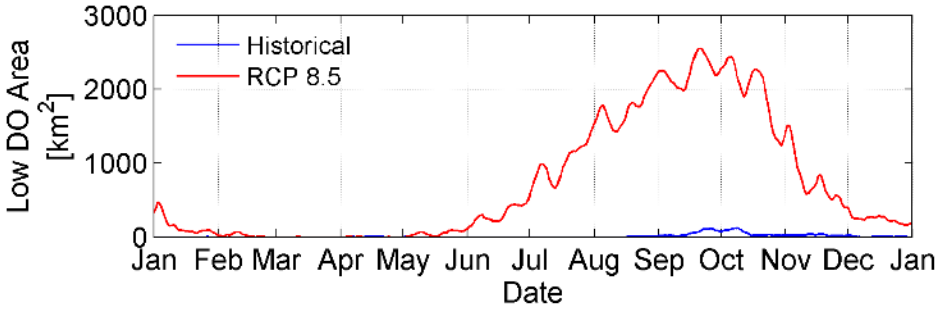

Figure 4.15. Comparison of Bottom Hypoxia Area Time Series between Scenarios

Exposure to hypoxic waters may be estimated by computing "area days" with DO concentrations less than 2 mg/L. For the historic scenario, the model predicts 4.2×10^3 km^2-days of hypoxia. In the future Y2095 scenario, the estimated exposure is two orders of magnitude higher at 2.6×10^5 km^2-days, representing a 62-fold increase in exposure to hypoxic bottom layer waters.

Figure 4.16 shows the increase in number of days and the expansion of hypoxic zone within Hood Canal using color-coded dots to illustrate the location and total number of days under hypoxia. Figure 4.17 summarizes Salish Sea-wide DO concentration statistics between historical and future RCP8.5 scenarios. In both scenarios, the annual mean DO (+) is higher than OBC mean DO (---), indicating that the circulation and mixing inside Salish Sea results in increasing the DO levels relative to levels over the continental shelf. Overall, the Salish Sea-wide annual mean DO is predicted to decrease by 0.74 mg/L in the future Y2095 RCP8.5 scenario relative to the historical scenario (reduction from 7.96 mg/L to 7.21 mg/L). This is less than half of the DO reduction of 1.7 mg/L predicted over the continental shelf due to global climate change induced changes to the ocean chemistry.

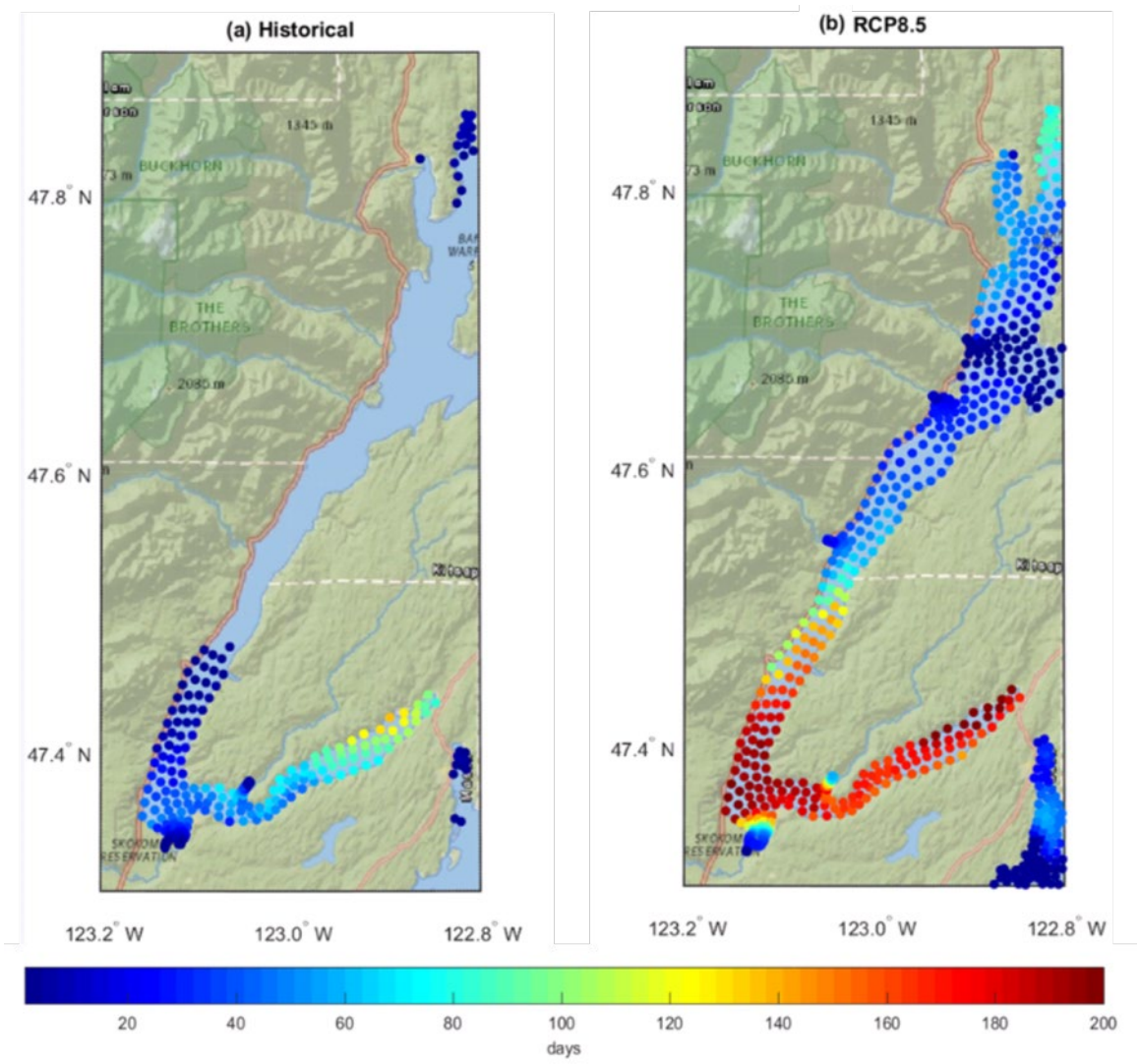

Figure 4.16. Comparison of Number of Days with Bottom DO at Hypoxic Levels in Hood Canal region of Salish Sea.

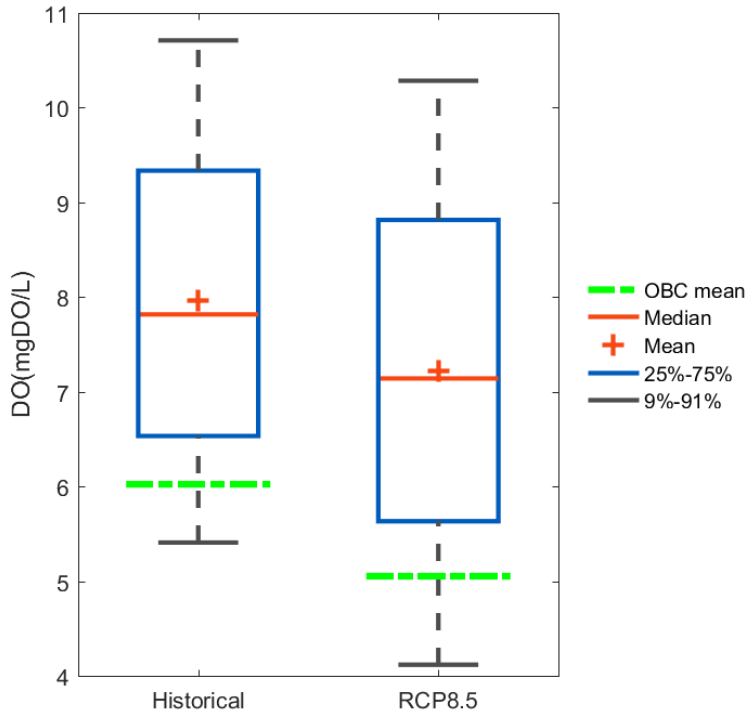

Figure 4.17. Comparisons of Salish Sea-wide DO Concentration Statistics

Comparison of Salish Sea-wide mean DO time series between historical and future RCP8.5 scenarios (Figure 4.18) shows that DO levels drop to the lowest point in late summer. However, deviation between the historical and future RCP8.5 scenarios varies seasonally. In the future scenario, the annual mean DO is 0.74 mg/L lower than historical scenario. The difference or relative DO depletion is significantly higher (≈1.4 mg/L) during late summer.

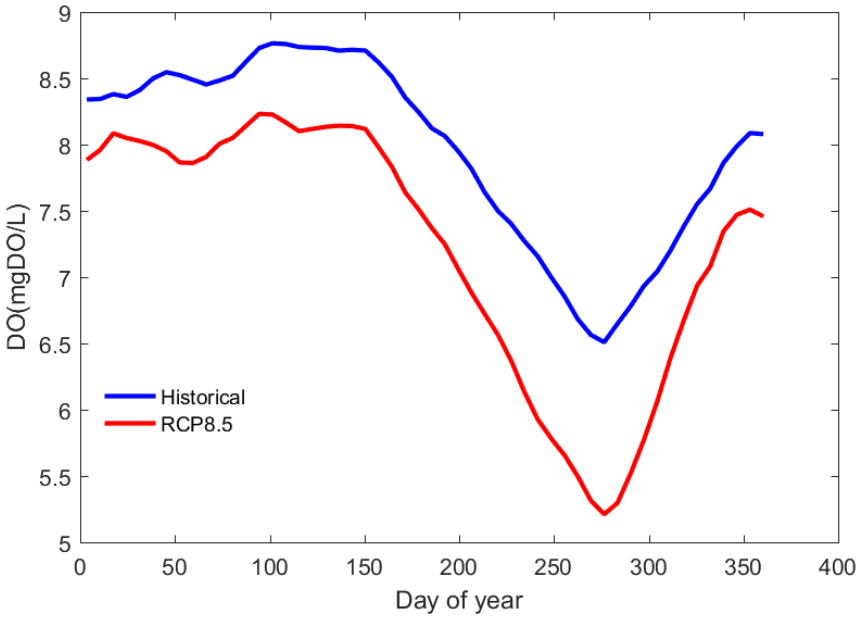

Figure 4.18. Comparison of Salish Sea-wide Mean DO Time Series

4.2.4 Ocean Acidification

Seawater is slightly basic (pH >7). Ocean acidification is the process of pH decrease caused by seawater's uptake of carbon dioxide (CO_2) from the atmosphere. Increasing acidity is potentially harmful for marine organisms, especially for the calcifying process of corals and shellfishes. Effects of sea level rise, upwelling of acidic waters from deeper ocean depths onto the continental shelf, and contributions from algal biomass decay on future pH levels in the Salish Sea are of much interest.

The SSM includes carbonate chemistry and simulates DIC, TA, pCO_2, and pH. Surface DO and pH in Puget Sound benefit from the effects of primary production that results near supersaturated DO levels and increase in pH or reduction in acidity due to consumption of DIC through algal growth. As in the case of DO, the focus is on near-bed pH. Near-bed low DO levels are often associated with carbonaceous biogeochemical oxygen demand due to decaying or organic matter. This decay is also associated with low pH levels due to release of DIC. Similar to low DO, low pH is also associated with incoming water from the continental shelf through the bottom layers.

Figure 4.19 through Figure 4.21 show the spatial and temporal patterns of bottom pH in Salish Sea for the historical and future RCP8.5 scenarios, and their differences. In the historical scenario representing the present conditions, the Puget Sound region south of Admiralty Inlet appears to be notably higher in pH relative to the outer sub-basins such as Strait of Juan de Fuca and waters surrounding the San Juan Islands. This spatial distribution result for pH is consistent with the results for temperature and DO where bottom layer waters in Puget Sound benefit from the strong circulation between embracing sills. Waters affected by high freshwater inflow such as the Skagit and Bellingham Bay show lower pH levels. Throughout the year, Hood Canal stands out with the lowest simulated pH levels. In the future Y2095 RCP8.5 scenario, pH in the Strait of Juan de Fuca, directly connected to the ocean boundary, is 0.4 unit lower than the historical scenario. Hood Canal bottom pH reaches levels as low as 7.2 units. Figure 4.21 shows that the largest pH reduction in the future is predicted for the continental shelf and the Strait of Juan de Fuca regions during the summer months.

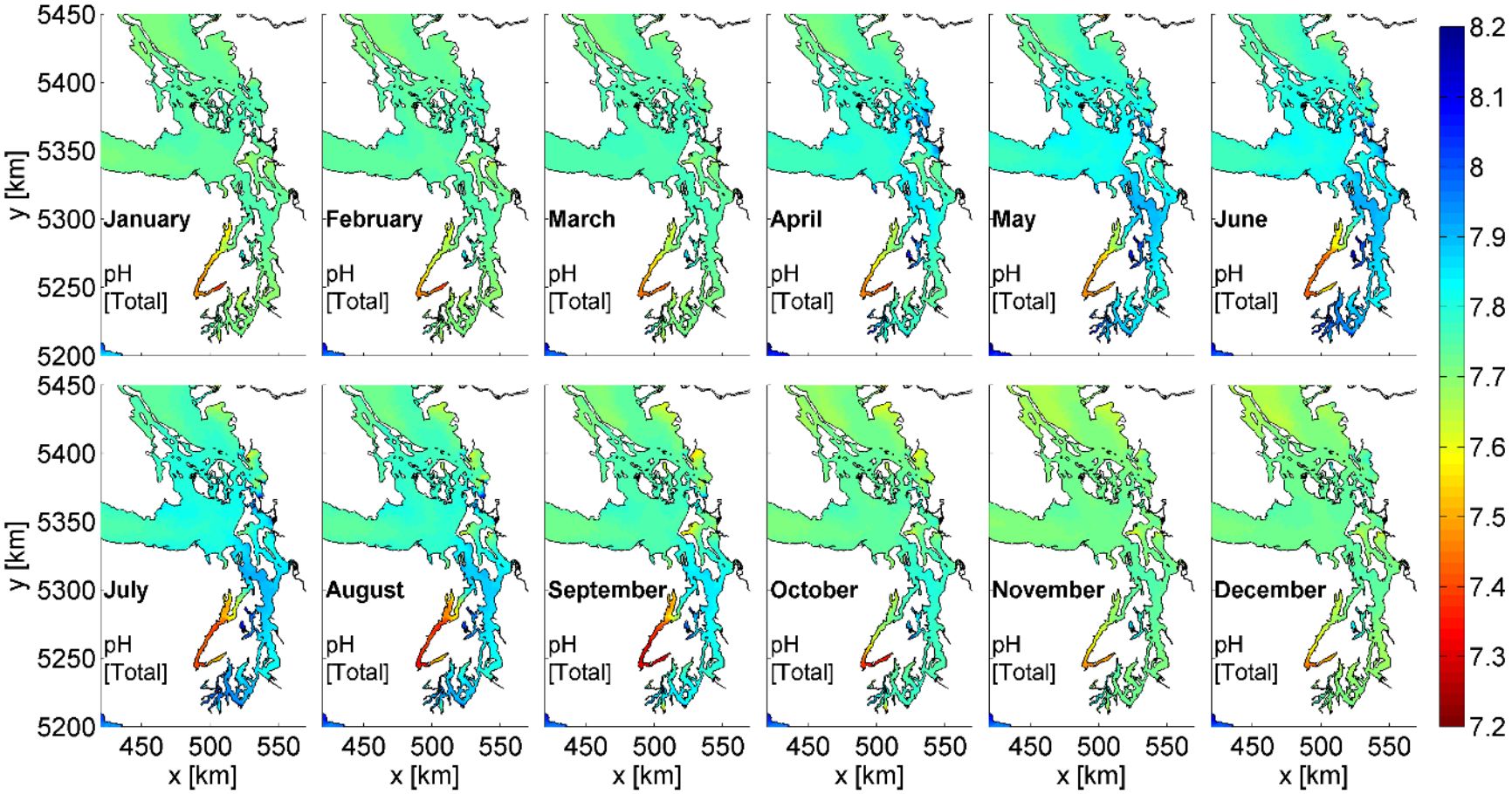

Figure 4.19. Monthly Average Bottom pH in Puget Sound for Historical Scenario

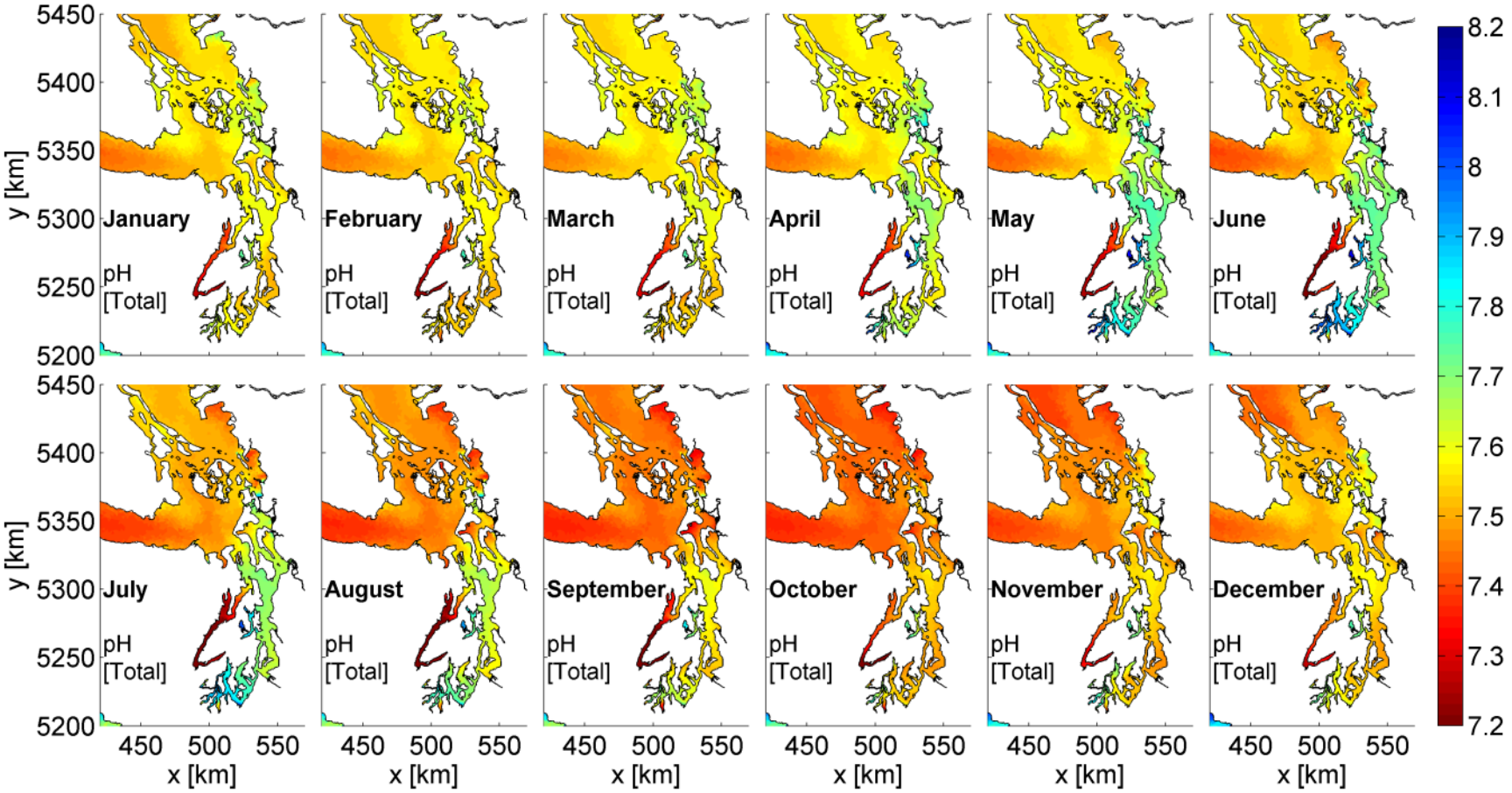

Figure 4.20. Monthly Average Bottom pH in Puget Sound for RCP8.5 Scenario

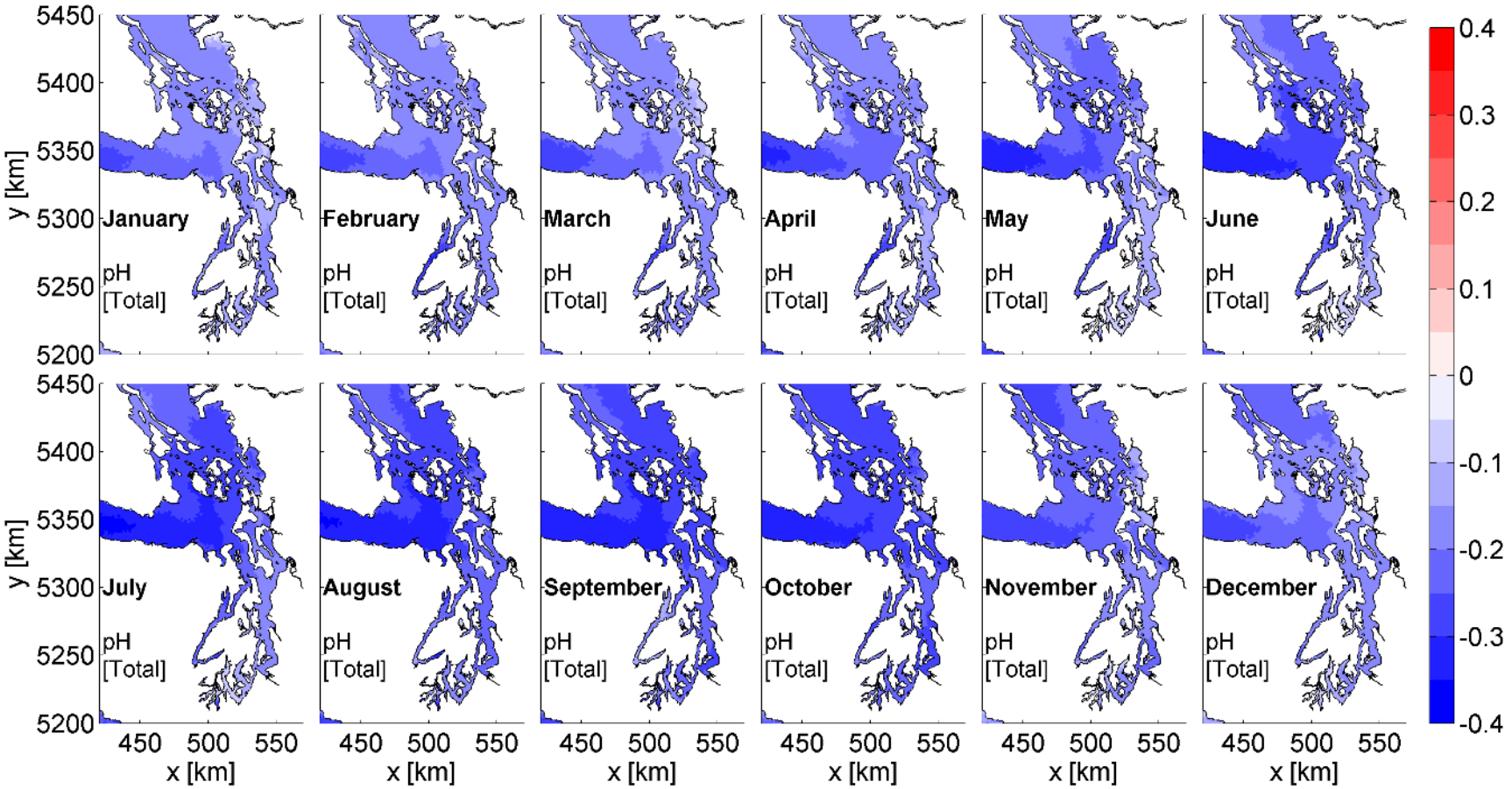

Figure 4.21. Monthly Average Bottom pH Differences between Scenarios

Figure 4.22 shows that CESM predicted the annual mean pH at the ocean boundaries (green line) reduced from 7.82 (historical) to 7.58 (RCP8.5), with a net reduction of 0.23. However, as explained above, the effect of ocean acidification within Salish Sea is less severe, mitigated by the combined effect of biogeochemical activity and circulation. Salish Sea-wide annual mean pH (+) reduced from 7.78 (historical) to 7.66 (RCP8.5) is a net reduction of 0.12 units within the Salish Sea.

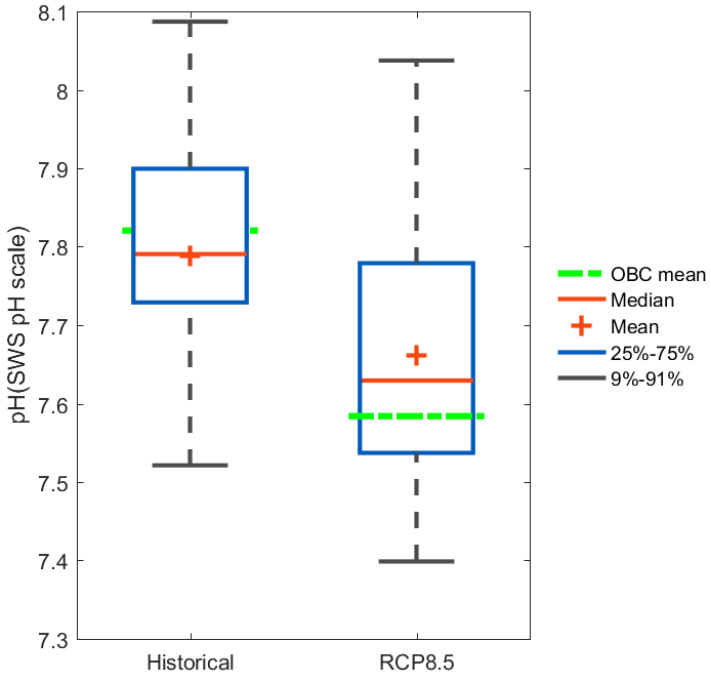

Figure 4.22. Comparisons of Salish Sea-wide average pH Concentration Statistics between Scenarios

The temporal variation of Salish Sea-wide mean pH through the annual seasons is similar for historical and future scenarios as shown in Figure 4.23. In spring, pH levels increase corresponding to algal growth and consumption of DIC. The pH levels reach a peak in summer and wain in the fall with the decline in primary productivity and conversion of algal biomass carbon to DIC. The difference between historical pH and the RCP8.5 scenario is fairly consistent throughout the year, indicating pH will be lower in all seasons under the RCP8.5 scenario.

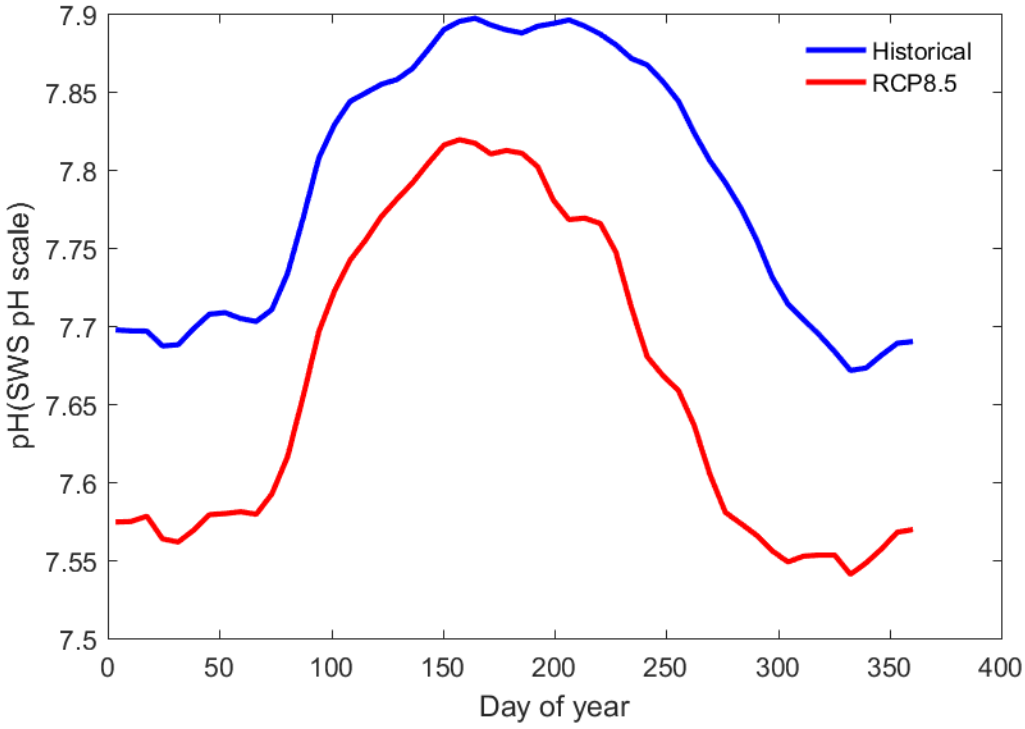

Figure 4.23. Salish Sea-wide Mean pH Seasonal Patterns

To fully recognize the ocean acidification and its impacts on the Salish Sea ecosystem and shellfish industry, a more detailed assessment of these results is needed. The information presented in this section is a first examination of new results through this proof-of-concept level application of the SSM.

5.0 Response to Future Climate in Intertidal Estuarine Reaches

Coastal ecosystems in the Pacific Northwest are composed of numerous tide flats, marshes, and eelgrass beds that support thousands of species of fish and wildlife, which in turn are vital to the regional economy, culture, and quality of life. Potential changes to coastal physical processes such as inundation, circulation, hydrodynamic transport, and biogeochemical cycles as a result of climate change and sea level rise are of utmost importance here. Specifically, inundation frequency, temperature, and salinity in the nearshore intertidal environment are some of the primary parameters that control the biological character of estuarine wetlands.

We selected the Snohomish River estuary as the test bed site for this proof-of-concept objective of simulating nearshore future climate impacts using a combination of global climate change products downscaled to the Pacific Northwest and the SSM. The Snohomish River estuary currently represents the third largest complex of tidally flooded estuarine and freshwater wetlands in Puget Sound (Collins and Sheikh 2005; Simensted et al. 2011). In addition, the Snohomish River estuary provides rearing and migration habitat for all anadromous Pacific salmon, steelhead, cutthroat, and bull trout, including listed Chinook, steelhead, and bull trout. NOAA Fisheries Science Center has been monitoring water surface elevations, temperature, and salinity in the Snohomish River estuary since 2001 and provides a comprehensive data set for model calibration.

Simulation of intertidal temperatures in the Snohomish River estuary required improvements to the heat flux computational scheme in FVCOM as described in section 3.1.2. Also, the SSM was refined in the Snohomish Estuary region to accommodate wetting and drying to best represent the conditions in the nearshore tidal marshlands. Setup, calibration, and application of the SSM with an embedded high-resolution representation of Snohomish Estuary are described below. Application of the model and estuarine response to historical and future climate predictions are then presented.

5.1 High-Resolution Model of the Snohomish Estuary

A high-resolution hydrodynamic model of the Snohomish River estuary, capable of resolving the fine-scale shoreline features, was embedded within the SSM for this analysis (Figure 5.1). This was based on a prior standalone model developed by Yang and Khangaonkar (2007), and Yang et al. (2010). It includes details such as river-training jetties, dikes, small islands, and connection to Port Gardiner through the braided distributaries. Major distributaries include the Snohomish River mainstem, Steamboat Slough, Union Slough, and Ebey Slough.

The term embedded is used to reflect that the existing Snohomish River grid in the SSM was replaced with approximately an order of magnitude finer resolution grid while retaining the original intermediate-scale grid over the rest of the domain. The grid cells in the estuary vary from as small as ≈20 m in the braided reaches to ≈200 m over the tide flats to smooth transition to SSM grid scale ≈1000 m for Possession Sound. The upgraded model grid size is only 1.5 times that of the original SSM and consists of 25,306 nodes and 41,431elements. However, the fine grid size (20 m) requires an external mode time step of 0.5 seconds and 2.5 seconds for the internal mode. All other model specifications are the same, including the sigma-stretched coordinate system with 10 terrain-following sigma layers distributed using

a power law function with an exponent P_Sigma = 1.5. This scale and the selected time step(s) offer sufficient resolution of the various major river channels and tidal marsh bathymetry while allowing year-long simulations within 48 hours of run time on a 384-processor cluster computer.

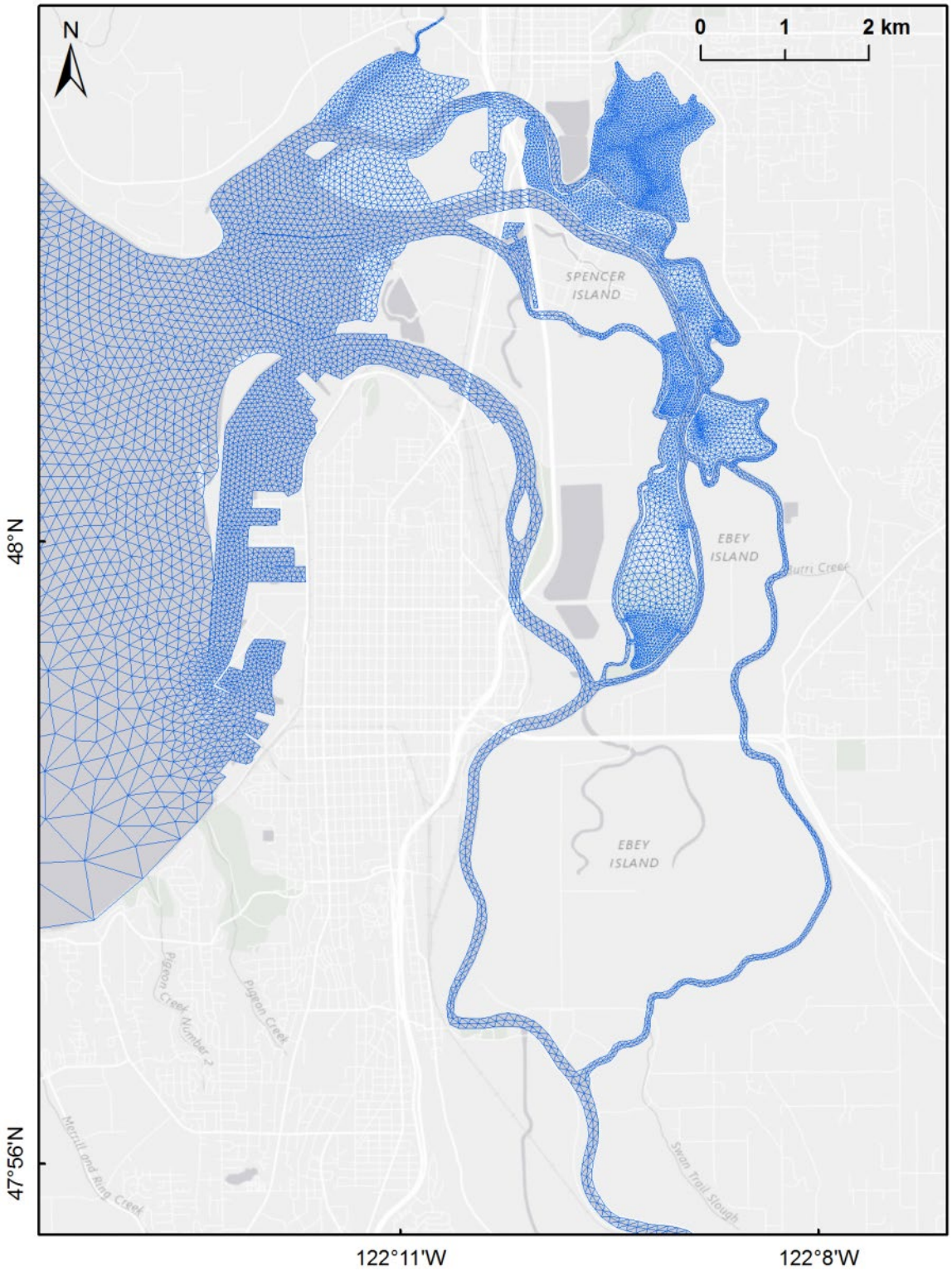

Figure 5.1. SSM Grid with Embedded high-resolution for Snohomish River Estuary

The bathymetry was derived from a combined data set consisting of data from the Puget Sound digital elevation model and high-resolution light detection and ranging bathymetric data collected by the Tulalip Tribes and Snohomish County. The bathymetry was smoothed in the estuary regions outside of the braided channels to minimize hydrostatic inconsistency associated with the use of the sigma coordinate system with steep bathymetric gradients. The associated slope-limiting ratio $\delta H/H = 0.2$ was specified within each grid element following guidance provided by Mellor et al. (1994) and using site-specific experience from Foreman et al. (2009), where H is the local depth at a node and δH is change in depth to the nearest neighbor. The smoothing procedure also includes adjustment of bathymetry to ensure the individual basin and total domain volumes remained with 1% of the original values.

The baseline year selected for this analysis was 2014 due to the availability of continuous time series measurements of temperature, salinity, and water surface elevation in the Snohomish River delta. NOAA Fisheries have implemented a system-wide network of continuous water sensors to measure basic hydrological parameters with the goal of providing improved baseline descriptions of salt intrusion and thermal conditions within the estuary prior to implementation of multiple restoration projects. This network will also provide a framework from which project-level and cumulative restoration responses could be evaluated within the Snohomish River estuary over time. These measurements at 10-minute intervals have been in place since 2013. Y2014 was selected as it provided a complete year of data prior to changes in the tidal prism as a result of Qwuloolt March restoration project on Ebey Slough line in August of 2015. Figure 5.2 shows the locations of the continuous measurement water sensors as black points with site names.

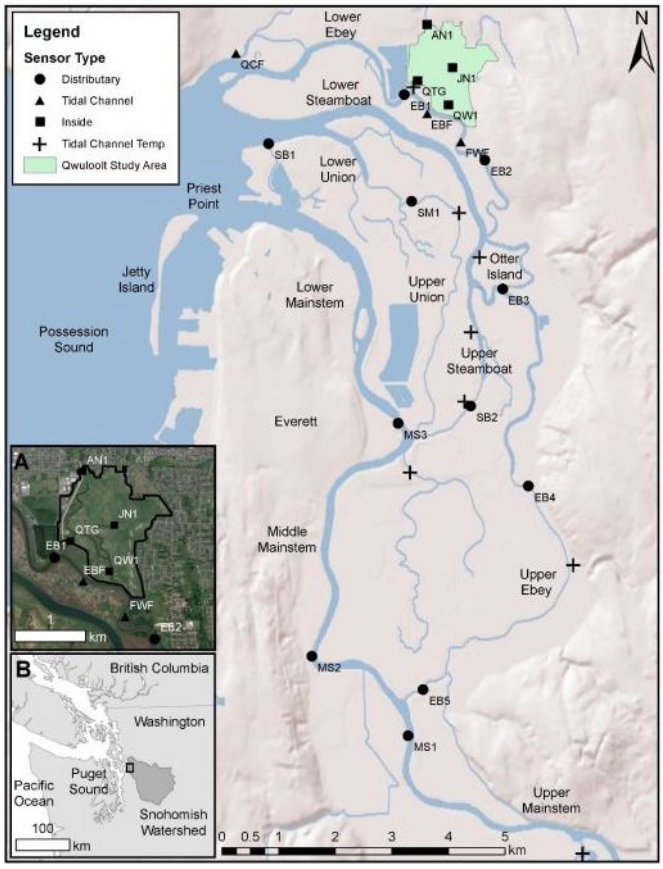

Figure 5.2. Snohomish River Estuary Braided Channel Network

The SSM with embedded Snohomish Estuary in high resolution was applied for Y2014 conditions with all inputs identical to those used for baseline calibration described section 3.3. Salish Sea-wide match with observed data from Ecology monitoring stations was first examined to ensure overall error statistics were comparable. The calibration effort then focused on iterative comparison with NOAA data from the Snohomish River estuary. As described in section 3.1.2, temperatures predictions were initially cooler than observed data. Sometimes this error can occur as a result of excessive mixing in the model. This typically also leads to lower than observed bottom salinity. However, predicted bottom salinity values appeared higher than observed data indicating that lower temperatures were the result of insufficient heat input to the water column. The heat flux computations were then modified such that shortwave solar radiation was correctly accounted for in the intertidal zone with wetting and drying regions.

Many of the stations were at locations that became very shallow during low tide where wetting and drying criteria resulted in stable but incorrect predictions for salinity and temperature. Calibration therefore focused on stations that remained wet during the computations and with data amenable for comparison for model predictions. Figure 5.3 shows a comparison of predicted water surface elevations and measured data in Ebey Slough and mainstem of Snohomish River. Figure 5.4 and Figure 5.10 show comparisons of surface temperatures and bottom salinities at the same stations. Error statistics at all stations are provided in Table 5.1 through Table 5.3 for elevation, temperature, and salinity respectively.

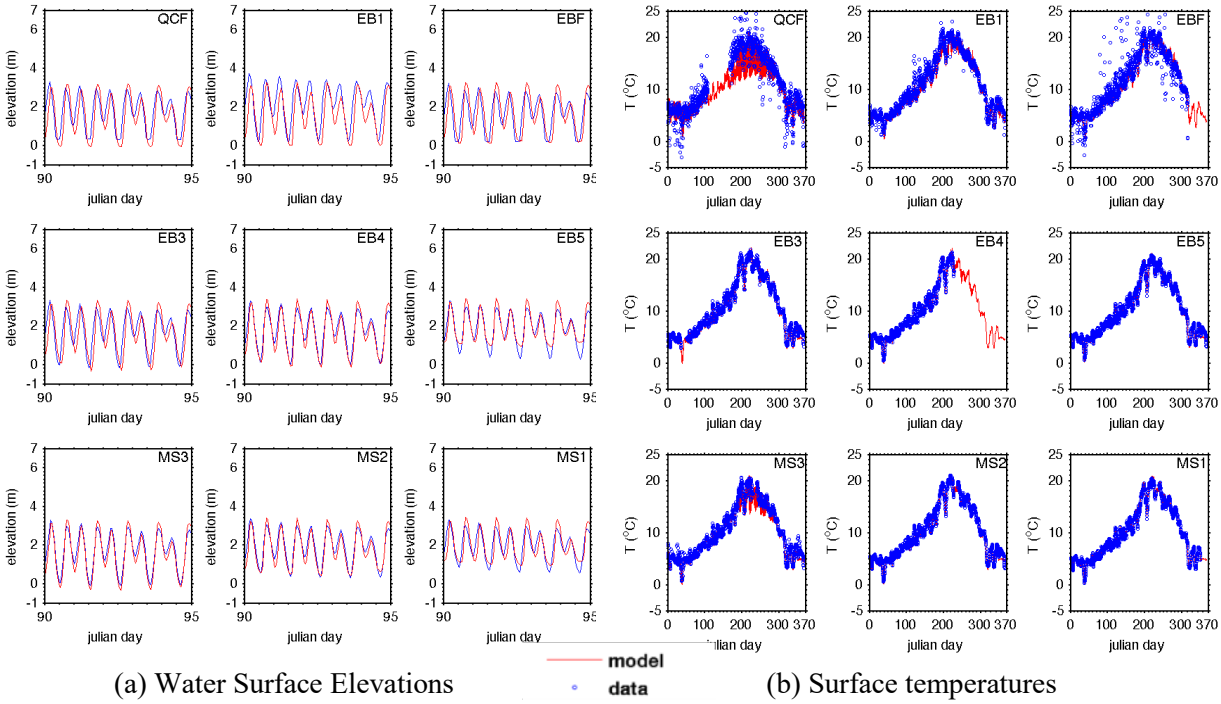

(a) Water Surface Elevations (b) Surface temperatures

Figure 5.3. Comparison of Surface Temperature at Ebey Slough and Mainstem Stations

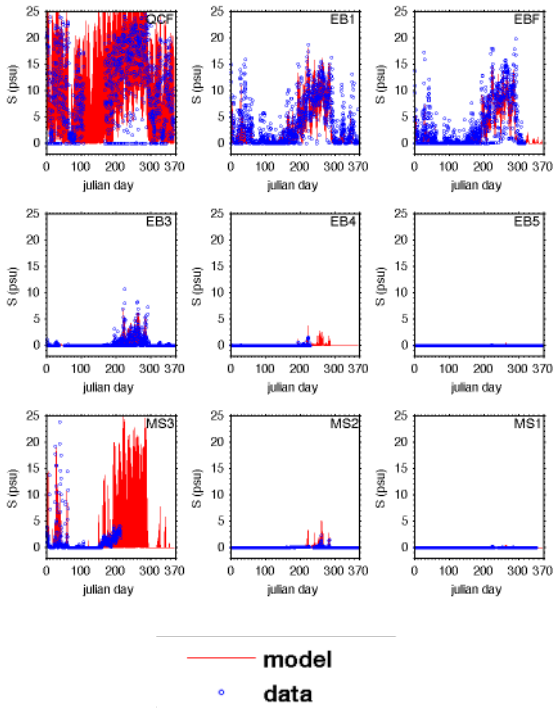

Figure 5.4. Comparison of Bottom Salinity Data at Ebey Slough and Mainstem Stations

Table 5.1. Water Surface Elevation Error Statistics for Snohomish River Stations

Station	ME (m)	RMSE (m)	R2
Water Surface Elevation (distributary stations)			
EB1	-0.33	0.73	0.86
EB2	0.14	0.54	0.92
EB3	-0.03	0.57	0.91
EB4	-0.01	0.34	0.97
EB5	0.10	0.49	0.92
SB1	-0.02	0.61	0.91
SB2	-2.89	0.07	0.42
MS3	0.01	0.32	0.97
MS2	-0.06	0.35	0.96
MS1	0.01	0.49	0.91
Mean	**-0.01**	**0.48**	**0.88**

Table 5.2. Temperature Error Statistics for Snohomish River Stations

Station	ME (^{0}C)	RMSE (^{0}C)	R2
Temperature (distributary stations)			
EB1	-1.23	2.50	0.94
EB2	-0.65	1.20	0.99
EB3	-0.56	1.16	0.99
EB4	-0.34	0.59	1.00
EB5	-0.15	0.37	1.00
SB1	-0.22	0.47	1.00
SB2	-1.68	2.10	0.95
MS3	0.52	1.41	0.97
MS2	-0.41	0.78	0.99
MS1	-0.30	0.50	1.00
Mean	**-0.29**	**1.11**	**0.98**

Table 5.3. Salinity Error Statistics for Snohomish River Stations

Station	ME (ppt)	RMSE (ppt)	R2
Salinity (distributary stations)			
EB1	-1.73	5.33	0.86
EB2	-1.68	3.12	0.83
EB3	1.18	2.71	0.07
EB4	-0.20	0.61	0.86
EB5	-0.02	0.08	0.82
SB1	-0.01	0.02	0.41
SB2	-2.27	5.41	0.84
MS3	-8.30	9.46	0.45
MS2	-0.56	2.60	0.50
MS1	-0.02	0.17	0.67
Mean	**-1.12**	**2.47**	**0.64**

Water surface elevations in the intertidal region are strongly influenced by the accuracy of the bathymetry. The mean sea level bias has been adjusted to -1 cm; however, amplitude of tidal variation is affected by accuracy in specification of the channel cross-section. As a result, the average RMSE is 48 cm. There is considerable room for improvement as the bathymetry of the major distributaries in this model application was based on data collected nearly a decade ago. Fine tuning of model calibration may best be done with a more recent bathymetric survey and was considered beyond the scope of this proof-of-concept effort for simulation of climate change effects.

The temperature bias and RMSE are -0.29ºC and 1.11ºC respectively. In general, the calibration target for temperature is less than 1ºC. Given the complexity of temperature predictions in the intertidal regions, this error was deemed acceptable. Similarly, a salinity bias of -1.12 psu and an RMSE of 2.47 psu are considered on the higher side and could be improved with more accurate bathymetry and iterative site-specific grid adjustment.

5.2 Model Setup under Climate Change Scenarios

The embedded high-resolution model for Snohomish Estuary uses the same boundary condition forcing as SSM to simulate climate change impacts. These boundary conditions were derived from CESM, as described in section 2.0. For the Snohomish River Estuary hydrodynamics, the most significant change from the historical Y2000 to the future Y2095 RCP8.5 scenario are the local changes in seawater temperature increase, air temperature increase, and reduction of Snohomish River summer flow.

5.3 Intertidal Response in Snohomish River Estuary

5.3.1 Temperature Increase

The Snohomish Estuary is predicted to be warmer under future climate conditions, with the highest temperature increases in the upstream portion of the estuary (Figure 5.5) away from mixing with the relatively cooler waters of Possession Sound that upwell on to the intertidal flats and distributaries. The difference in annual mean temperatures between the historical and future RCP8.5 scenarios is ≈1.75˚C in Possession Sound; however, the temperature difference is greater than 3˚C in the mainstem of the Snohomish River and Steamboat Slough.

Figure 5.6 shows the temporal variation in the Snohomish River estuary stations. Although all stations show temperature increases under climate change, the response varied depending on location relative to the river mouth. Simulation results at Lower Ebey Slough stations (EB1, EB2, EBF, and FWF) showed significant temperature increase in winter, but summer temperature increase was not as significant. In the historical scenario, QCF and SB1 stations showed high diurnal temperature fluctuation, indicating that their temperature was influenced by tides. In the future Y2095 RCP8.5 scenario, the tidal effects move further upstream and diurnal variation effects are also observed at the stations that are further upstream such as SB2 and MS3. For the remaining stations, temperatures rise about equal amount in winter and summer. Across all stations, the mean temperature increase predicted was 3.23˚C.

This result is interesting because the effect of future meteorology is already reflected in the SSM response that reaches Possession Sound, resulting in a muted temperature increase of ≈1.75˚C, benefitting from the circulation and mixing effects in the Salish Sea. The higher temperature in the intertidal flats and

upstream river stations of ≈3.23˚C reflect the effect of inflow temperatures from the Snohomish River that increase from mean temperature of 10.39˚C in the historic scenario to 14.33˚C in the future scenario, a Δ T of 3.94˚C.

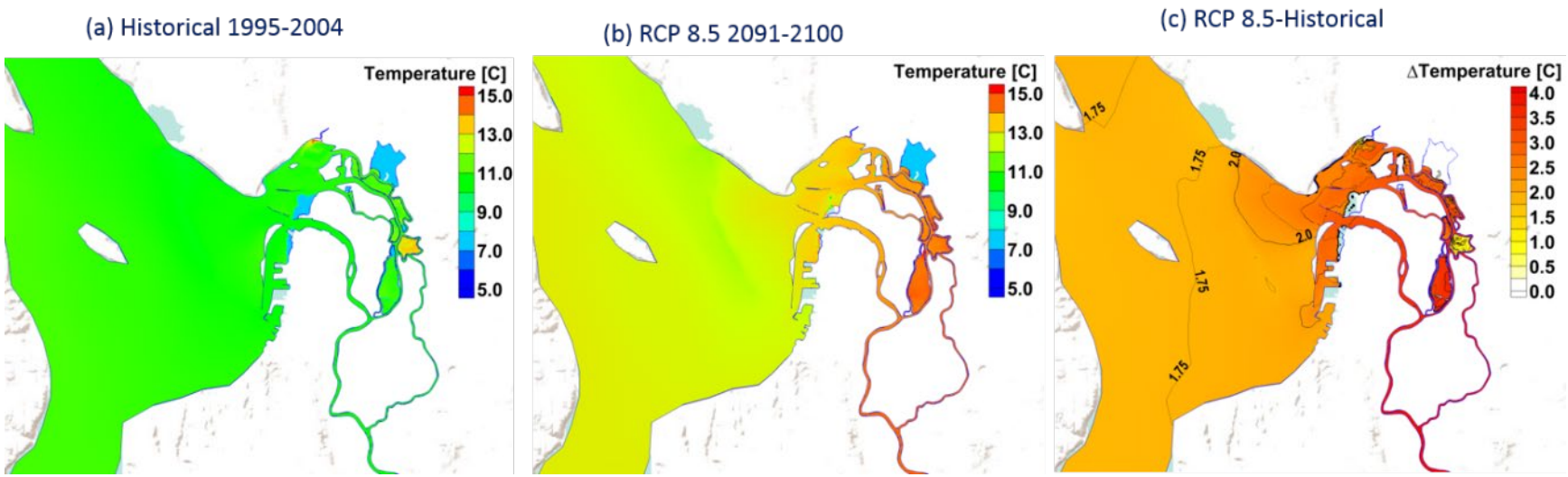

Figure 5.5. Snohomish Estuary Annual Mean Sea Surface Temperatures

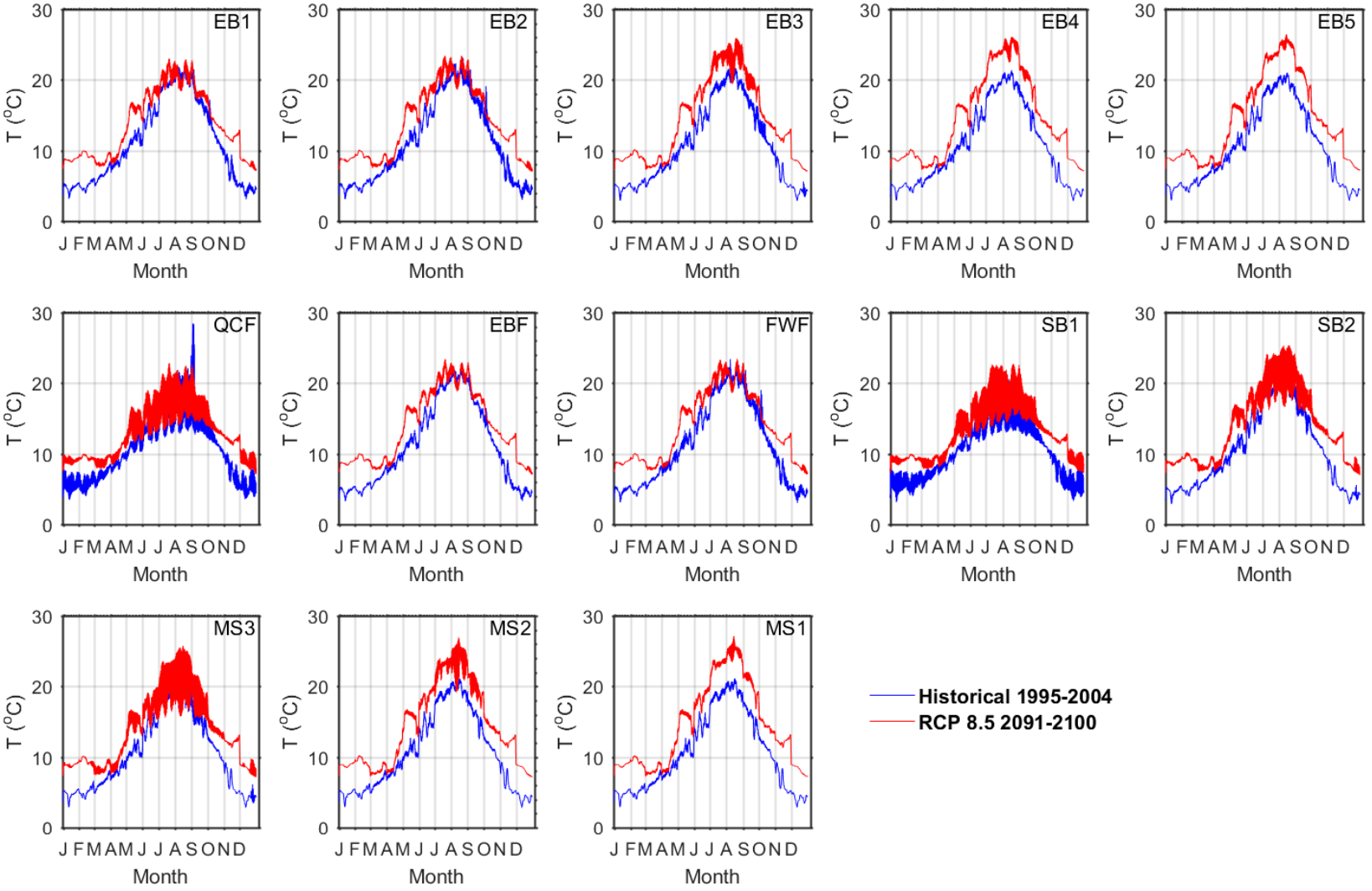

Figure 5.6. Temperature Comparisons at Snohomish River Estuary Stations

The Snohomish River estuary provides important habitat for juvenile salmon during their smoltification process. Fish rearing in the estuary includes endangered species like Coho salmon and bull trout. The state of Washington's spawning and rearing temperature criteria is 13˚C in estuaries, meaning that when temperatures exceed 13˚C, spawning and rearing fish may be negatively affected by the thermal stress. We used 13˚C as a temperature benchmark to quantify the ecological impacts of future temperature increases on fish habitat. Figure 5.7 shows the number of days when daily average temperatures exceeds 13˚C at the Snohomish Estuary stations under historical Y2000 and future Y2095 scenarios. Simulation results show that at most stations, the number of days in the future climate scenario increases by nearly 50%.

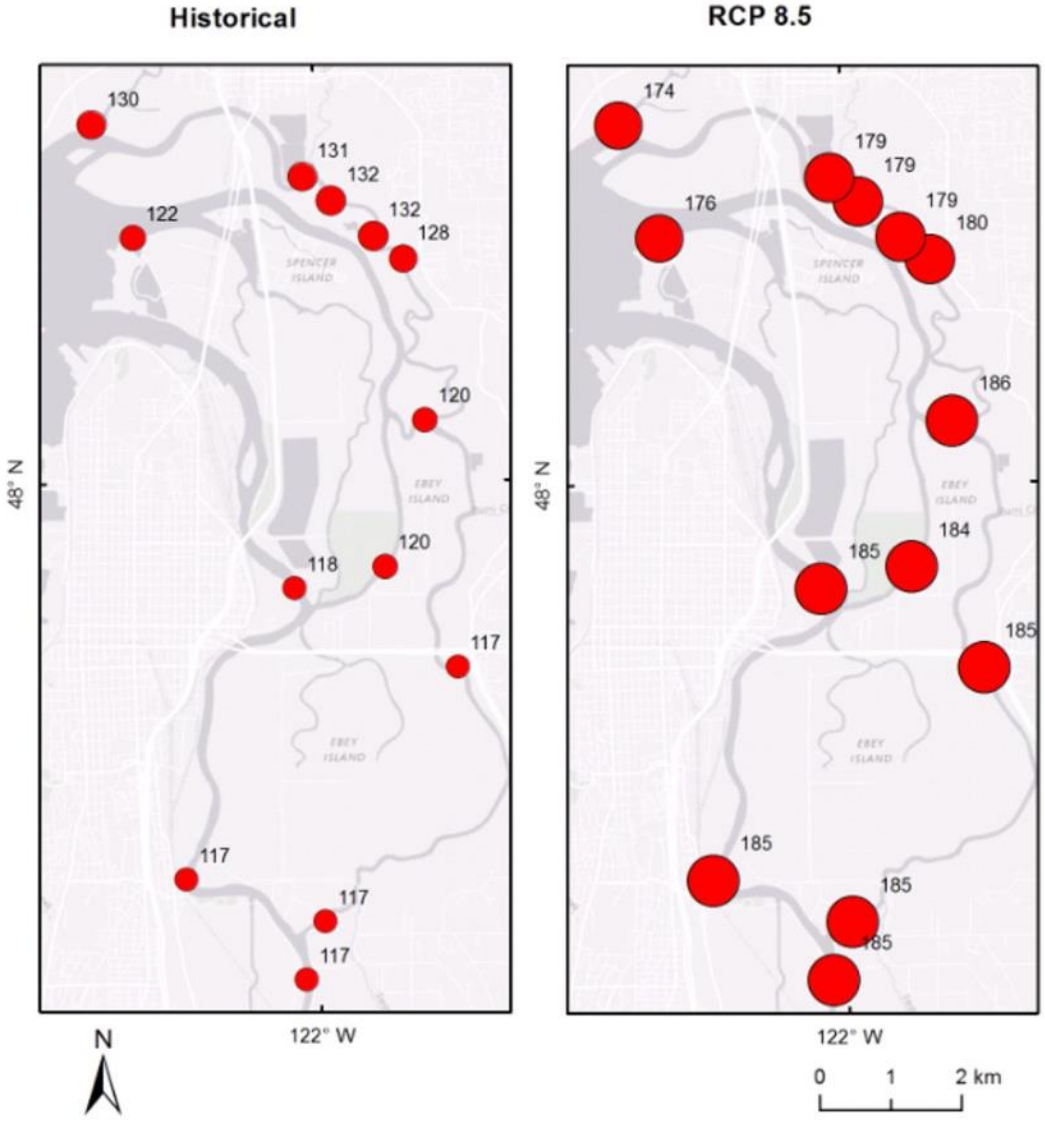

Figure 5.7. Count of Days Daily Mean Temperatures Exceed 13˚C

5.3.2 Sea Level Rise and Seawater Intrusion

In the future scenario, we assumed 1.5 m sea level rise at the ocean boundary, which is less than the global mean due to upward land movement in the Pacific Northwest. Our model results show that mean sea level rise over the Snohomish River Estuary stations is lower than the incident sea level rise over the continental shelf and Neah Bay. This is likely due to the difference in mean sea level data over the Snohomish River estuary shelf. The Snohomish stations experience an average rise of 1.3 m (Table 5.4).

Table 5.4. Annual Mean Sea Surface Elevation Rise in Future Scenario

Station	Elevation Rise (m)
EB1	1.34
EB2	1.34
EB3	1.35
EB4	1.32
EB5	1.11
QCF	1.36
EBF	1.33
FWF	1.33
SB1	1.37
SB2	1.34
MS3	1.35
MS2	1.22
MS1	1.10

Higher sea surface elevation during high tides results in increased seawater intrusion into the estuary. Figure 5.8 shows that water is more saline in the future Y2095 RCP8.5 scenario than the historical scenario. In Possession Sound, the simulation results show surface salinity increases by 1-2 psu. The lower Ebey Slough experiences the highest salinity increase of 6 psu.

Figure 5.9 shows temporal variation of salinity in Snohomish River estuary stations. In the historical scenario, eleven out of the 13 stations (EB1, EB2, EB3, EB4, EB5, EBF, EWF, SB2, MS1, MS2, and MS3) only experience a spike of salinity in late summer months when the freshwater flow is at its lowest. In the future scenario, these eleven stations experience a higher salinity (up to 25 psu) over longer duration, with some stations affected by seawater intrusion throughout the year.

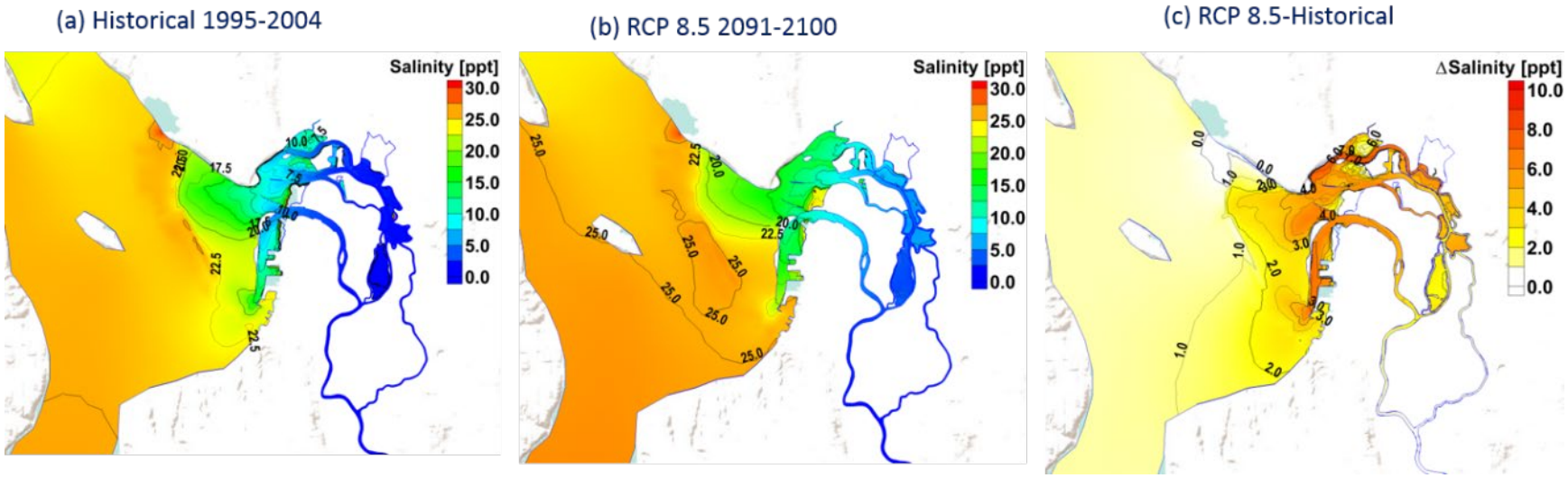

Figure 5.8. Snohomish Estuary Annual Mean Sea Surface Salinity

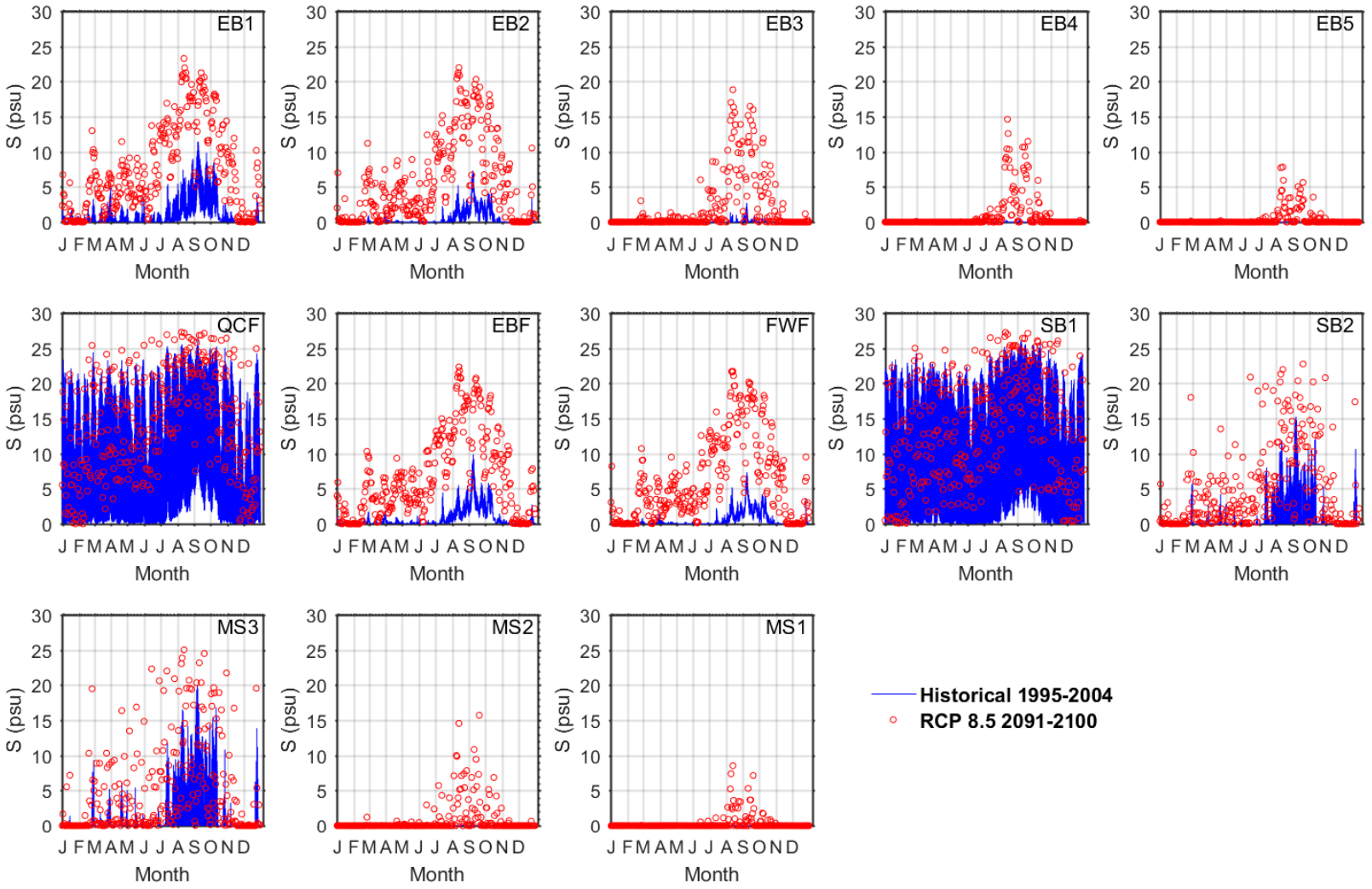

Figure 5.9. Salinity Comparisons at Snohomish River Estuary Stations

The salinity gradient in estuaries, from fresh to salt water, is necessary for juvenile salmonid to adapt to life in the marine environment. We used 5 psu, the upper bound of oligohaline condition (0.5-5.0 psu), to measure the extent of seawater intrusion in Snohomish Estuary and its ecological impacts on fish habitat. Figure 5.10 plots the count of days when daily maximum salinity exceeds 5 psu at the Snohomish River estuary stations. For Ebey Slough stations, for more than 200 days in a year the daily maximum salinity is predicted to exceed 5 psu in the future 2095 RCP8.5 scenario. This indicates the possibility of a large reduction of oligohaline habitat. A similar trend is observed at SB2 and MS3 stations. Salinity intrusion is predicted to reach as upstream as MS1 station and exceeds 5 ppt for 27 days during summer low-flow conditions.

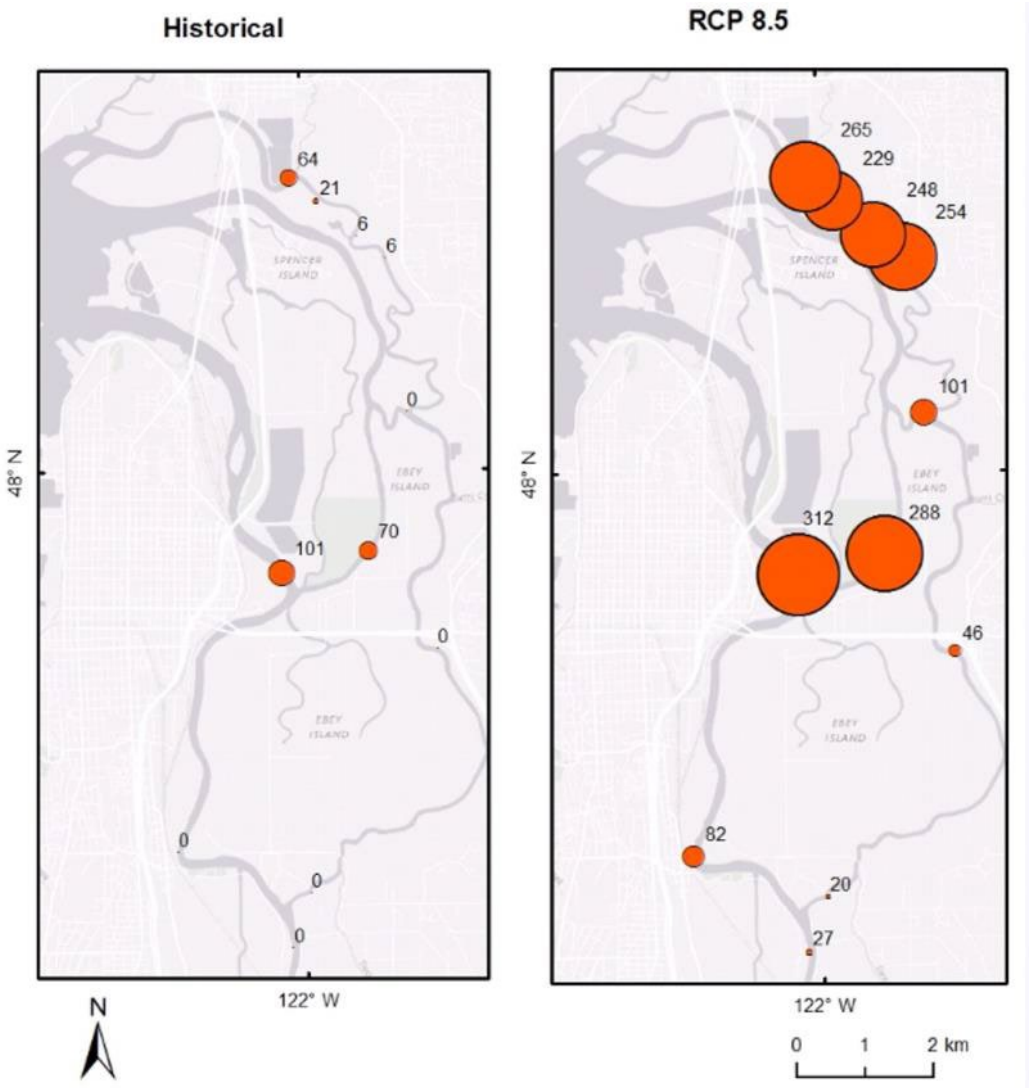

Figure 5.10. Count of Days with Maximum Salinity Above 5 psu

6.0 Summary and Conclusion

This section presents the results of SSM application to simulate hydrodynamic and water quality response in the Salish Sea using historical and future meteorological and hydrological inputs, and ocean boundary conditions including sea level rise. This was a proof-of-concept effort where the objective was to evaluate feasibility of simulating nearshore estuarine response using off-the-shelf products available from the climate change research community to provide the inputs and boundary conditions. This effort also evaluated whether SSM, used by water quality management agencies such as the EPA and Ecology, had sufficient resolution and sophisticated kinetics suitable for propagating the climate change effects into the nearshore coastal environment.

SSM has been improved recently with new kinetics for sediment diagenesis and carbonate chemistry. This project expanded the domain to encompass Vancouver Island and covering the continental shelf. The model ocean boundary was adjusted to align better with the shelf break. An added effort was made to refine the grid and test model performance in one of the Salish Sea sub-basins, the Snohomish River estuary. The SSM grid was refined to better represent the intertidal region including periodic wetting and drying. The effort focused on salinity and temperature response in the Snohomish River distributaries to future climate conditions. An improvement to heat flux routines was implemented that allowed the model to function in a stable manner in regions with shallow/dry or standing water.

The inputs and boundary conditions were obtained from the latest CMIP5 future climate predictions, a set of coordinated model experiments of future emissions scenarios that were simulated by numerous modeling groups around the world and used in the development of IPCC's 5th assessment report. The CESM global circulation model from the National Centre for Climate Research was selected for this study based on the availability of future ocean biogeochemistry directly from CESM and derived downscaled meteorological and hydrological predictions for the Pacific Northwest. Results were extracted from model scenarios corresponding to historical Y2000 emissions and a future Y2095 high-emission scenario titled RCP8.5.

Climate change effects on Salish Sea circulation and biogeochemistry were predicted relative to present conditions defined by a 10-year average of simulations from 1995 to 2004 representing the historic Y2000 scenario. The future scenario was defined by conditions averaged over a 10-year of simulation from 2091 to 2100 representing the future Y2095 RCP8.5 scenario. The historical conditions from downscaled CESM products were bias corrected to observed data and bias correction applied to inputs for future simulations with SSM.

6.1 Results and Findings

By comparing SSM simulations under the historical and future RCP8.5 scenarios, potential climate change impacts on the Salish Sea were quantified. These results are caveated by the limitations described in the next chapter below. Consistent with the premise that the scope of this effort was a proof-of-concept assessment, only major results are summarized below:

- Salish Sea-wide warming is predicted in the future. Annual mean water temperature inside the Salish Sea is predicted to increase by 1.77˚C in the future Y2095 RCP8.5 scenario. The warming, especially at estuaries and inner bays, are likely to increase exposure to high temperatures indicating potential for increased thermal stress for the ecosystem.
- Maximum area of near-bed hypoxia (DO <2mg/L) is predicted to occupy as much as 16% of the Salish Sea and the majority of Hood Canal in the future Y2095 RCP8.5 scenario. Annual mean Salish Sea-wide DO is predicted to decrease by 0.7 mg/L.
- Model simulations predict that higher temperatures in the future have the potential to cause algal species shifts. Based on the simple kinetics in the model, dinoflagellates were favored (increase by 196%) and diatoms were hindered (decrease by 14%). The overall annual mean algal biomass is predicted to increase by 23% in the RCP8.5 simulation relative to historical levels as a result of higher temperatures and higher nutrient loads.
- A 9% higher concentration of nitrates in the tidally averaged estuarine inflow from the Pacific Ocean, 44% increase in nitrate loads from rivers, and near doubling of wastewater inflows is estimated for future Y2095 RCP8.5 scenario.
- Ocean acidification effects propagate with a Salish Sea-wide mean pH reduction of 0.12 units predicted in the future Y2095 RCP8.5 simulation relative to historical levels.
- The temperature increase, DO depletion, and pH reduction levels listed above are domain-wide averages that are considerably muted relative to levels at the ocean boundaries and inflows. The strong vertical circulation and mixing with the Salish Sea and biogeochemical activity in the inner Salish Sea sub-basins provide a buffering effect reducing the impacts from global temperature increase, DO depletion, and acidification.
- The intertidal reaches of the Snohomish River estuary, an inner Salish Sea sub-basin, is predicted to experience up to 3˚C annual mean surface temperature increase based on RCP8.5 simulation. The projected temperature-increase in the estuary relative to historical conditions is dominated by the temperature increase from Snohomish River inflow over the delta.
- As a result of sea level rise, seawater intrusion frequency and distance are predicted to increase. In the future Y2095 RCP8.5 scenario, salinity intrusion is predicted to extend as far upstream as RKM 18 relative to RKM 7 in historical conditions.

6.2 Model Limitations

All models have errors and limitations that arise from a combination of simplification of complex hydrodynamic and biogeochemical processes in the mathematical formulation, errors in the discretization solution scheme, lack of adequate site-specific data, and temporal and spatial resolution in model inputs and forcing parameters. Understanding model limitations is essential to ensure that application results are not misused or applied beyond their intended performance design and the deliverables presented are correctly interpreted. The following is a list of model limitations and model interpretation guidelines.

- Projections of future climate vary across different GCMs due to several reasons, such as: (1) uncertainty in forcing applied, (2) differences in parametrizations, and (3) internal variability associated with each model. One common approach for reducing the uncertainty is the use of an ‘ensemble’, where the mean across several models is used to indicate the general direction of change.

Studies of atmospheric activities have shown that using multiple high-performing models can reduce the bias introduced by an individual model. The challenges of using multiple models are primarily computational costs and availability of downscaled global atmospheric data to the Salish Sea region for meteorology, hydrology, and ocean biogeochemistry. Rupp et al. (2013) and Gao et al. (2014) showed that CESM ranks among the top CMIP5 models with regards to its ability to simulate Pacific Northwest climate and the multi-model mean for both temperature and precipitation and was selected for this study. However, it is still a single model and inputs for historical and future scenarios were developed using results from only the CESM. We therefore recommend that the results presented be tested against similar simulations with multiple downscaled products to increase in the confidence level of these future projections.

- The hydrological boundary conditions for SSM were developed using downscaled river flow and temperature from a relatively coarse resolution (one-eighth of a degree) national-scale hydrological model. The procedure for developing flow and water quality inputs for SSM relied on hydrological procedure based on multi-variate regression relations developed from monitoring data. Significant bias correction was needed to match observed historical hydrological records within the Salish Sea. It was assumed that the bias corrections and hydrological regression-based procedures were valid in the present/historical and future scenarios. The hydrological boundary conditions can be improved by using a finer resolution routing model for distributing flows from downscaled products.
- Effects of future population change and land use on water quality variables could only be computed for nitrogen loads using the procedure developed by Ecology. Inputs to SSM from river and wastewater loads reflect change in nitrogen concentrations from future land-use change; however, concentrations of other river water quality variables were left unchanged. The model results may be improved in the future by using physics-based river water quality models or statistical methods to project future concentrations of variables such as DO, DOC, particulate organic carbon, alkalinity, DIC, pH, and PO4.
- The results presented in this report were generated using uniform meteorological forcing as a simplification. The available downscaled meteorological data were available on 0.125 deg (≈14 km.) resolution allowing only a limited number of data points inside the Salish Sea domain. The results could be improved in the future using downscaled results generated from a finer 4 km grid distributed meteorological forcing.
- The results indicate a potential future impact on suitable fish habitat in estuaries due to seawater intrusion and temperature increase based on present use. As the estuarine mixing zone moves upstream due to sea level rise, it is likely that geomorphological changes will occur, and suitable habitat may form in upstream reaches. Geomorphological changes associated with sediment transport, erosion, and deposition were not considered in this effort.

6.3 Conclusion

Prior research recommends integrated modeling of multiple stressors to realistically assess climate change impacts on coastal ecosystems. This report summarizes an integrated assessment, where cumulative effects of multiple stressors were examined, including sea level rise, air temperature increase, river temperature increase, urbanization, and ocean chemistry changes on Salish Sea hydrodynamics and biogeochemistry. The model used was an unstructured grid FVCOM-ICM to simulate the response of Salish Sea to climate change and sea level rise scenarios.

Global climate models within the framework of CMIP5 experiments as part of IPCC 5th assessment report were reviewed. The CESM model results available from the National Center for Atmosphere Research and associated downscaled products from PNNL were selected to construct inputs and boundary conditions for SSM. The future emissions scenario RCP8.5, the projected most-extreme scenario available in CMIP5, was used to examine the impacts on the Salish Sea in combination with a sea level rise of 1.5 m. Future impacts were computed for Y2095 relative to historical conditions of Y2000.

The model results show that under the RCP8.5 scenario, at the Salish Sea scale, several changes are predicted. These changes, driven primarily by global changes, include overall warming, depletion of DO levels, algal species shift towards those with preference for higher temperatures, and continued ocean acidification. However, the results provide a new finding that the Salish Sea response in the future is less severe in magnitude when compared to the response of the outer ocean. The apparent resilience is attributed to benefits from the existence of strong estuarine circulation and healthy primary production. At the intertidal scale, the combined effects of the warming freshwater streamflow and seawater intrusion have the potential to reduce the available fish habitat in estuaries such as the Snohomish River estuary based on simulated future scenarios.

This study accomplished the primary objective to demonstrate the feasibility of using a leading coastal estuarine hydrodynamic and biogeochemical model to propagate climate change effects from a global scale to the nearshore estuarine scale. Downscaled products from global climate change experiments of future emissions scenarios are available for major U.S. coastal estuaries, such as the Chesapeake Bay and Salish Sea. These products may be used for testing the response in the nearshore environment using a suitable coastal ocean model that has been tested and reached an acceptable level of robustness and maturity. The SSM developed by PNNL in collaboration with Ecology with funding from the EPA demonstrated a readiness level for this assessment and successfully simulated Salish Sea response to future climate conditions.

7.0 References

Albertson SL, J Bos, G Pelletier, and M Roberts. 2007. *Estuarine flow into the south basin of Puget Sound and its effects on near-bottom dissolved oxygen*. Washington Department of Ecology, Olympia, Washington.

Albertson SL, K Erickson, JA Newton, G Pelletier, RA Reynolds, and M Roberts. 2002. *South Puget Sound Water Quality Study Phase 1*. Washington Department of Ecology, Olympia, Washington.

Barnes CA and EE Collias. 1958. Some considerations of oxygen utilization rates in Puget Sound. *J Mar Res* 17(1):68-80.

Brocca L, S Hasenauer, T Lacava, F Melone, T Moramarco, W Wagner, and J Latron. 2011. Soil moisture estimation through ASCAT and AMSR-E sensors: An intercomparison and validation study across Europe. *Remote Sensing of Environment*, 115(12), 3390-3408.

Cerco C, SC Kim, and N Noel. 2010. *2010 Chesapeake Bay Eutrophication Model – 1080 A Report to the US Environmental Protection Agency Chesapeake Bay Program and to The US Army Engineer Baltimore District.* U.S. Army Engineer Research and Development Center, Vicksburg, Mississippi.

Collins BD and AJ Sheikh. 2005. *Historical Reconstruction, Classification, and Change Analysis of Puget Sound Tidal Marshes*. Prepared for the Washington Department of Natural Resources. University of Washington, Seattle, Washington.

Embrey SS and EL Inkpen. 1998. *Water-Quality Assessment of the Puget Sound Basin, Washington, Nutrient Transport in Rivers, 1980-93. U.S. Geological Survey Water Quality Investigations Report*. U.S. Geological Survey 97-4270. bhttp://pubs.er.usgs.gov/publication/wri974270.

Fairall CW, EF Bradley, JE Hare, AA Grachev, & JB Edson. 2003. Bulk parameterization of air–sea fluxes: Updates and verification for the COARE algorithm. *Journal of climate*, *16*(4), 571-591.

Gao Y, LR Leung, J Lu, Y Liu, M Huang, & Y Qian. 2014. Robust spring drying in the southwestern US and seasonal migration of wet/dry patterns in a warmer climate. Geophysical Research Letters, 41(5), 1745-1751.

Hurrell JW, MM Holland, PR Gent, S Ghan, JE Kay, PJ Kushner, and WH Lipscomb. 2013. "The community earth system model: a framework for collaborative research." *Bulletin of the American Meteorological Societ*y, 94(9), 1339-1360.

Hejazi MI, N Voisin, L Liu, LM Bramer, DC Fortin, JE Hathaway, and Y Liu. 2015. "21st century United States emissions mitigation could increase water stress more than the climate change it is mitigating." *Proceedings of the National Academy of Sciences*, 112(34), 10635-10640.

Ianson et al. (2017) Personal communication from Debby Ianson of Department of Fisheries and Oceans, Canada to L. Bianucci of PNNL, Seattle, WA.

IPCC. 2014. *Climate Change 2014: Synthesis Report. Contribution of Working Groups I, II and III to the Fifth Assessment Report of the Intergovernmental Panel on Climate Change.* Core Writing Team: RK Pachauri and LA Meyer (eds.)]. IPCC, Geneva, Switzerland, 151 pp.

Irby ID, MAM Friedrichs, CT Friedrichs, AJ Bever, RR Hood, LWJ Lanerolle, M Li, L Linker, ME Scully, K Sellner, J Shen, J Testa, H Wang, P Wang, and M Xia. 2016. "Challenges associated with modeling low-oxygen waters in Chesapeake Bay: a multiple model comparison." *Biogeosciences*, 2011-2028. doi: 10.5194/bg-13-2011-2016. ***Open Access.***

Jiang L and M Xia. 2016. "Dynamics of the Chesapeake Bay outflow plume Realistic plume simulations and its seasonal, interannual variability." *Journal of Geophysical Research: Oceans* 121 (2), 1424-1445.

Kay JE, C Deser, A Phillips, A Mai, C Hannay, G Strand, J Arblaster, S Bates, G Danabasoglu, J Edwards, M Holland, P Kushner, JF Lamarque, D Lawrence, K Lindsay, A Middleton, E Munoz, R Neale, K Oleson, L Polvani, and M Vertenstein. 2015. "The Community Earth System Model (CESM) Large Ensemble Project: A Community Resource for Studying Climate Change in the Presence of Internal Climate Variability." *Bulletin of the American Meteorological Society*, doi: 10.1175/BAMS-D-13-00255.1, 96, 1333-1349.

Khangaonkar T, W Long, and W Xu. 2017. "Assessment of circulation and inter-basin transport in the Salish Sea including Johnstone Strait and Discovery Islands pathways." *Ocean Modelling*, 109, 11-32.

Khangaonkar T, A Nugraha, W Xu, W Long, L Bianucci, A Ahmed, T Mohamedali, and G Pelletier. (Under review December 2017). "Analysis of Hypoxia and Sensitivity to Nutrient Pollution in Salish Sea." JGR-Oceans.

Li H, MS Wigmosta, H Wu, M Huang, Y Ke, AM Coleman, and LR Leung. 2013. "A physically based runoff routing model for land surface and earth system models." *Journal of Hydrometeorology*, 14(3), 808-828.

Li HY, L Ruby Leung, T Tesfa, N Voisin, M Hejazi, L Liu, and X Yang. 2015. "Modeling stream temperature in the Anthropocene: An earth system modeling approach." *Journal of Advances in Modeling Earth Systems*, 7(4), 1661-1679.

Lindsay K, GB Bonan, SC Doney, FM Hoffman, DM Lawrence, MC Long, and PE Thornton. 2014. "Preindustrial-control and twentieth-century carbon cycle experiments with the Earth system model CESM1 (BGC)." *Journal of Climate*, 27(24), 8981-9005.

Newton JA, AL Thomson, LB Eisner, GA Hannach, and SL Albertson. 1995. "Dissolved oxygen concentrations in Hood Canal: are conditions different than forty years ago?" Puget Sound Research '95 Proceedings, Puget Sound Water Quality Authority, Olympia, Washington, pp. 1002–1008.

Gent PR, G Danabasoglu, LJ Donner, MM Holland, EC Hunke, SR Jayne, and PH Worley. 2011. "The community climate system model version 4." *Journal of Climate*, 24(19), 4973-4991.

Mohamedali T, M Roberts, B Sackmann, and A Kolosseus. 2011. *Puget Sound Dissolved Oxygen Model Nutrient Load Summary for 1999-2008*. Washington State Department of Ecology, Olympia, Washington. Publication No. 11-03-057.

Moss RH, JA Edmonds, KA Hibbard, MR Manning, SK Rose, DP Van Vuuren, and GA Meehl. 2010. "The next generation of scenarios for climate change research and assessment." *Nature*, 463(7282), 747-756.

Paulson A, C Konrad, L Frans, M Noble, C Kendall, E Josberger, R Huffman, and T Olsen. 2006. *Freshwater and Saline Loads of Inorganic Nitrogen to Hood Canal and Lynch Cove, Washington.* U.S. Geological Survey in cooperation with Hood Canal Dissolved Oxygen Program. Scientific Investigations Report 2006–5106. www.pubs.usgs.gov/sir/2006/5106.

PSAT. 2007. *2007 Puget Sound Update: Ninth Report of the Puget Sound Assessment and Monitoring Program.* Puget Sound Action Team. Olympia, Washington. 260 pp.

Roberts M, J Bos, and SL Albertson. 2008. *South Puget Sound Dissolved Oxygen Study Interim Data Report.* Washington Department of Ecology, Olympia, Washington.

Roberts M, T Mohamedali, and B Sackmann. 2014. *Puget Sound and the Straits Dissolved Oxygen Assessment: Impacts of Current and Future Human Nitrogen Sources and Climate Change Through 2070.* Washington State Department of Ecology, Environmental Assessment Program, Olympia, Washington.

Rupp, DE, JT Abatzoglou, KC Hegewisch, & PW Mote. (2013). Evaluation of CMIP5 20th century climate simulations for the Pacific Northwest USA. Journal of Geophysical Research: Atmospheres, 118(19).

Simenstad C**,** M Ramirez, J Burke, M Logsdon, H Shipman, C Tanner, J Toft, B Craig, C Davis, J Fung, P Bloch, K Fresh, S Champbell, D Myers, E Iverson, A Bailey, P Schlenger, C Kiblinger, P Myre, WI Gertsel, and A MacLennan. 2011. *Historical Change and Impairment of Puget Sound Shorelines: Atlas and Interpretation of Puget Sound Nearshore Ecosystem Restoration Project Change Analysis*. Puget Sound Nearshore Ecosystem Restoration Project, Technical Report 2011-01.

Stockner JG, DD Cliff, and KRS Shortreed. 1979. "Phytoplankton Ecology of British Columbia." *Journal of the Fisheries Research Board of Canada*, **36**, 657–666

Sutherland DA, P MacCready, NS Banas, and LF Smedstad. 2011. "A model study of the Salish Sea estuarine circulation." *Journal of Physical Oceanography*, 41(6), 1125-1143.

Taylor KE, RJ Stouffer, and GA Meehl. 2012. "An overview of CMIP5 and the experiment design." *Bulletin of the American Meteorological Society*, 93(4), 485-498.

Ye F, YJ Zhang, HV Wang, MA Friedrichs, ID Irby, A Valle-Levinson, J Shen, Z Wang, H Huang, J Shen, and J Du. 2017. *Assessment of a 3D Unstructured-Grid Model for the Chesapeake Bay and Adjacent Shelf: Supplementary Materials.* Virginia Institute of Marine Science, College of William & Mary. doi:10.21220/V5HK5S

Wood AW, LR Leung, V Sridhar, and DP Lettenmaier. 2004. “Hydrologic implications of dynamical and statistical approaches to downscaling climate model outputs.” *Climatic Change* **62**: 189–216.

Appendix A: Ocean Boundary Conditions from CESM Verification and Bias Correction

A.1 Temperature and Salinity Ocean Boundary Conditions Verification

Figure A.1 shows the temperature and salinity profile comparisons between the CESM historical scenario and DFO measurements. Node 45, which is in the middle of 87 SSM boundary nodes, is used as an example node for all the plots. Because the DFO OBC profiles are only available for 5 years (2000-2004) within the historical scenario timeframe of 1995-2004, we compared the CESM profiles with individual years from 2000-2004 from DFO, but also an ensemble mean of 2000-2004 DFO profiles to represent the climatological mean. Temperature mean error is 0.34˚C and RMSE is 1.02˚C. The CESM temperature profiles are within the variation of the DFO individual year profiles, indicating that CESM derived OBC is consistent with reality.

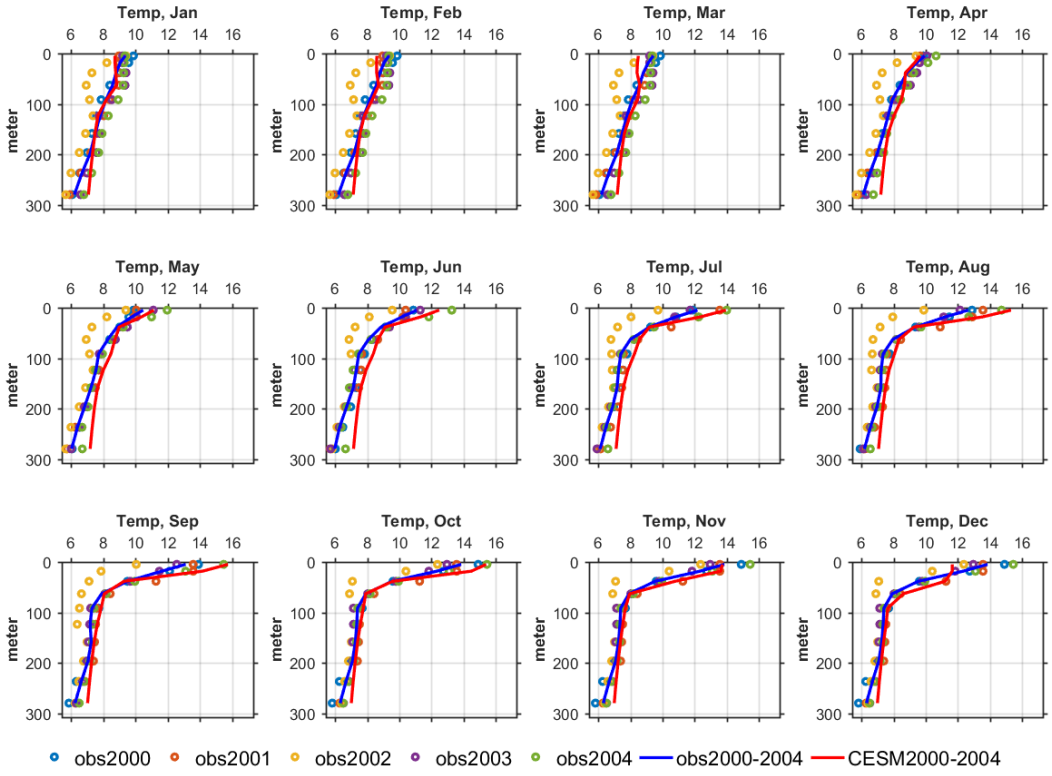

Figure A.1 Comparison of SSM Node 45 Temperature Profiles

The CESM salinity profiles are overall underestimating the salinity at the ocean boundary, but the bias is small. Salinity mean error is -0.54; RMSE is 0.6 (Figure A.2). Hence, CESM temperature and salinity OBC profiles are used as model inputs without bias correction required.

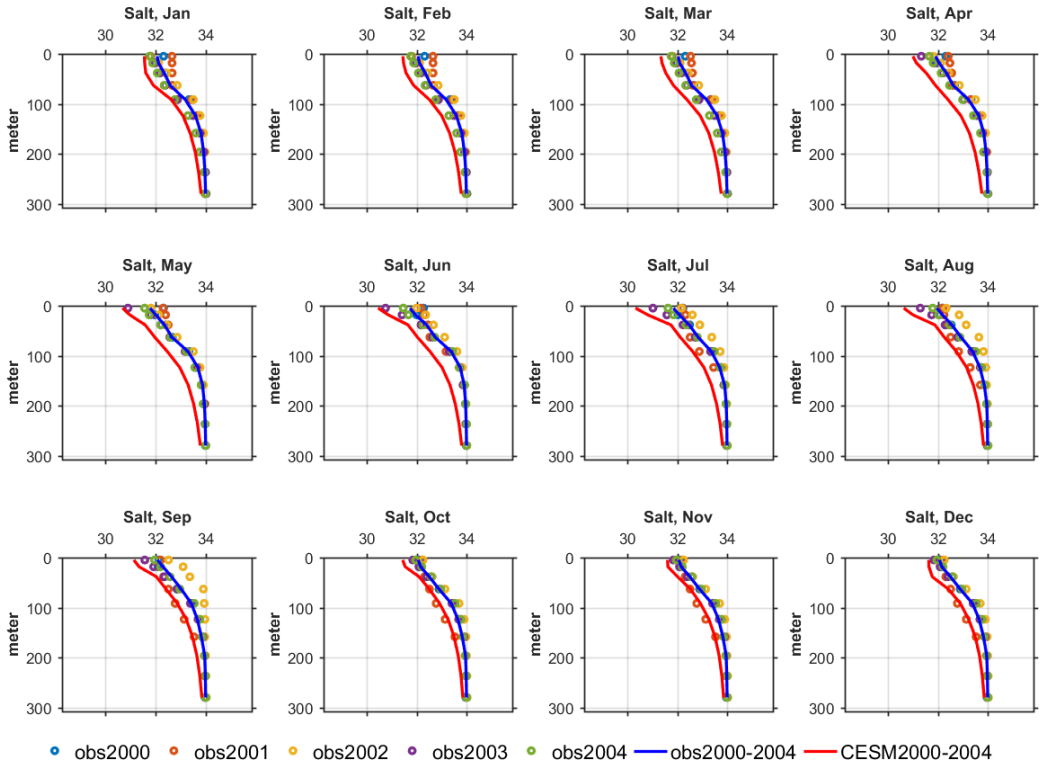

Figure A.2. Comparison of SSM Node 45 Salinity Profiles

A.2 Water Quality Ocean Boundary Conditions

The water quality profiles from the CESM historical scenario and DFO were compared and Node 45, which is in the middle of 87 SSM boundary nodes, was used as an example node for all the plots. CESM-derived OBC profiles were overestimating DO and underestimating NO3 and PO4. Constant values, either positive or negative, were added to water quality profiles as a simple approach for bias correction.

CESM-derived OBC profiles correctly predicted bottom algal concentration as close to zero, although surface algal concentrations were underestimated. Since the ocean boundary inflow was mostly at the bottom, the algal concentrations were not bias corrected.

The bias correction values being applied to CESM-derived OBC water quality profiles are summarized in Table A.1; other variables are not bias corrected due to lack of DFO data to compare with. Figure A.3 through Figure A.8 are the CESM water quality OBC profiles compared with DFO before and after bias corrections. Figure A.9 and Figure A.10 show the CESM algal concentration OBC profiles compared with DFO without bias correction.

Table A.1. Water Quality OBC from CESM Bias Correction Summary

Variable	FVCOM Units	Bias Correction
NH4	gN/m^3	
NO3	gN/m^3	0.085
PO4	gP/m^3	0.012
ALK	mmol/m^3	
DIC	mmol/m^3	
DO	mgO2/L	-0.7
Dinoflagellates Chlorophyll (Algae 2)	gC/m^3	
Diatom Chlorophyll (Algae 1)	gC/m^3	
DOC	gC/m^3	
DON	gN/m^3	
DOP	gP/m^3	

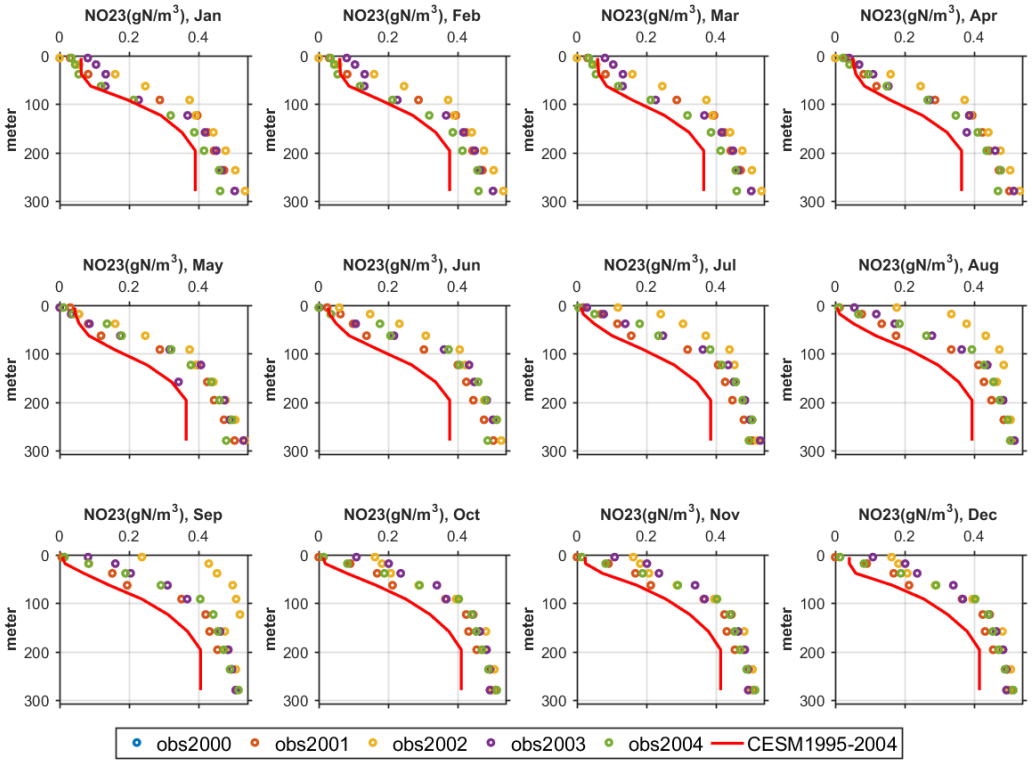

Figure A.3. Comparison of SSM Node 45 NO3 Profiles Before Bias Correction

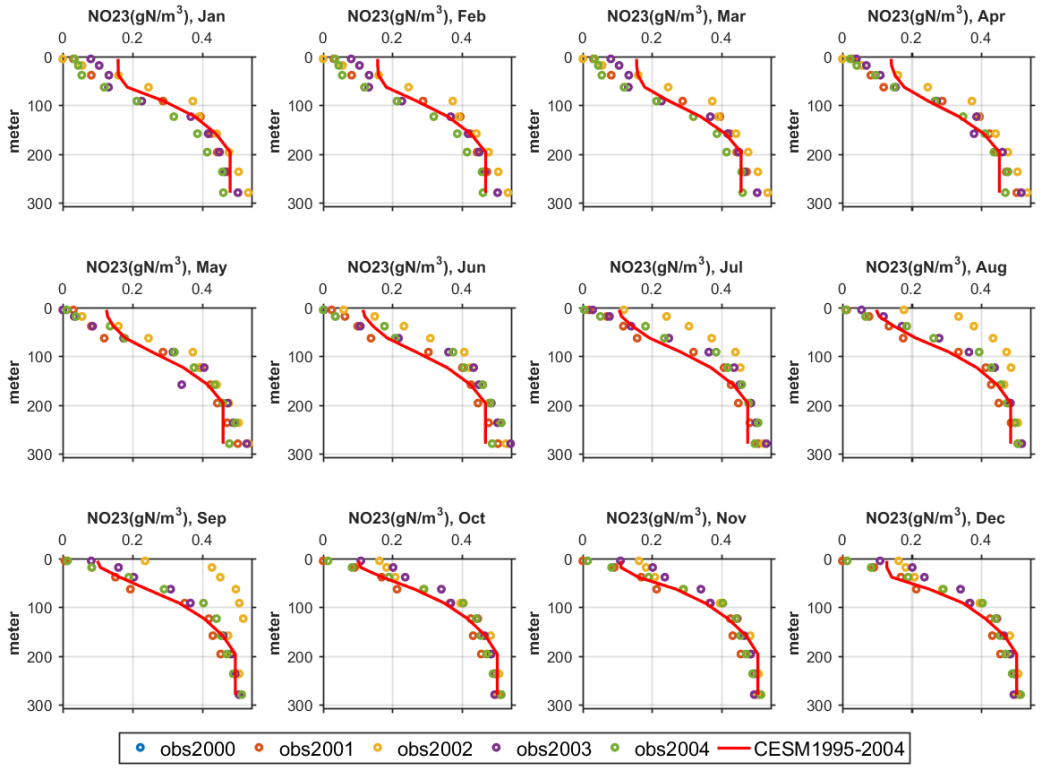

Figure A.4. Comparison of SSM Node 45 NO3 Profiles After Bias Correction

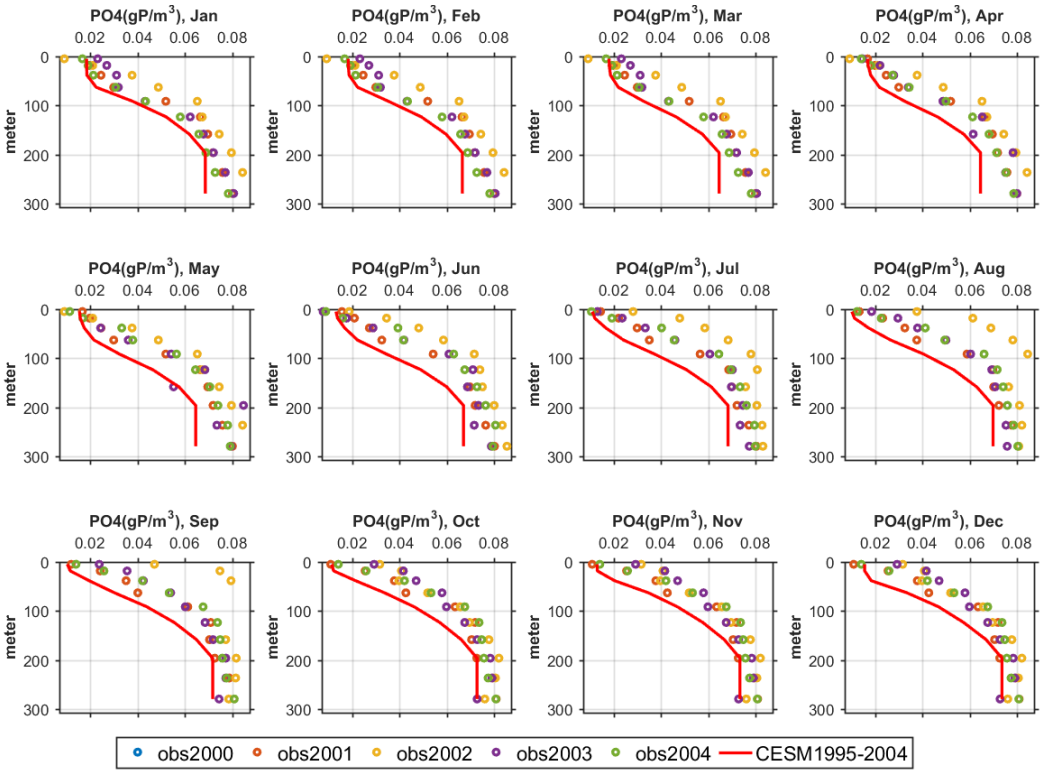

Figure A.5. Comparison of SSM Node 45 PO4 Profiles Before Bias Correction

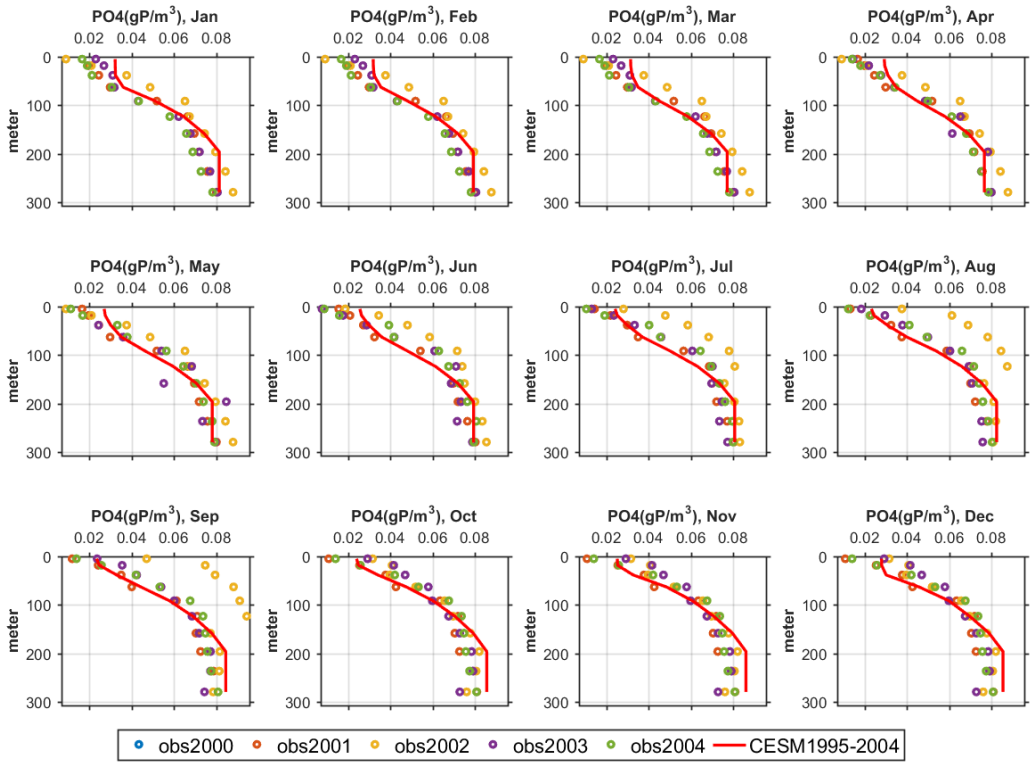

Figure A.6. Comparison of SSM Node 45 PO4 Profiles After Bias Correction

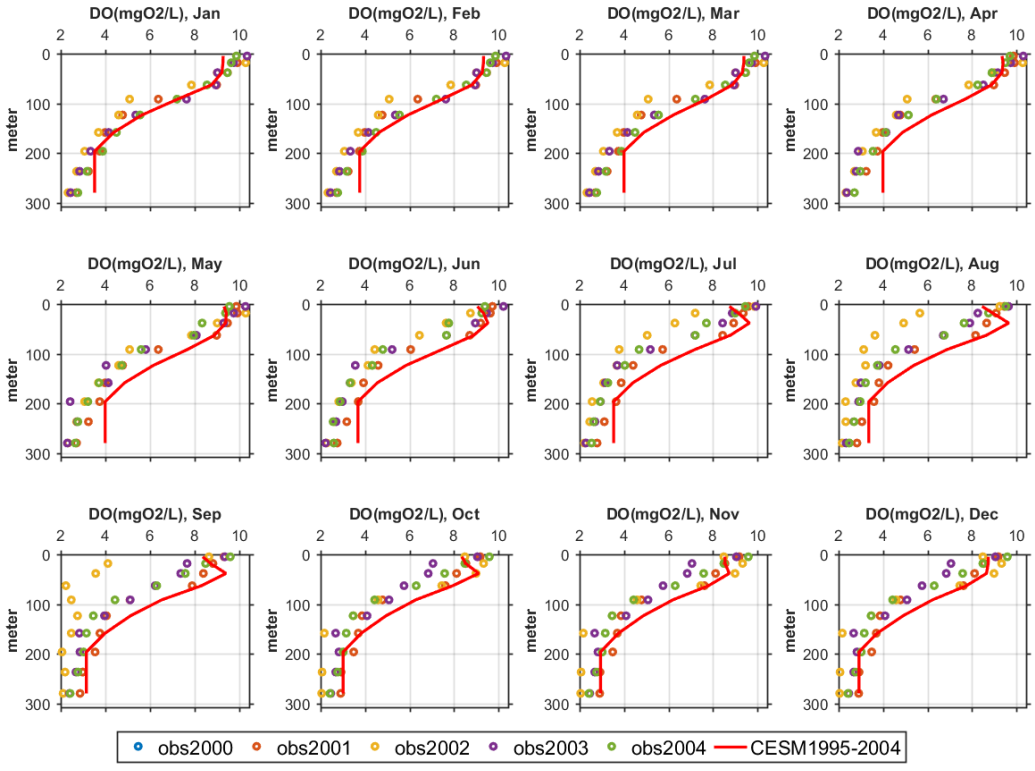

Figure A.7. Comparison of SSM Node 45 DO Profiles Before Bias Correction

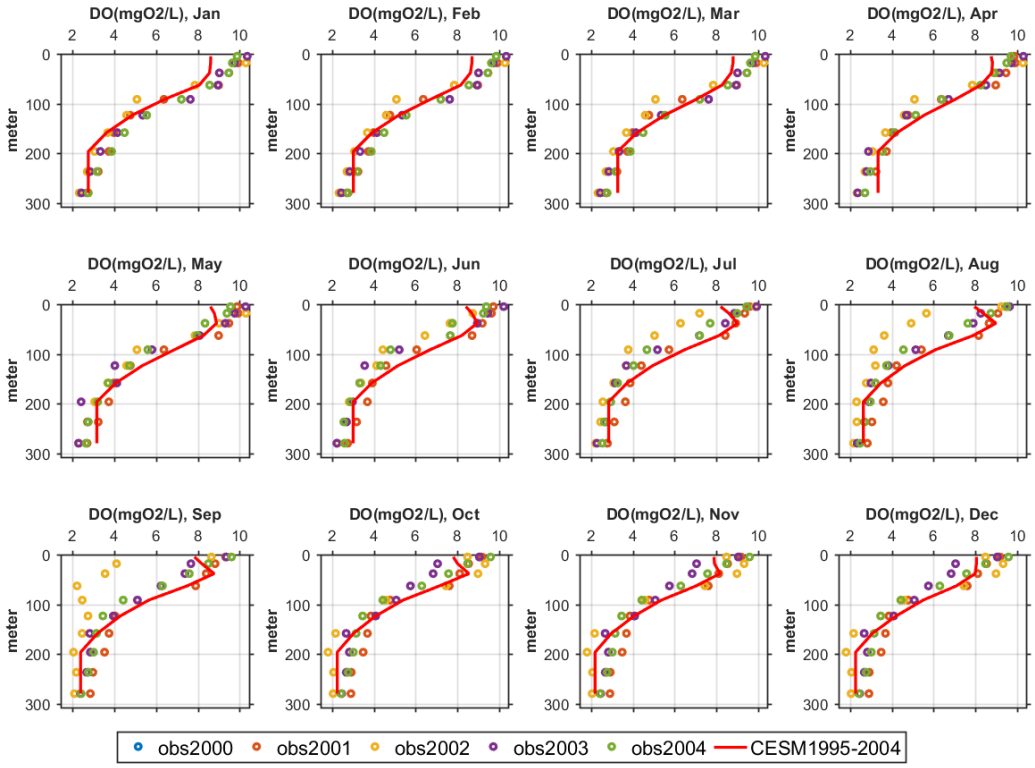

Figure A.8. Comparison of SSM Node 45 NO3 Profiles Before Bias Correction

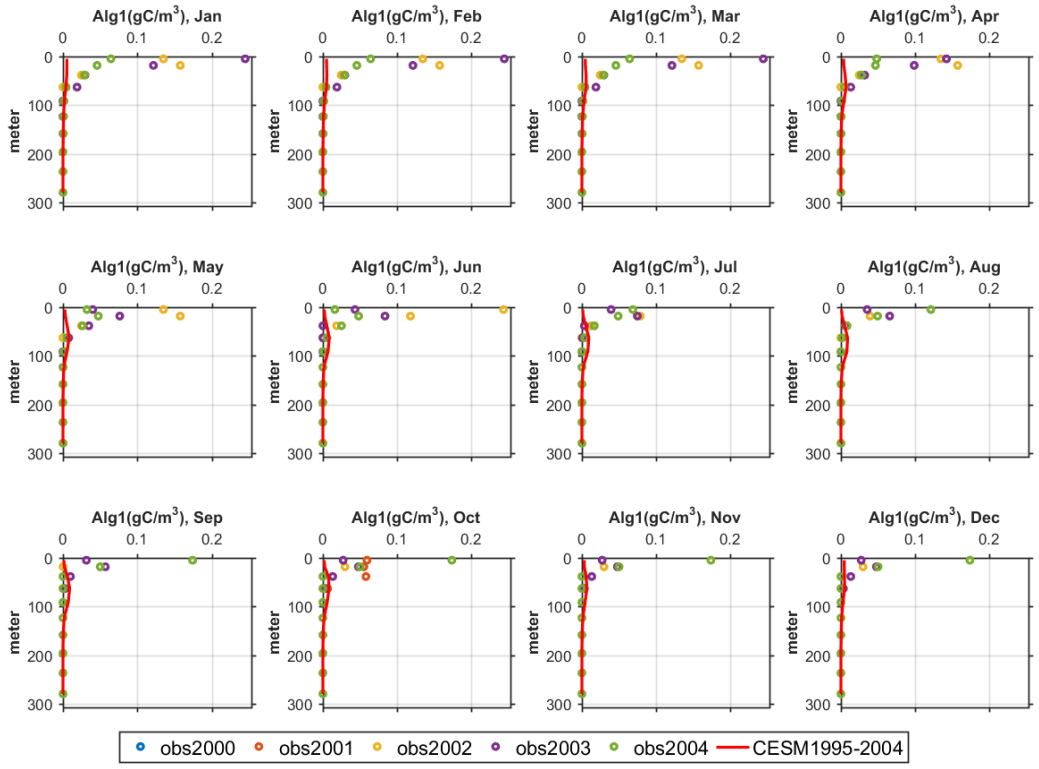

Figure A.9. Comparison of SSM Node 45 ALG1 Profiles Without Bias Correction

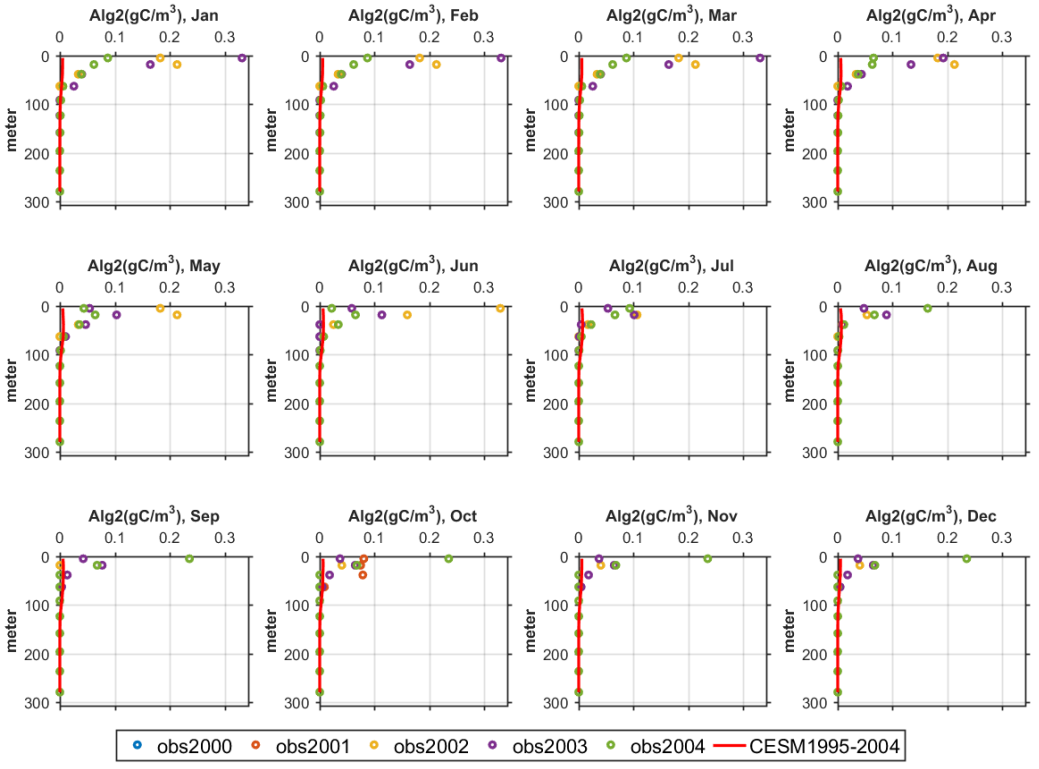

Figure A.10. Comparison of SSM Node 45 ALG2 Profiles Without Bias Correction

Appendix B: FVCOM-ICM Model Equations

Biogeochemical Model Kinetics for Algae, Nitrate, and DO

Phytoplankton (gC/m^3)

Two groups of algae are simulated, B_1 (diatoms) and B_2 (dinoflagellates). Equations for change in algal biomass are as follows

$$\frac{dB_1}{dt} = NP_{B1} - PR_1 - WS_{B1} \times dB_1/dz$$

where NP_{B1} is the net primary production defined as:

$$NP_{B1} = (P_1.min(NL_1, PL_1) \times (1 - \gamma_1)/\alpha_{CCHL1} - BM_1) \times B_1 ,$$

and

$$P_1 = PM_1 \times f_{PM}(T) \times FI_1$$

where $f_{PM}(T)$ is the temperature control on algal growth rate (0-1), and NL_1, PL_1, and FI_1 are the nitrogen, phosphorous, and light limitation parameters respectively that vary from 0-1. γ_1 is the fraction of photosynthesis that is lost due to photochemical respiration (0-1). α_{CCHL1} is carbon to chlorophyll ratio ($gC/gCHL$). PM_1 is the maximum photosynthesis rate ($gC/gCHL/day$). BM_1 is the rate of biomass loss due to basal metabolism (1/day). PR_1 is the rate of loss due to predation ($gC/m^3/day$). WS_{B1} is the algal settling speed (m/day). Equations for B_2 are similar with the subscript 2 to represent the second algae group.

Nitrate (gN/m^3)

Change in nitrate concentration is described by the equation

$$\frac{dNO3}{dt} = NT - \alpha_{NC} \times DN - NO3_{A1} - NO3_{A2}$$

where NT is the gain of nitrate ($gN/m^3/day$) due to nitrification.

DN ($gC/m^3/day$) is the loss of labile DOC due to denitrification and α_{NC} is the stoichiometric ratio of NO3 to labile DOC in denitrification (gN/gC) and is governed by the equation.

$$DN = K_{LDOC} \times \alpha_{ANOX} \times \left[\frac{K_{HO,DOC}}{K_{HO,DOC} + O_2} \right] \times \left[\frac{NO3}{K_{HNDN} + NO3} \right] \times LDOC$$

where K_{LDOC} is labile DOC respiration rate (1/day). α_{ANOX} is the ratio of denitrification to oxic carbon respiration rate (0-1), $K_{HO,DOC}$ is the half-saturation concentration of dissolved oxygen for oxic respiration (gO_2/m^3). K_{HNDN} is the half-saturation concentration of nitrate for denitrification (gN/m^3). Labile DOC is the concentration of labile dissolved organic matter (gC/m^3). $NO3_{A1}$ ($gN/m^3/day$) is the uptake of NO3 by first algae group, $NO3_{A2}$ is the uptake of NO3 by the second algae group.

Oxygen (gO_2/m^3)

Dissolved oxygen kinetics are described by the following equation.

$$\frac{dO_2}{dt} = DOR_1 + DOR_2 - DOP_1 - DOP_2 - DO_{DOC} - DO_{NIT}$$

$$+\{KR_{DO}/dzs \times (DO_{Sat} - O_2)\} - \{SOD/dzb)\}$$

Where DOR_1 ($gO_2/m^3/day$) is the sum of production of oxygen due to photosynthesis, consumption of oxygen due to photochemical respiration and metabolism of algae group 1. DOR_2 is sum of production of oxygen due to photosynthesis, consumption of oxygen due to photochemical respiration and metabolism of group 2 algae. DOP_1 and DOP_2 are loss of oxygen due to predation of algae 1 and algae 2 groups respectively. DO_{DOC} is the oxygen consumption due to mineralization of labile and refractory DOC ($gO_2/m^3/day$).

$$DOR_1 = ((1.3 - 0.3PN_1) \times P1_{NNF} \times B1 - f_{RDO1} \times CP_1) \times \alpha_{OC,R}$$

$$DOR_2 = ((1.3 - 0.3PN_2) \times P2_{NNF} \times B2 - f_{RDO2} \times CP_2) \times \alpha_{OC,R}$$

where

$$f_{RDO1} = (1 - f_{CLD1} - f_{CRD1} - f_{CLP1} - f_{CRP1}) \times \frac{O_2}{K_{HR1} + O_2} = F_{CI1} \times (1 - f_{DOCBM1})$$

$$f_{RDO2} = (1 - f_{CLD2} - f_{CRD2} - f_{CLP2} - f_{CRP2}) \times \frac{O_2}{K_{HR2} + O_2} = f_{CI2} \times (1 - f_{DOCBM2})$$

$$DOP_1 = f_{DOP} \times PR_1 \times \frac{O_2}{K_{HR1} + O_2} \times \alpha_{OC,R}$$

$$DOP_2 = f_{DOP} \times PR_2 \times \frac{O_2}{K_{HR2} + O_2} \times \alpha_{OC,R}$$

$$DO_{DOC} = (MNL_{LDOC} + MNL_{RDOC}) \times \alpha_{OC,R}$$

$\alpha_{OC,R}$ is oxygen to carbon stoichiometric ratio (gO_2/gC). For surface layer, KR_{DO} is the surface reaeration rate for dissolved oxygen (m/day) and dzs is surface layer thickness (m). For the bottom layer, SOD is sediment oxygen demand ($gO_2/m^3/day$) and dzb is bottom layer thickness (m). SOD is calculated by the sediment diagenesis model. PN_1 and PN_2 are ammonia preference for nitrogen uptake by first and second algae groups respectively (0 -1).

Pacific Northwest
NATIONAL LABORATORY

Proudly Operated by **Battelle** *Since 1965*

U.S. DEPARTMENT OF
ENERGY

902 Battelle Boulevard
P.O. Box 999
Richland, WA 99352
1-888-375-PNNL (7665)

www.pnnl.gov